Spring 2024

Monitoring and Control of Coal Dust Exposure Using Low-Cost PM Sensors and Computational Fluid Dynamics

Nana Kobina Amoako Amoah
Missouri University of Science and Technology

Department: Mining Engineering

MONITORING AND CONTROL OF COAL DUST EXPOSURE USING LOW-COST PM SENSORS AND COMPUTATIONAL FLUID DYNAMICS

by

NANA KOBINA AMOAKO AMOAH

A DISSERTATION

Presented to the Graduate Faculty of the

MISSOURI UNIVERSITY OF SCIENCE AND TECHNOLOGY

In Partial Fulfillment of the Requirements for the Degree

DOCTOR OF PHILOSOPHY

in

MINING ENGINEERING

2023

Approved by:

Guang Xu, Advisor
Kwame Awuah-Offei
Yang Wang
Taghi Sherizadeh
Emanuele Cauda

PUBLICATION DISSERTATION OPTION

This dissertation consists of the following four articles, formatted in the style used by the Missouri University of Science and Technology:

Paper I, found on pages 11 - 60, has been published in the *International Journal of Mining Science and Technology*.

Paper II, found on pages 61 - 99, has been published in the *Science of the Total Environment journal*.

Paper III, found on pages 100 - 136, has been submitted to the *journal of ACS Sensors.*

Paper IV, found on pages 137 - 163, has been submitted to *international journal of mining science and technology*.

ABSTRACT

Overexposure to respirable coal mine dust has been linked to causing serious health problems including coal workers pneumoconiosis (CWP) and chronic massive fibrosis. The prevalence of these health problems has been on the increase since the 2000s due to increased exposure levels with roof bolter operators having the highest exposure levels. The currently used PDM3700 is too expensive, heavy and bulky which limits their use only for regulatory monitoring failing to measure miners' personal exposure levels. Also, since roof bolter opeartors are more prone to elevated coal dust levels, the canopy air curtain (CAC) was developed to protect then high coal dust concentrations. However, the current generation CAC only provides a 46% coal dust reduction efficiency leaving room for improvement. Insifficient coal dust monitors in mines make it challenging to effectively evaluate the performance of these CACs.

The objectives of this research are therefore, to develop a small, light weight, low-cost coal dust monitor using a low-cost PM sensor for personal coal dust monitoring in underground coal mines; to develop statistical and machine learing calibration models for low-cost PM sensors to accurately measure coal dust concentrations; and to optimize the design of the CAC using computational fluid dynamics for improved coal dust protection. This study has led to the development and calibration of a low-cost coal dust monitor which will potentially reduce monitoring cost by ~$15,000 per unit while achieving 95% the accuracy of the PDM3700. The CAC design was optimized using CFD simulations improving the uniformity of the CAC. Further, the low-cost sensors present an opportunity to effectively measure the dust control efficiency of the CACs.

ACKNOWLEDGMENTS

I express sincere gratitude to my research advisor Dr. Guang Xu for his mentorship throughout my program. He provided me with opportunities to work on vital research projects and guided me with his knowledge and experience to ensure my research was completed successfully. I also express appreciation for the research funding he provided for the completion of my research.

I am thankful to Dr. Ashish Kumar for the many hours he spent with me in the lab setting up and performing experiments. He was always available to answer my questions and share his knowledge on CFD which was instrumental in my research. The support from other members of the Ventilation, Safety and Health research group in running experiments is also appreciated.

I acknowledge my committee members Dr. Kwame Awuah-Offei, Dr. Taghi Sherizadeh, Dr. Yang Wang, and Dr. Emanuele Cauda who took the time to contribute to my research to excellence. I am thankful that they had genuine interest in my research and worked diligently to ensure excellent work was done.

An immense thank you to my parents Richmond Amoah and Victoria Akorah for their love and support throughout my studies. None of this would have been possible without their support throughout my stay away from home. I also acknowledge my siblings Michael, Richmond and Stella Amoah, as well as my cousin Ellen Afful for their love and support over the years.

To all my friends in Rolla, I appreciate you all for the friendships we shared.

TABLE OF CONTENTS

Page

LIST OF ILLUSTRATIONS

SECTION Page

LIST OF TABLES

PAPER II Page

PAPER IV

1. INTRODUCTION

Particulate matter is a general hazard associated with mining. High levels of PM are generated from many activities and processes involved in the extraction and processing of minerals including drilling, blasting, excavation, loading, hauling, tipping and crushing of ore. Different mines are associated with different PM characteristics and chemical composition. In coal mining, miners are exposed to respirable coal mine dust in the mine atmosphere generated by coal minig activities. Coal dust concentrations measured in underground mines can be considerably higher than in surface mines due to limited ventilation to dilute coal dust. As a result, underground coal miners are exposed to elevated levels of coal dust.

Overexposure to respirable coal mine dust is known to cause irreversible respiratory diseases such as coal workers pneumoconiosis (CWP), emphysema and chronic bronchitis, collectively known as “black lung” which causes permanent disability and premature deaths. Coal miners have also been diagnosed with silicosis due to exposure to coal dust with high silica content. The prevalence of the advanced form of black lung known as progressive massive fibrosis has been exponentially increasing since 2000. This recent prevalence is considered the most serious in history, causig thousands of deaths and about $44 billion in compensation paid to affected families by the federal government. While all miners are at risk, underground roof bolter operators are the occupation exposed to some of the highest levels of coal dust in underground coal mines.

The Mine Safety and Health Administration (MSHA) has promulgaed coal dust rules which are aimed at protecting coal miners from excessive coal dust exposure. In the

new coal dust rule implemented in August 2014, underground coal mines are required to limit personal exposure to respirable coal dust to 1.5 mg/m^3 end of shift average. Accurate real time personal exposure monitoring is needed to ensure that personal exposure levels for miners do not exceed the regulated concentration as this was required within the new coal rule. However, the currently used personal coal dust monitoring unit, the PDM3700, which costs $20,000 and weighs 5 kg is too expensive, too heavy and too bulky. Because of these drawbacks, mines are not able to measure all miners' personal exposure levels, leaving most miners exposed to unknown coal dsut concentrations. This has resulted in the use of the PDM3700 primarily for regulatory monitoring purposes.

Low-cost light scattering PM sensors offer an advantageous solution. These low-cost PM sensors measure PM concentrations in real time using light scattering principles, and come in a small, light weight package. Even though these sensors have been previously explored for domestic air quality montoring applications and have demonstrated promising results, this technology has never been explored for any mining applications. Moreover, their accuracy for measuring mining induced coal dust concentrations in underground mine conditions are questionable due to errors and performance issues pointed out in the past. The objectives of this work are therefore to develop low-cost coal dust monitors using low-cost PM sensors and to calibrate them using statistical and machine learning algorithms. These sensors will be necessary to inform timely dust control measures. They will also provide a more effective measure of the efficiency of dust control devices such as the CAC with high density motitoring capacity.

Effective dust control technology is crucial in underground coal mining to ensure timely intervention when elevated coal dust conentrations are detected. Roof bolter operators are exposed to some of the highest coal dust conentrations in underground mines. This is due to their exposure to dust falling off from their operations drilling in the roof, their position downwind of other operations and limited ventilation in underground mines. The canopy air curtain (CAC) was therefore developed by NIOSH to control their exposure to coal dust and has been through several redesigns over the years with the aim of improving its dust control efficiency. It is known that with a uniformly distributed airflow over the plenum of the CAC, an air curtain will be formed preventing dust laden air from penetrating the protected zone. Previous internal structures of the CAC have been incorporated with deflectors and louvers to ensure a uniform airflow distribution over the plenum area. However, the third and current generation CAC has an efficiency of 42% which leaves room for further improvement. The objective of this study was therefore to optimize the design of the CAC to ensure optimum dust protection efficiency.

The combined application of the low-cost PM sensors and the optimized CAC design in underground coal mines aim to achieve improved underground mine air quality and the protection of miners against coal dust overexposure. This is achieved through real time personal exposure monitoring and timely dust control using the optimized CAC for roof bolters. This study also presents a more effective technology to measure the dust control efficiency of the CACs with their high special and temporal capabilities.

2. LITERATURE REVIEW

According to data from the International Energy Agency (IEA), global demand for coal for power generation has more than doubled since the 1970s making up 29.03% of global energy production [1]. In the United States, coal fired power plants account for about 30% of the nation's electricity generation produced from the 700 million tons of coal mined yearly [1], [2].

The national and global production of coal at these levels by coal mines exposes miners to high levels of coal dust. Nearly all stages in the coal mining process generate various levels of coal dust in the mine atmosphere. Overexposure to high concentrations of coal dust causes serious respiratory diseases. The most common among these diseases is the coal workers pneumoconiosis (CWP), also known as black lung [3], [4] whereby inhaled coal particles cause scarring within lung tissues impairing one’s ability to breathe. An advanced form of CWP, known as progressive massive fibrosis causes large conglomerate masses to grow within the lungs which can be potentially fatal [5], [6]. In the US, the prevalence of CWP and progressive massive fibrosis had been steadily decreasing since the early 2000s from 3.5% in 1975 to 0.5% in in 1997 as can be seen in Figure 2.1. However, a resurgence in progressive massive fibrosis prevalence has been observed since early 2000s, which is considered the most serious in history with prevalence rates rising back up from 0.5% to 5.3% in recent years [7]. Moreover, while data on miners diagnosed with CWP in China is limited, a recent study found prevalence of 6.02% through a systematic evaluation of reported data between 2001 and 2011 [8]. This suggests that coal miners in China are more susceptible to CWP than actual numbers

may predict as unreported data could be misleading. Another study also observed increased reports of CWP in Australia even though there is not national reporting system [9]. All this evidence points to CWP being a global problem linked to thousands of deaths globally each year [10].

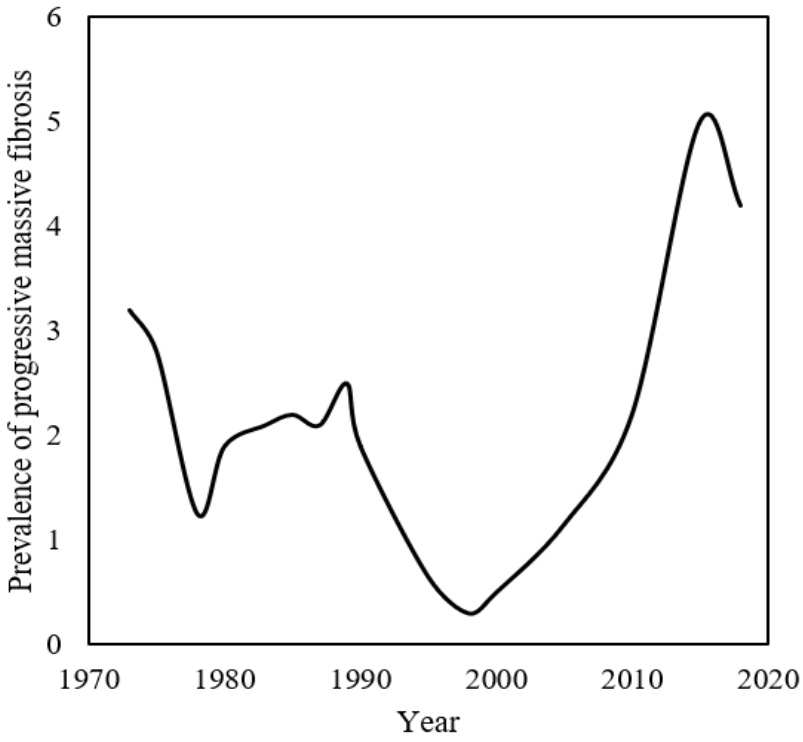

Figure 2.1. Prevalence of progressive massive fibrosis among underground coal miners within the US's Appalachia region

To control coal dust exposure and protect miners from CWP and progressive massive fibrosis, MSHA promulgated the new coal rule on August 1st, 2014, to regulate mines from exposing miners to unhealthy coal mine dust concentrations [11]. Some provisions within this rule were that: miners are required to sample airflow to measure personal exposure levels to coal dust throughout the shift and implement corrective

measures if high levels of coal dust are detected; miners are required to increase monitoring locations within the mine to cover the entire mine; miners are required to increase medical surveillance and transfer miners with evidence of CWP (also known as part 90 miners) to areas of the mine with lower coal dust concentrations. Two years after this rule was passed, an additional provision was implemented reducing permissible exposure levels and introducing the continuous personal dust monitor (CPDM). First, the concentration limits for respirable coal mine dust in underground miners was reduced to 1.5 mg/m^3 from 2.0 mg/m^3. Second, respirable coal dust exposure limit for part 90 miners was lowered from 1.0 mg/m^3 to 0.5 mg/m^3. This provision further required the new CPDM to be worn by all part 90 miners and other miners exposed to high concentrations of coal dust. This was expected to increase sampling frequency and miners would receive sampling results faster.

The currently used CPDM model 3700, also known as PDM3700 or simply PDM, measures personal coal dust exposure levels every minute and displays the minute-by-minute rolling averages. This monitor measures coal dust exposure levels based on the tapered element oscillating microbalance (TEOM) technique [12], [13]. Prior to its introduction, the federal equivalent TEOM was used to measure miners' exposure levels by sampling air from their breathing zone throughout the miner's shift onto a filter to determine exposure levels [14]. The TEOM, however, was too large to be used as a personal monitoring unit. Moreover, it took several to complete analysis and receive sampling results which made it difficult to implement dust control measures in time. The TEOM technology was therefore miniaturized into the PDM3700 as a smaller unit and thus portable for personal monitoring. The PDM is known to measure coal dust

concentrations with high accuracy and is approved by NIOSH for monitoring in underground coal mines. NIOSH laboratory tests have demonstrated that there is 95% confidence that PDM measurements are within ±25% of true concentrations. Their field precision tests also show that the PDM monitors have a 0.078% standard deviation [15]. The PDM is equipped with a respirable size coal dust cyclone with a cut-off size modelled to closely simulate the human respiratory system respirable curve. Therefore, only respirable size particles go through to the mass transducer where the mass concentration is determined using the tapered element oscillation microbalance (TEOM).

Light scattering low-cost PM sensors are compact, consume little power, and are able to provide particle concentrations in particle size categories in real time using light scattering principles. This technology has been studied over the years for their ability to measure PM concentrations in domestic conditions, occupational environments and in the cities [16]–[18]. Light scattering is sensitive to particle size and composition [19]. Therefore, several focused previously focused on calibrating low-cost PM sensors using specific dust types for which they will be deployed. Previous studies have calibrated then for particle types including Arizona road dust [20]–[22], cigarette smoke [23], coal dust [24], polystyrene latex (PDL) particles [20], welding fumes [20], [25], salt [20], [21], [26], wood smoke [27], diesel particulate matter (DPM) [28], [29], incense [26], [30], [31] and sugars [26].

Multiple studies have established that low-cost PM sensors are effective for measuring particle mass concentrations for PM relative to research-grade monitors [22], [23], [32], [33]. For example, Wang et al. [26] reported a high correlation with reference monitors with coefficient of determination (R2) of >0.89 for various types of sensors

evaluated in a laboratory for PM2.5. Feenstra et al. [34] also recorded a correlation of >0.7 for 6 out of 12 sensors tested in a field evaluation for PM2.5. However, studies have also reported poor performance scenarios of these sensors due to errors related to meteorological conditions [35].

The canopy air curtain was developed by NIOSH to protect roof bolters from excessive coal dust exposure. Roof bolter operators install roof bolts into the roof of the mine by drilling into the roof to install the bolts. They are protected by a canopy over their working area to protect them from falling objects. However, the canopy provides no protection from coal dust. These operators therefore are exposed to some of the highest coal dust concentrations within the mine mainly resulting from dust generated from their operations, dust generated by other operations such as continuous mining which are carried over to their working area and lack of ventilation capacity in underground mines to dilute high coal dust concentrations [36], [37]. According to some NIOSH studies which monitored roof bolter operators personal exposure levels over long periods of time, these miners recorded concentrations as high as 7.0 mg/m^3 [38]. Over the years, the design of the CAC has gone through several iterations aiming to provide adequate coal dust protection to roof bolter operators.

The CAC was originally designed for continuous miner operator cabs and was modified to fit on the roof bolter. Since then, the National Institute for Occupational Safety and Health (NIOSH) has made many iterations of improvement to the design of CACs. Initial laboratory evaluation showed a dust reduction of up to 62% [39]. A new prototype design was presented by Listak and Beck [38] that covers the entire operating area under the roof bolter canopy. The CAC was optimized to provide uniformed airflow

over the entire plenum using computational fluid dynamics (CFD) simulation and trial-and-error process, and has achieved dust reduction of more than 67% for entry velocities up to 0.61 m/s (120 fpm). Based on the NIOSH design, J.H. Fletcher & Co. incorporated the CAC into the roof bolter canopy as part of the machine [40]. However, based on NIOSH mine gallery test, its dust reduction efficiency was only 24%. Based on NIOSH CFD analysis and recommendations, Fletcher designed the 2nd and 3rd generation CAC that is redesigned to prevent contaminated air infiltrating the protected zone while maintaining the initial NIOSH design with uniform airflow from the plenum using equally spaced holes [36], [41]. Although the 3rd generation CAC lab test dust reduction has improved up to 49.3% [42], field test has shown variable dust control efficiencies indicating rooms to further improve. Previous NIOSH CAC research has indicated that an even distribution of airflow across the plenum of the CAC at a velocity higher than 0.51 m/s (100 fpm) is a key for improved efficiency.

A manifold is an important device used in many industrial processes to distribute a large fluid stream into several parallel streams. It consists of a main flow header, and several outlets. A uniform flow distribution is commonly required in most engineering applications, such as piping system in pumping stations, heat exchangers, and flow distribution system in treatment plants. However, it is challenging for a typical manifold with a constant cross-sectional area header to achieve uniform flow distribution. This is due to the static pressure build up toward the end of the header, which causes a higher efflux through the downstream outflows. Studies have, however, shown that the manifold with a tapered longitudinal section can achieve nearly uniform flow distribution if properly optimized [43]. This is because the pressure distribution is more uniform in the

header [44]. Instead of using trial-and error approaches, CFD has been successfully used to optimized the tapered manifold parameters to achieve uniform outlet flows [43]–[46] [16-20]. This allowed researchers in these studies to explore the impact of factors such as varying manifold outlet sizes, increasing main header size, linear and non-linear tapering of main header. Among these factors studied in literature, it is apparent that linear tapering of a main header of a manifold is the most effective strategy to achieve a uniform distribution of manifold outlets.

PAPER

I. APPLICATION OF LOW-COST PARTICULATE MATTER SENSORS FOR AIR QUALITY MONITORING AND EXPOSURE ASSESSMENT IN UNDERGROUND MINES: A REVIEW

ABSTRACT

Exposure to mining-induced particulate matter (PM) including coal dust and diesel particulate matter (DPM) causes severe respiratory diseases such as coal workers' pneumoconiosis (CWP) and lung cancer. Limited spatiotemporal resolution of current PM monitors causes miners to be exposed to unknown PM concentrations, with increased overexposure risk. Low-cost PM sensors offer a potential solution to this challenge with their capability in characterizing PM concentrations with high spatiotemporal resolution. However, their application in underground mines has not been explored. With the aim of examining the potential application of low-cost sensors in underground mines, a critical review of the present status of PM sensor research is conducted. The working principles of present PM monitors and low-cost sensors are compared. Sensor error sources are identified, and comprehensive calibration processes are presented to correct them. Evaluation protocols are proposed to evaluate sensor performance prior to deployment, and the potential application of low-cost sensors is discussed.

1. INTRODUCTION

Poor air quality in underground mines causes severe health impacts to underground mine workers as mining activities generate various types of particulate matter (PM). In underground mines, PM concentration is much higher than the surface open environments due to limited ventilation capacities, which causes severe health impacts to underground miners. Coal dust and diesel particulate matter (DPM) are the two primary types of PM pollutants in underground mines. For coal dust, overexposure to respirable coal dust causes various lung diseases among miners, including coal workers' pneumoconiosis (CWP), also known as black lung, a potentially fatal lung disease with no cure [1]. The prevalence of CWP has considerably decreased since the 1980s. However, a resurgence of CWP has been observed in the U.S. coal mines based on the data reported from the Coal Workers' Health Surveillance Program [2]. This recent resurgence has been the most serious in history, and miners are at an increased risk. Contrary to prior finding that only long term exposure to coal dust leads to CWP, recent studies have identified cases occurred to miners who just started working in the mine and have never worked in other mining environments before [3]. DPM also presents a health threat to underground miners. DPM concentrations in underground mines are significantly higher than typical surface environments [4–5]. Currently, DPM is classified as an occupational carcinogen by the United States National Institute for Occupational Safety and Health (NIOSH) and increases the risk of lung cancer by 20%–50% [6]. Non-cancer health effects, such as respiratory and cardiovascular health effects, are also associated with underground DPM exposure.

Different countries have different standards for regulating underground mine coal dust and DPM exposure levels. Exposures to concentrations higher than the regulated levels are regarded as overexposure that causes negative health impacts. In the United States, the Mine Safety and Health Administration (MSHA) promulgated the coal dust permissible exposure levels (PEL) to be 1.5 mg/m^3 for underground mines. For DPM, the Occupational Safety and Health Administration (OSHA) regulations requires that a miner's personal exposure to DPM must not exceed 160 $\mu g/m^3$. Accurate personal PM monitoring is an essential way to protect the miners from overexposure. In US underground mines, the PDM3700 [7] and the FLIR Airtec DPM monitor [8] are the most commonly used portable monitors measuring coal dust and DPM, respectively. The PDM3700 uses a miniature of a tapered-element oscillating microbalance (TEOM) to measure PM concentration, which generally requires to be in an upright position and carefully protected as a hit or bumping has adverse effects on the measurement accuracy. The FLIR Airtec is a filter-based DPM monitor which uses light extinction to measure elemental carbon (EC, a surrogate for DPM) mass concentration and reports results in a 5-min rolling average. However, these monitors have the disadvantages of high cost, heavyweight, and limited measuring capabilities (only measure mass concentrations) [9–10]. Typically, regulatory grade PM monitors cost more than $20000 per unit. The PDM on the other hand cost ~$17000 per unit and the Airtec DPM monitor cost ~$5000 per unit. At these prices, they are still too expensive for mines to purchase one for each miner on duty to ensure each miner wears one unit. As a result, these monitors are worn only by a small number of miners primarily for regulatory compliance sampling purposes. This practice has serious drawbacks, most notably that the exposure levels for the majority of

the miners are unknown due to low spatio-temporal resolution of current monitoring system. Besides, due to the lack of sufficient data, mining engineers are unable to directly quantify the coal dust and DPM control effectiveness caused by modified engineering control strategies. Finally, there is a lack of sufficient personal exposure data to accurately correlate personal coal dust and DPM exposure to their related-health data in more detailed epidemiology studies.

Low-cost light scattering PM sensors offer a potential solution to these problems. These sensors are compact, consume little power, and can even provide particle size distribution information if sensors have multiple size bins and are properly calibrated. Based on these characteristics, low-cost sensors can be deployed for personal monitoring to achieve a real-time highly dense monitoring data which can be necessary to monitor and improve air quality, ventilation designs, and underground conditions. These sensors are available from different commercial supplies as packed modules, and previous evaluations have demonstrated promising results in comparison with federal equivalent methods (FEMs) or research-grade instruments for air quality PM monitoring [11–13]. Currently, there is no research available in the application of low-cost PM sensors in mines [14–15]. However, the few advances in this field have been dominated with surface mine applications which have shown good results whereas underground mine application still remains unexplored [15]. Therefore, there is still limited understanding of the performance specifications of these emerging low-cost sensors, and their performance varies with operating conditions (relative humidity and temperature), particle properties (particle composition and size distribution), and the choice of reference instruments [16]. There is basically no comprehensive study available in the literature using a standard

protocol assessing these sensors for monitoring coal dust and DPM, which hinders an in-depth understanding of their performance and application for underground PM monitoring due to lack of knowledge about the accuracy, precision, and stability of such sensors.

As shown in the flow chart in Figure , the objective of this review paper is to summarize the current status of low-cost PM sensor research and propose research directions on how it can be applied to underground mines. The working principles of current PM monitors and low-cost PM sensors are presented and compared to help understand the differences between them. The accuracy of the sensors largely depends on the control and correction of errors. Thus, both the internal and external error sources for the low-cost PM sensor are analyzed, revealing their impact on sensor accuracy. Laboratory calibration is an important step before sensor field deployment. We explained commonly used calibration methods, with a discussion on the setup of a calibration chamber and its key components. We have introduced the linear and multivariate calibration models which are developed using laboratory chamber tests. Sensors have to be evaluated before applications; therefore, we have proposed standardized evaluation procedures and indices. Lastly, the challenges and application potentials of low-cost PM sensors in underground mines are discussed. This paper provides a theoretical and practical guide to the application of low-cost PM sensors to the underground mining industry where PM exposures cause significant health issues. Low-cost PM sensor with a high spatio-temporal resolution is expected to improve underground structure and ventilation designs, protect the health of miners, and provide high quality “big data” that facilitate the health studies related to respiratory diseases caused by PM.

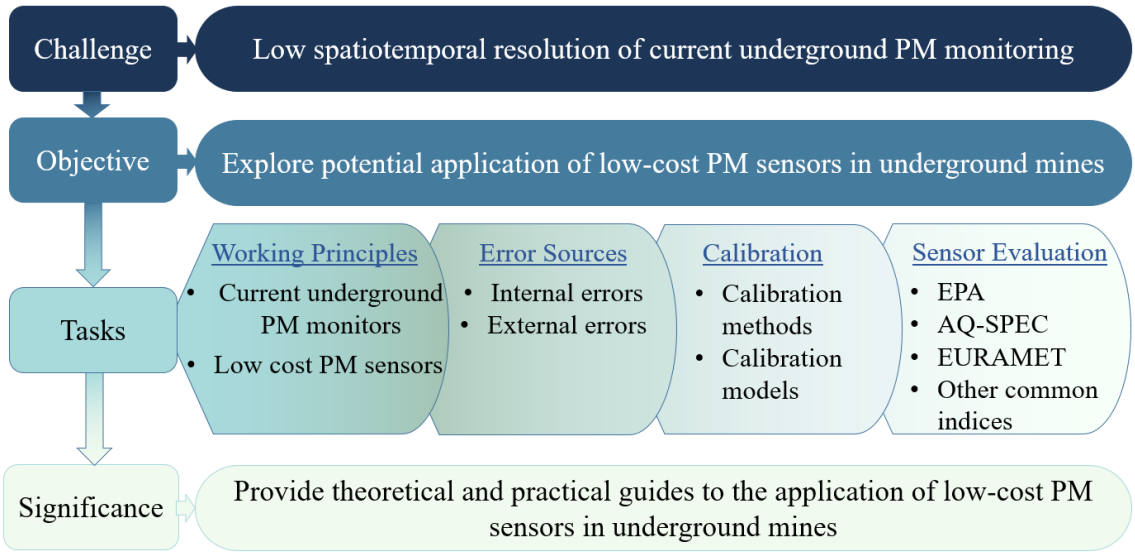

Figure 1. Low-cost PM sensor review flow chart.

2. WORKING PRINCIPLES OF PM MONITORS

2.1. CURRENT UNDERGROUND PM MONITORS

Coal dust and DPM are the two most perilous PMs whose concentrations are regulated in underground mines. To protect mineworkers from overexposure, the Personal Dust Monitor model 3700 (PDM3700) was developed under a NIOSH funded program for portable real-time monitoring of underground coal dust concentrations. The working principle is based on tapered element oscillating microbalance (TEOM) which has been designated as Federal Equivalent Methods by the U.S. Environmental Protection Agency (EPA) for environmental air quality PM monitoring [17].

The federal equivalent TEOM monitors are too large to be used as a personal portable monitor. The PDM3700 is a small sized miniature of TEOM, and thus portable for underground coal mine applications. As shown in Figure 2, a sample inlet is mounted

on the bill of a miner's hard hat to sample dust within the miner's breathing zone at a constant flow rate of 2.2 L/min [18], which passes through the flexible conductive tube towards the cyclone. An in-built cyclone screens particles to allow only respirable sized particles in the air stream to flow through to the heated section for moisture removal. The air stream reaches the exchangeable filter cartridge where particles settle as filtered air proceeds to the monitor's orifice. The microbalance applies gravimetric equivalent techniques to measure mass of coal dust collected on the filter, and the dust concentration is reported every minute. A 1.05 correction multiplier is used to compensate for errors between manual gravimetric reference and the PDM3700 results to meet the MSHA standard for underground coal mine compliance monitoring [18–19].

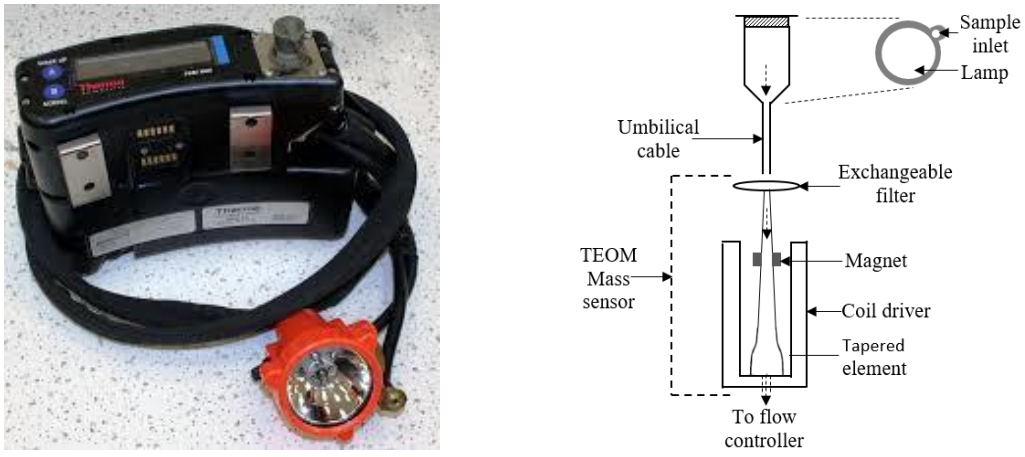

(a) (b)

Figure 2. (a) Commercial PDM 3700 set up and (b) schematic diagram.

Momentum compensation is the key technology used in PDM3700 to miniaturize the traditional large TEOM [18]. The tapered element in the traditional TEOM is large

because it needs to be mounted on a base of significant mass to reduce energy loss and maintain its oscillation frequency. To overcome this, as shown in Figure 2(b), a coil driver and magnet are incorporated with the TEOM mass sensor. The coil driver pulsates against the magnets on the tapered element to initiate an oscillation. The magnetic field created by the magnet provides momentum compensation to the tapered element by oscillating in an equal but opposite motion. This patented concept of momentum compensation substantially reduces the energy loss from the tempered element oscillator, which enables the size and weight reduction of the TEOM.

NIOSH has validated the PDM3700's accuracy, precision, and comfortability before MSHA approves this equipment as the regulatory compliance monitoring device [18,20]. Laboratory tests verified that the PDM3700 met the criteria of ±25% accuracy compared to reference measurement with 95% confidence [18]. Their underground tests also revealed a field measurement precision of 0.078 (relative standard deviation) [21].

For DPM measurement, the NIOSH method 5040 is the standard procedure for measuring DPM concentrations [22]. This method analyzes EC concentration on a DPM laden filter through a thermal-optical analyzer in a burning process. Although this method is accurate, it only provides average concentration over an entire shift, and the analysis results are only available after weeks [6,23–24]. To measure DPM in real-time in underground, the FLIR Airtec DPM monitor (Airtec, United States), shown in Figure 3, has been developed and calibrated against the NIOSH 5040 method [22]. It measures DPM concentration based on light extinction principles with EC as the analyte [25]. The Airtec's diaphragm pump draws in ambient air at 1.71 L/min through the inlet, where an impactor makes a size cut of 0.8 μm. A conductive air tube is used for preventing DPM

from sticking to the tube walls. The Teflon filter housed in a specially designed cassette traps DPM and darkens. A 650 nm wavelength laser is shot through the filter, and the transmittance of the filter is measured by a photodetector. The measured optical density is calibrated against the NIOSH 5040 method, thus able to measure EC concentrations in a 5 min rolling average. The total carbon (TC) concentration can be obtained by multiply a factor of 1.3 to the measured EC data.

Noll and Janisko [25] carried out assessments of the accuracy, precision, and susceptibility to interferences of the Airtec. They observed accuracy of 12% at 95% confidence compared to the NIOSH 5040 method. Interferences from non-DPM dust and cigarette smoke particles were found not to affect Airtec measurements only when a submicron impactor was used. Laboratory test results showed that 50–250 µg/m3 concentration of cigarette dust resulted in additional interference of 8–98 µg/m3 of DPM while lower interference was recorded at lower cigarette smoke concentration. It is established that non-DPM particles do not affect light extinction directly. However, they can affect the accuracy when they are coagulated with DPM and attached to the filter, or in case a compactor is not used. The Airtec was not certified by MSHA as a regulatory compliance monitoring device, and the manufacturer has discontinued it as of 2019.

In recent times, light scattering has become an emerging technology used for PM monitoring in mining environments. Many real-time PM monitors utilize light scattering and sensing elements to characterize PM concentrations. For example, the Thermos Personal Dataram (PDR) models 1000 [26] and 1500 [27] PM monitors are both instantaneous samplers that use light scattering principles to provide airborne respirable dust concentrations in underground mines. The PDR1000 uses light scattering and

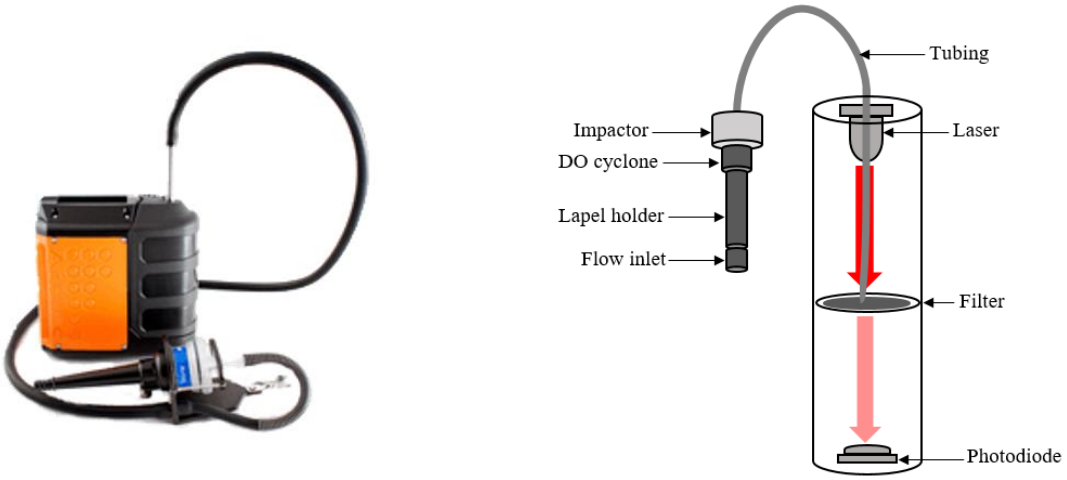

(a) (b)

Figure 3. FLIR Airtec DPM monitor: (a) external features of the FLIR Airtec DPM monitor; (b) schematic diagram showing the internal components and principles of operation of the Airtec.

sensing principles which is optimized to monitor respirable sized PM such as PM2.5, smoke, fumes, and mist. It uses the natural ambient airflow to draw air samples. The PDR1500 model is a similar but more advanced model which equipped with a flow control pump to give users some level of flexibility. An evaluation conducted by the Respirable Hazard Control branch of NIOSH on these monitors yielded accurate PM measurements using gravimetric sampling as reference monitoring [28]. Other established light scattering based PM monitors which are commercially available include AM520 TSI monitor and GRIMM model 1.107 [10,29–30]. Even though these models perform accurately as compared with gravitational samplers, they still possess size and cost disadvantages which make them inapplicable for personal monitoring in underground mines.

2.2. LOW-COST PM SENSORS

In view of the limitations presented by the current underground personal PM monitors, there remains the need for an efficient method that can provide accurate real-time continuous PM monitoring. Considerable recent research has led to the development of a new generation of monitors in the form of inexpensive, portable, low power, real-time PM sensors termed as “low-cost PM sensors.” These sensors operate on light scattering principles. The main components of a typical low-cost PM sensor are a light source which could be a laser, white light or infrared light emitting diode (LED), a photodetector, focusing lenses, an airflow controller, and a microprocessor. Figure 4 illustrates the components and working principles of low-cost sensors. Three techniques are used to draw air into the sensor. The first type uses a thermal resistor installed close to the inlet, as can be seen in Figure 4(a). It is electrically heated to create natural convection that results in an updraft of particles through the inlet to the sensing volume [31–32]. The second type is equipped with a small direct current (DC) fan, as shown in Figure 4(b), to draw air into the sensor [10]. The third type does not require any specific configurations, and it only relies on a hole through the center of the sensors’ body to allow for convection of particles through the sensing volume. With any of these techniques employed, sampled airflow travels through the inlet to the sensing volume and eventually exits from the sensor. In the flow path, particles pass through the sensing volume where the light beam is focused. The intensity light scattered by particles is detected by the photodetector and converted to mass or number concentration of PM by a microprocessor. Scattering angles of low-cost sensors are between 90° to 120° [33–34].

Most PM sensors also have a light trap (Figure 4(b)) at the end of the focusing path to avoid spurious light scattering [13].

There are two types of low-cost PM sensors: the nephelometer type, as shown in Figure 4(a), and the optical particle counter (OPC) type, as shown in Figure 4(b). Nephelometer type PM sensors employ forward scattering principles to measure the amount of light scattered by the particle cloud within the sensing volume. These sensors infer mass concentration from the intensity of the light scattered from the incident light source. The OPC type sensors, on the other hand, operate as though they are single particle counters. As shown in Figure 4(b), only a small sensing volume is illuminated by a beam of the incident light, through which sample airstream flows, so that one particle at a time is illuminated. The intensity of light scattered by each particle is converted to number and mass concentration for different particle sizes across various size bins.

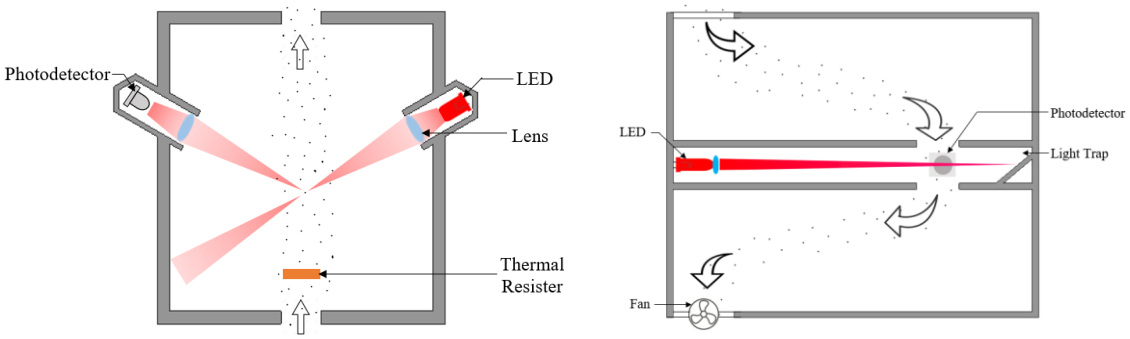

(a) (b)

Figure 4. Low-cost PM sensor schematic diagram: (a) nephelometer type PM sensor; (b) OPC type low-cost sensor.

Low-cost PM sensors generally weigh less than 200 g, mostly consume less than 1 W and cost from <$10 to $500s. Most low-cost PM sensors are sold as individual

sensor modules and require to be incorporated with alternating current (AC)/direct current (DC) adaptor or batteries to provide power. For air quality monitoring, low-cost sensors are integrated into other products such as mobile phones [35–37], multi-sensor devices [38], or a body-worn monitor [39] and consequently equipped with a microcontroller for data-logging. Light scattering low-cost PM sensors currently used and commercially available include Plantower (PMS3003 and PMS5003) [9,33], OPC-(N1, N2) [40], Sharp GP2Y1010 [34,41], SYhitech DSM50 [42–44], Dylos (DC1100, DC1100 pro, and DC1700) [10,42], and Shinyei (PPD42NS, PPD 20 PV, PPD 60 PV, and AES-1) [45].

Numerous experiments have established that low-cost sensors are effective for measuring mass concentration of PM using research-grade monitors as reference [13,16,42,46]. For example, Wang *et al.* [41] reported a high correlation with reference monitors with coefficient of determination (R^2) of >0.89 for various types of sensors evaluated in a laboratory for PM2.5. Feenstra *et al.* [11] also recorded a correlation of >0.7 for 6 out of 12 sensors tested in a field evaluation for PM2.5. However, studies have also reported poor performance scenarios of these sensors due to errors related to meteorological conditions [47]. Some of the major error sources are discussed in the next section and followed by sensor calibration methods for improving the sensor accuracy.

3. PM SENSOR ERROR SOURCES

Measurement errors cause inaccurate and misleading results. In a case of erroneously underestimation of PM concentration, miners face the risk of unknown

overexposure to PM concentrations higher than the safe exposure levels. It is, therefore, crucial to identify the PM sensor error sources and apply appropriate calibration pre- and post-deployment. Based on a critical review of error sources investigated in the literature, we classify them into two general categories; internal and external error sources.

3.1. INTERNAL ERROR SOURCES

Internal error sources, also called instrument errors, are due to the working principles that are independent of deployment conditions, even though they may also be develop after deployment [10]. These errors are caused by imperfect working principles, defective and imperfect manufacture of parts, inaccurate installation, changes in instrument properties with time, and unsteady flow control systems [10,32,48]. The following section discusses the main types of internal error sources.

3.1.1. Measurement Boundary Error. The measurement boundary is generally the range of PM concentration a PM sensor is sensitive to. It includes two aspects: Upper limit of quantification (ULOQ), and lower limit of quantification (LLOQ). ULOQ and LLOQ are the highest and lowest PM concentrations the sensors can accurately measure [10,49]. Outside this range, particles do not scatter enough light to be detected [39,42,48,50–51].

These performance characteristics are either provided by the manufacturer on the sensor datasheet or derived by experiments. A widely used technique set out in [52] to experimentally determine these parameters has been successfully applied in many recent studies [13,41], which is elaborated in Section 5 of this paper. Outside these boundaries, PM sensors encounter measurement boundary errors where measurement outputs are

reported as their boundary values [42,46]. This was demonstrated in a test [42] of the TSI AirAssure low-cost PM monitor, which uses a Sharp GP2Y1010AU0F sensor with a limit of quantification from 5 to 300 µg/m3. With this boundary, they reported concentrations above 300 µg/m3 as ~300 µg/m3 and concentrations below 5 µg/m3 as ~5 µg/m3.

3.1.2. Systematic Errors. As in Figure 5(a), data affected by systematic error have three main characteristics: a drift [11], overestimation [9,13], and underestimation [32,40] of the true concentration. These errors are identified using mean bias error (MBE) and mean absolute error (MAE). They are calculated using Eqs. (1) and (2), respectively,

$$\mathrm{MBE} = \frac{1}{n}\sum_{i=1}^{n}(X_i - X_t) \tag{1}$$

$$\mathrm{MAE} = \frac{1}{n}\sum_{i=1}^{n}|(X_i - X_t)| \tag{2}$$

where X_i is the measurement by the low-cost sensor, X_t is that by the reference monitor, and n is the number of measurements. MBE quantifies both overestimated and underestimated errors into a single matric [53–54]. MAE, on the other hand, uses the absolute overestimation and underestimation differences to provide the mean total error [38]. Among low-cost sensors, Feenstra *et al.* [11] observed systematic errors to be dominant in the 12 sensors tested. Moreover, Budde *et al.* [35] recorded a linear drift of the measurement from two sensors that were evaluated for dust concentration

measurement. Wang *et al.* [41] also observed a systematic deviation in a pairwise correlation between sensors of the same type for all three sensors tested.

The source of this error has been associated with sensor degradation due to extended use. Budde *et al.* [48] attributed systematic errors to the thermal resister not able to maintain a constant temperature within the sensor caused by unstable voltage supplies. Collingwood *et al.* [10] pointed out that the inability to measure and control flow rates in the sensor results in systematic errors. They further explained that voltage fluctuation causes fluctuation of fan speed and consequently changes the inlet air flow rate, which impacts measurement accuracy and contributes to systematic errors.

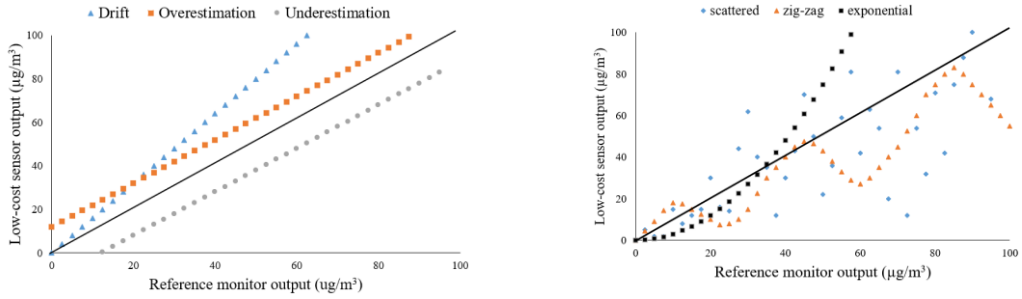

(a) (b)

Figure 5. Low-cost PM sensor error types demonstrating their data structure: (a) systematic error; (b) non-linear response error.

3.1.3. Non-linear Response. An ideal sensor should have a linear relationship between its measurements and that of the referencing instrument. In an ideal situation where a low-cost sensor perfectly matches a reference monitor, the slope of the line of best fit should be 1.0, intercept of 0.0, and R2 of 1.0. Measurement data that are affected

by a non-linear error may be characterized by an exponential curve, zig-zag curve, or a scattered plot, as demonstrated in Figure 5(b).

The non-linear nature of low-cost sensors have been widely reported by numerous researchers [45,50] recording an R^2 of less than 0.9 even though a few other studies have reported higher linearity ($R^2 > 0.9$) [41]. Kelly *et al.* [13] observed a linear relationship for Plantower PMS 1003/3003 sensors below 40 µg/m^3, and above that concentrations, the non-linear relationship started to occur. Austin *et al.* [45] observed low-cost sensors showed a non-linear response when measuring particles with smaller diameter while a linear relationship was observed when measuring larger diameter particles.

When making low-cost sensors, manufacturers calibrate them to achieve a linear response under manufacture conditions. However, differences in calibration condition and deployment condition could result in non-linear responses [55]. Moreover, dual-channel principles of certain PM sensors are likely to be the cause of non-linearity in such sensors. For example, in the Dylos sensor, PM concentrations are obtained by subtracting particles in the >2.5 µm channel from that in the >0.5 µm channel, which may be the source of non-linearity [42].

3.1.4. Reproducibility. Reproducibility of measurements of a sensor unit and/or units of the same sensor model is the measure of the ability of the low-cost PM sensors to repeat a measurement output under the same conditions. Reproducibility of low-cost sensors is determined by the precision of the sensors which can be measured either as relative precision or absolute precision. Relative precision evaluates the reproducibility of different sensors of the same type when measuring the same condition. Absolute precision measures the reproducibility of the same monitor over the same concentration.

Lack of precision among low-cost sensors has been attributed to factors including unsteady wavelengths of sensor light source, orientation of the light source and photodetector, mode of particle transfer from the inlet to sensing volume, and difference in airflow rates among PM sensors [42]. Low-cost PM sensors are not able to maintain their measurement precision and accuracy over a long period of time as a result of aging and dirt effects [10]. Reproducibility is quantified and regulated with coefficient of variation (CV) which is further elaborated in Section 5 of this paper. The US EPA requires acceptable sensor CV values to be less than 10% [17].

3.2. EXTERNAL ERROR SOURCES

External error sources come from deployment conditions and external factors. PM sensors are calibrated by manufacturers at a certain ambient condition. Changes in such conditions are likely to affect the sensor's function. External error sources include meteorological factors and measured particle characteristics.

Meteorological conditions known to have significant impacts on PM sensors are relative humidity [9] and temperature [56]. To overcome the effects of relative humidity, most high-end reference monitors are equipped with drying systems that remove water vapor from "in-flow" air before measurement. This system also maintains a constant temperature within the measured airstream. Low-cost sensors, however, do not have such technology, which introduces errors.

High humidity causes overestimation of PM sensor readings. Jayaratne *et al.* [57] reported a significant overestimation of particle number and particle mass concentrations at relative humidity greater than 75%. Laboratory tests revealed that PM10 and PM2.5

mass concentrations began to increase exponentially at relative humidity (RH) of 78% and increased by a factor of 2 at RH of 89%. Their field experiment data also showed that foggy weather conditions cause overestimation of PM2.5 by over 50% and PM10 by 46%. Field evaluations in another study revealed that the highest overestimated PM2.5 concentrations occurred in the mornings (6–9 am) and evenings (18–20 pm) when RH was high, and temperatures were low [9]. Humidity generally overestimates particle number and mass concentrations in low-cost PM sensors. Water particles possess light scattering properties which make them scatter additional amount of light if they enter low-cost PM sensors' sensing volume. Water vapor can also condense on aerosol particles, making them grow hygroscopically causing overestimation of particle size and concentration. Additionally, highly concentrated water may lead to a failure of the sensor circuits which can cause a bias in measurement outputs [41].

It is normal that temperature variation causes a change of RH, thus indirectly leads to errors related to the above-mentioned RH variations. This error type is particularly evident at lower ambient temperatures when RH is high. For example, Wang *et al.* [41] observed that the sensors experienced an overestimation of PM concentration generally at low concentrations at 5°C. Another study reports a significant temperature effect for low-cost PM sensors during winter-time at temperatures between −3.5 to −19.2°C [58]. For PM sensors that use a thermal resister to generate airflow, the ambient air temperature has a direct influence on the air flow rate. The thermal resistor heats to produce a temperature gradient between the inlet and outlet, relative to the ambient temperature, to create airflow. Therefore, ambient temperature fluctuations result in airflow rate perturbations within the sensor. This results in unexpected PM concentration

fluctuations [39,51]. This effect can be exacerbated when the sensor is disoriented. Typically, such sensors are required to be vertically oriented (with thermal resister side pointing downward) to cause hot air to move up, forcing ambient air into the sensor. Other orientations will cause airflow direction change and flow rate variations, thus generating errors [59].

Another error source is from different particle characteristics. The intensity of light scattered by particles depends on the particles' physical characteristics, including particle size, and refractive index of particles [60–62]. The Refractive index is a measure of the speed of light through a particle. Different particles possess different refractive indexes [63]. Light travels at a lower speed in particles with a high refractive index and faster in particles with a lower refractive index. Therefore, particles with different refractive indexes refract and reflect different intensities of light. Ideally, PM sensors should be calibrated using PM with known refractive indexes that are closely similar to the PM to be monitored. Particle refractive index is often not considered during sensor calibration. This causes significant erroneous readings when low-cost PM sensors are deployed for measuring PM with different refractive indices [64]. In addition, particle size significantly influences the intensity of light scattered by dust particles [61]. Particles smaller than 1 μm scatter light by Rayleigh scattering while particles equal to and larger than 1 μm (in this case also larger than the wavelength of the sensor light source) scatter light by Mie scattering. In both principles, the intensity of light scattered is strongly dependent on particle size. Low-cost PM sensors are generally more sensitive to larger size particles and less sensitive to smaller ones. This causes underestimation in mass concentrations when monitoring smaller size PM and a possible overestimation when

monitoring larger particles. One study has shown that the outputs of the tested sensor became higher as particle size increased from 300 to 900 nm [41].

4. CALIBRATION OF LOW-COST PM SENSORS

Accurate calibration has proven to be an effective tool for improving the low-cost PM sensor's data quality [65–66]. Low-cost PM sensors are either purchased uncalibrated or calibrated under the factory calibration conditions, which differs from intended deployment conditions. In addition, a calibrated sensor can get de-calibrated due to sensor aging over extended use. Therefore, low-cost PM sensors need to be pre-calibrated and re-calibrated periodically after deployment.

Low-cost PM sensor calibrations follow an evaluation assessment carried out in a collocated field or laboratory test to ascertain the accuracy, precision, and the sources of errors that affect the measurements of low-cost sensors. The required calibration is dependent on these outcomes with the aim of converting raw (non-calibrated or de-calibrated) data into a more acceptable quality. The following sections, therefore, elaborate calibration methods available in existing literature that can be applied to low-cost sensors for underground mine PM monitoring.

4.1. LABORATORY CALIBRATION CHAMBER

Laboratory calibration chambers are custom built chambers with the purpose of evaluating the performance and calibrating low-cost PM sensors under controlled environmental conditions. These chambers can control environmental conditions,

including PM concentration, temperature, and humidity [41–42]. The performances of the low-cost PM sensors are evaluated, and the influence of these varied environmental factors are quantified by collocated measurements between sensors and reference monitors. Based on laboratory evaluation results, the sensor responses are adjusted to those of the reference monitors.

As shown in Figure 6, the major components of a laboratory calibration chamber include the chamber enclosure, a particle generator, a dry particle-free air generator system, and a temperature and RH monitor. The chamber enclosure is generally made of metal frame [67] with acrylic glasses on the sides that allows visualization of the physical processes in the chamber [42,68–70]. At the rear end of the chamber is an exhaust system to collect exiting dust particles and moisture to prevent contaminating the laboratory environment.

The particle generator generates particles into the calibration chamber which is uniformly mixed by a small mixing fan. There are two types of particle generators: particle dispensers [71] and atomizers [34]. Particle dispensers dispense dry aerosolized dust directly into the chamber. Particle dispensers have a dust reservoir with specified dry dust particles. In particle dispensers, dust is fed from a reservoir into the dispensing unit by an in-built conveyor belt, which uses high pressure compressed air to deagglomerate dust particles and aerosolize it directly into the chamber. Commercially available particle dispensers include Palas RGB 1000-C [68], TSI fluidized bed dust generator [6,18,46], and Topas model SAG 410/U [71].

The second type of particle generator is the atomizer. It produces PM from liquid suspensions, which are made by dissolving particles in a solvent. With pressure from

compressed air, the solution is nebulized through a nozzle to a diffusion drying system to remove the moisture content and produce completely dry aerosolized dust particles prior to entry into the chamber. The amount of aerosol generated is dependent on the pressure of compressed air applied to the nozzle, and the mass flow rate is adjusted by the volume flow through the nozzle. Commercially available atomizers include PALAS AGK 2000 [72], Collision atomizer TSI 3076 [33,41,73], and single jet atomizer TSI 9302 [68].

Ideally, PM used for this test should be of similar characteristics with the measured particles the sensors will be deployed for. Dust types that have been used in previous low-cost PM sensor laboratory calibration chamber studies include Arizona road dust (ARD) [40,43,46], cigarette smoke [42], coal dust [74], polystyrene latex (PSL) particles [40], welding fumes [40,61], salt [40–41,43], wood smoke [75], DPM [23,76], incense [41,56,77], and sugars [41].

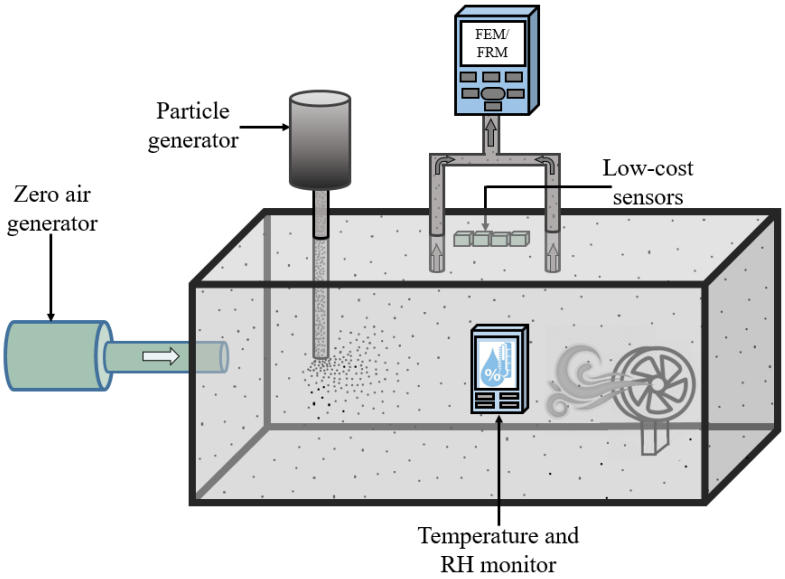

Figure 6. Laboratory calibration chamber.

Temperature and relative humidity can be controlled in the chamber. Temperature can be controlled by the laboratory's heating, ventilation, and air condition (HVAC) system [42,56] or by placing ice packs or heating tapes around the chamber. In the US EPA's laboratory calibration chamber, the temperature is regulated using the laboratory's HVAC system and supplemented with heating pads and dry ice [78]. This temperature regulation technique has been widely adapted in other studies [41,71]. Relative humidity is controlled through a water bubbler system which flows dry air through a deionized water to channel water vapor into the chamber to increase relative humidity [39,41,56,78]. Another method is by using a humidifier and pumps humid air into the chamber [71]. Dehumidification is achieved by eliminating excess water condensed on the cooling coils [71–72]. Commonly used temperature and relative humidity sensors include AOSONG AM2302 temperature-humidity sensor [13], AD22100 temperature sensor [56], platinum resistive temperature sensor for temperature measurement, and monolithic integrated circuit capacitance sensors for relative humidity measurement [78].

A diffusion dryer is connected to the atomizer to remove the moisture from the generated particles and ensure dry particles are dispensed into the chamber [68,73,79–80]. Diffusion dryers are composed of a cartridge containing silica gel, which absorbs moisture. As the wet aerosol goes through the cylindrical cartridge, water vapor diffuses into the silica gel and only dry dust aerosol is injected into the chamber. A microporous structure interlocking cavities gives silica gel a high surface area and makes it a high capacity desiccant. Water vapor is adsorbed to the silica gel due to the lower pressure in the silica gel caused by its large surface area. Examples of factory-made diffusion dryers are PALAS model TR2000 [71] and TSI model 3062 [68]. It can also be custom-built in

the laboratory using the major component of the silica gel desiccant cartridge [41,81]. As shown in Figure 7, it is built as a double layer cylindrical tube with granules of silica gel in-between the layers. The inner cylinder is made with fine stainless steel wire mesh to allow moisture to diffuse in the silica and avoid substantial particle loss. The initial red color of the silica gel in the cartridge turns green as it gets saturated, and the silica gel can be reused after drying.

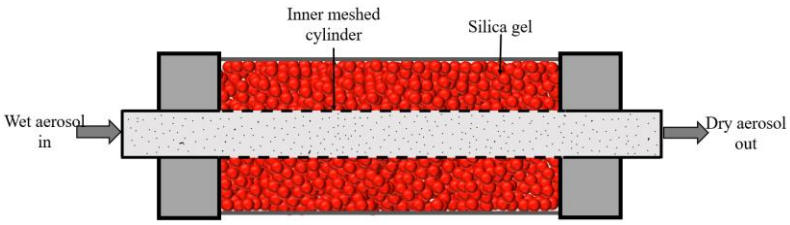

Figure 7. Diagram for a custom-built diffusion dryer.

When environmental conditions are controlled to the desirable conditions, and desired PM concentrations attained at a steady-state, evaluation and calibration can begin. Low-cost PM sensors and reference monitors are collocated in the chamber and challenged with a wide range of controlled PM concentrations and environmental conditions. Different sensors or sensors of the same type can be calibrated with this method. The basic principle employed is that low-cost PM sensors should have a perfect linear relationship with reference monitors used in the calibration. The difference between low-cost PM sensor readings and reference monitor readings are studied. The influence of relative humidity on low-cost PM sensor readings are then observed and quantified. Finally, the influence of temperature on low-cost sensor readings is studied and quantified based on the evaluation test with a variety of temperatures. A combination

of these factors can also be studied since they occur simultaneously in real life. At the end of the calibration process, various calibration models and algorithms will be used to adjust the sensor response to that of the reference monitors, thus improving the low-cost PM sensor's data quality.

4.2. CALIBRATION MODELS

Eliminating errors from low-cost PM sensors is a difficult and complex process. However, calibration models developed based on laboratory chamber tests allow for the best estimate of true concentration using low-cost PM sensors. Accurate and precise calibration models are important for successful and effective field deployment.

The most used calibration model is the linear calibration model [55,82]. It assumes that low-cost sensors respond linearly with the PM concentrations, which simplifies the calibration procedures. A single variable linear model that only includes the PM concentration as the only independent variable is called a univariate linear calibration model. The linearity of response is usually assessed using the least-square regression. The calibration function is in the form of (3) where a and b represent calibration variables, X represents reference monitor measurement, and R_s represents low-cost sensor response [83]. Subsequently, (3) is rearranged into (4) to determine the calibrated concentration.

$$R_s = a \cdot X + b \tag{3}$$

$$X = \frac{R_s - b}{a} \tag{4}$$

Low-cost PM sensors are susceptible to errors caused by change in ambient temperature and relative humidity in the deployment environment [84]. For this reason, temperature and humidity levels should be included in the algorithms that are used to calibrate the PM concentration output of sensors. Multivariate calibration models are mostly used to take the impact of temperature and humidity into considerations. A recent study [85] developed a RH correction factor as shown in (5):

$$F = \frac{R_s}{R_m} = \alpha + \beta \times \frac{\mathrm{RH}^2}{1 - \mathrm{RH}} \tag{5}$$

where F is the RH correction factor, Rs is the low-cost PM sensor readings, Rm is the reference instrument readings, α and β are empirical regression parameters, and RH is the relative humidity measured within the chamber environment. These empirical regression parameters are obtained by ordinary least-squares regression. The dependent variable is the RH correction factors calculated as the ratio of low-cost PM sensor readings averaged across all the sensor units to the corresponding reference instrument readings at a given RH, and the independent variable is the term RH2/(1 − RH). Based on this derived equation, the RH adjusted concentration is generated using the RH correction factor equation as shown in (6):

$$P = \frac{R_s}{F} \tag{6}$$

where *P* is the RH adjusted PM concentration. This method reduced the mean error of PMS3003 sensor from 27% to 10% [85].

Correction of low-cost sensor readings for RH alone was found to be insufficient to meet the measurements by reference monitors likely due to additional interference from temperature. To compensate for temperature in addition RH in a multivariate linear regression, temperature is used as an additional term in the linear calibration model to generate a generalized empirical correction equation, as shown in (7):

$$P = \beta_0 + (\beta_1 \cdot R_m) + (\beta_2 \cdot t) \tag{7}$$

where β_0, β_1, and β_2 are calibration coefficients and t is the temperature [38,82,85]. Standard linear regression is used to fit these parameters in the equation to generate these coefficients, and the temperature adjusted PM concentration is calculated using (8):

$$\rho = \frac{P - \beta_0 - \beta_2 \times t}{\beta_1} \tag{8}$$

where ρ is the temperature and RH corrected concentration. The application of this model further reduced the mean error from 10% (error after RH correction) to 6%. Even though this temperature may be seen as trivial, the combination of both RH and temperature adjustments succeeded in lowering the mean errors from 27% to 6%, which falls within US EPA's acceptable sensor requirements [85].

5. SENSOR EVALUATION PROTOCOLS

Low-cost PM sensors need to be calibrated and evaluated before deployment. This is because the manufacturer calibration and evaluation procedures are normally not sufficient covering the range of deployment conditions, and thus are often of limited use. To address this challenge, standard PM sensor evaluation protocols are developed to systematically assess the accuracy and reliability of the sensors. These protocols allow for cross comparison among different PM sensor studies and establish accuracy between low-cost PM sensors and highly accurate federal reference methods (FRM)/federal equivalent methods (FEM) monitors. With the recent interest in low-cost PM sensors by governmental and regulatory agencies globally, it is important to standardize evaluation procedures and indices to evaluate the performance of low-cost PM sensors.

Seven performance evaluation indices have been established by the US Environmental Protection Agency (EPA) [78,86], including (1) linearity of response, (2) precision of measurement, (3) limit of detection (LOD), (4) concentration resolution, (5) response time, (6) interference equivalence, and (7) temperature and relative humidity influence. The US Air quality Sensor Performance Evaluation Center (AQ-SPEC) [71–72] reiterated some of these indices and additionally proposed the inclusion of four more indices: (8) data recovery, (9) accuracy, (11) intra-model variability, and (12) baseline drift. The European Metrology Research Program (EURAMET) [87] employs similar protocols based on indices used by the US EPA and AQ-SPEC protocols. Additional important indices that have been used in the literature include: (13) root mean square error (RMSE), (14) measurement bias [88], (15) dependence on particle size, and (16)

dependence on particle composition [41]. The above 16 indices will be discussed sequentially in the following paragraphs.

The coefficient of determination (R^2) from linear regression is a primary parameter to evaluate correlation of low-cost PM sensor outputs with reference monitors. This indicates the level of agreement between measurements of low-cost PM sensors and reference monitors over a range of PM concentrations. To test the correlation of a sensor, the sensor and reference monitor are challenged with a wide range of PM concentrations in a laboratory calibration chamber. The output from low-cost PM sensors is plotted against the output from reference monitor to generate a best fitted regression curve. Based on this curve, the fitted linear equation is generated and used to optimize the accuracy of the low-cost PM sensor's outputs. The R^2 is reported for evaluating the strength of correlation on a scale of 0 to 1 (or 0 to 100%). An R^2 of 1 indicates a perfect correlation with the reference monitor, while an R^2 of 0 indicates a complete lack of correlation.

The coefficient of variation (CV) is another parameter that is used to evaluate the precision of measurement. The precision of low-cost PM sensor measurements is evaluated by conducting three replicate measurements. A stable concentration is generated within the controlled laboratory chamber. Once this is attained, three replicate measurements are taken with the sensor. Based on data from this experiment, the coefficient of variation calculates the dispersion of data points around the mean value expressed as a percentage, and it should be less than 10% for acceptable performance [17]. This parameter is defined by (9):

$$\mathrm{CV} = \frac{\sigma}{\mu} \tag{9}$$

where σ represents standard deviation, and μ is the mean value of measurements.

The limit of detection (LOD) describes the lowest detectable concentration that is detected from blank concentration by a low-cost PM sensor. A PM monitor's reading is only considered reliable and meaningful when the dust concentrations exceed the LOD [41]. LOD evaluation is performed by challenging low-cost PM sensors with several blank concentrations. The LOD is then calculated using (10).

$$\mathrm{LOD} = \frac{3\sigma_{\mathrm{blk}}}{k} \tag{10}$$

where k is the slope from the fitted linear regression model, and σ_{blk} is the standard deviation at blank PM conditions. The k value is obtained as the slope from the linear correlation curve generated over the range of concentration (as measured in R2). The σ_{blk} is calculated over the extended measurement time for the test with all sensor readings using (11):

$$\sigma_{\mathrm{blk}} = \sqrt{\frac{\sum_{i=1}^{N}\left(R_i - \overline{R}\right)^2}{N-1}} \tag{11}$$

where R_i is the individual measurements, $\overline{R}$ is the average concentration measured by sensor, and N is the number of measurements.

Concentration resolution is the smallest amount concentration that the sensor can detect. This term is defined by the noise of the sensor. A sensor's noise is the spontaneous short-term change in sensor response at a constant PM concentration. Concentration resolution is quantified by the standard deviation of a sensor's measurements about a steady concentration. To evaluate this parameter, low-cost PM sensor is exposed to a zero-concentration for 10 measurements ($r_i,\ldots,r_{10}$) with a 2-min time interval between successive measurements. The standard deviation is calculated using (12):

$$S = \sqrt{\frac{1}{n-1}\left[\sum_{i=1}^{n} r_i^2 - \frac{1}{n}\left(\sum_{i=1}^{n} r_i\right)^2\right]} \qquad (12)$$

where S is the concentration resolution, r_i is sensor reading for each measurement, and n is the number of measurements (10 in this case). This procedure is repeated for a concentration 80% of the sensor's upper detectable limit.

Response time generally measures the time taken for a low-cost PM sensor to respond to a change in input concentration. US EPA classifies response time into lag time and rise time. Lag time is the time interval between a step change in input concentration and the first observable corresponding change in measurement response by the sensor. Rise time, however, is the time interval between the first observable measurement response (the lag time) and the final response after a step increase in input concentration. Response time is a vital sensor evaluation index as it assesses if the sensor is suitable for mobile monitoring in conditions like an underground mine where PM concentrations

change rapidly. Low-cost PM sensors deployed for personal monitoring are preferred to have response time approaching 0.

Interference equivalence is the positive or negative measurement response caused by particles and substances other than the one being targeted to be measured. The test to evaluate this parameter involves exposing low-cost PM sensors to a zero-air test atmosphere and taking the sensor output. This is followed by challenging the sensors with potential interfering particle types at a known concentration which is substantially higher than that likely to be found in the ambient air where the sensor will be deployed. The interference equivalence (IE) is calculated using Eq. (13):

$$\mathrm{IE} = Z_i - Z \tag{13}$$

where Z_i is the sensor output at zero concentration and Z is the sensor output with the interferent.

RH and temperature influence on low-cost PM sensors are tested to know how real-life changes in temperature and relative humidity influence the sensor performance. Within a controlled laboratory chamber environment, temperature variations ranging from low temperatures (~0ºC) to high (>30ºC) and relative humidity from <25% to >85% are challenged with the low-cost PM sensors to measure their impact on low-cost sensors [78].

Data recovery measures the effectiveness of collecting valid data. It is calculated using a percentage ratio of valid sensor data points as a percentage of the total number of data points collected over a testing period.

Accuracy is the degree of closeness between sensors' measured values to the true concentration. The test for a sensor's accuracy (A) exposes low-cost PM sensors and reference monitors to the same steady-state conditions and calculated using Eq. (15):

$$A = 100\% - \left(\frac{|\bar{X} - \bar{C}|}{\bar{C}} \times 100\%\right) \quad (14)$$

where $\bar{X}$ is the average concentration measured by the sensor throughout the steady-state period and $\bar{C}$ is that measured by the reference monitor. The accuracy criterion used by MSHA and the EPA protocol requires that a sensor yields an accuracy within ±25% of the true concentration with a probability of 0.95.

Intra-model variability is the closeness of measurements from sensors of the same type under the same concentration. Test for this parameter involves sensors closely deployed in a laboratory chamber with a steady state PM concentration, as calculated by Eq. (15):

$$V = \frac{X_{\text{highest}} - X_{\text{lowest}}}{X_{\text{average}}} \times 100\% \quad (15)$$

where V is the intra-model variability, X_{highest} is the sensor reading with the highest concentration, X_{lowest} is the sensor reading for the lowest concentration, and X_{average} is the total average of all the three sensors.

Baseline drift is the gradual systematic change in sensor response to a fixed set of environmental conditions over a period of time without a change in input concentration.

Drifts are evaluated by exposing the sensor to a zero concentration. A sensor which is affected by baseline drift has its response gradually but systematically deviates from the true zero concentration. This test is repeated for 80% of the sensor's upper detectable limit.

The evaluation sensor bias is imperative to measure the error percentage of low-cost sensor output compared to reference monitors. This value needs to be less than ±10% to ensure measurement accuracy. It is calculated by using Eq. (16):

$$\text{Bias} = \frac{1}{n}\sum_{i=1}^{n}\frac{C_{\text{HD}} - C_{\text{rf}}}{C_{\text{rf}}} \times 100\% \tag{16}$$

where n is the total number of measurements, C_{HD} is the concentration measured by low-cost PM sensor, and C_{rf} is the concentration measured by reference monitor. A positive bias indicates an overestimation of actual PM concentration and a negative measurement indicates an underestimation.

RMSE measures how close the observed data points are to the calibration model's predicted value. To determine this index, low-cost PM sensors are exposed to a wide range of known PM concentrations (model concentrations,M_i). Based on measurement outputs (observed concentrations, O_i) by the sensors, residual values ($O_i - M_i$) are determined to calculate RMSE using Eq. (17), where n and i indicates the time step.

$$\text{RMSE} = \sqrt{\frac{1}{n}\sum_{i=1}^{n}(O_i - M_i)^2} \tag{17}$$

Dependence on particle size is imperative as light scattering principle is strongly dependent on particle size both in Rayleigh and Mie regimes. To evaluate the impact of size dependence, spherical particles such as water solutions of polystyrene latex [41] with uniform diameters are generated for three size categories. The same constant steady concentration is maintained for all three tests using the three different particle size distributions. Sensor performance is evaluated by comparing their outputs with actual mass concentrations measured by reference monitors.

Dependence on particle composition is likely to be a problem with low-cost PM sensors due to their light scattering working principles which depend on particle characteristics such as refractive index. This is tested by exposing low-cost PM sensors and reference monitors to the same concentration of particles known to have different refractive indices for three particle types. Particles used for this test should be of equal aerodynamic diameters to avoid the interference of particle size.

6. FRAMEWORK FOR UNDERGROUND MINE APPLICATION

The application of low-cost PM sensors in underground mines for real-time personal monitoring of coal dust and DPM concentration will be a powerful tool to protect miners from overexposure to these PM. The implementation of this technology will additionally yield several economic and operational benefits to mines, such as a reduction in productive work time due to problems with high PM concentration, a considerable reduction in cost incurred through hospital bills and compensation due to PM-related health conditions, and accident prevention caused by high PM levels. It is,

therefore, imperative to discuss the framework for the implementation of low-cost PM sensors in underground mines effectively to facilitate the control of PM exposure.

6.1. USABILITY

It is important to note that low-cost sensors, only refer to the PM measuring component described in Section 2.2 which is not entirely functional as a measuring system all by itself since it has no inbuilt digital converters and unable to display results. In order to operate as a complete monitor, low-cost sensors are converted into complete PM monitors together with other important components such as microprocessor which functions as an anolog to digital converter and a platform to program the sensor and the monitor as a whole, other sensors including temperature and RH sensors to provide supplementary environmental monitoring data and inclusion into the calibration algorithms, battery or another power source to provide power for the monitor, and a display screen to allow data to be viewed by miners. Therefore, for the purpose of application in underground mines, low-cost PM monitors are what will be deployed and not the sensor alone.

Low-cost PM monitors made from PM sensors may be worn on a miner's chest region or on the bill of a hard hat where it can monitor the PM within the miner's breathing zone—within 0.3 m (12 in.) radius of the miner's mouth or nose [89]. The lightweight and small size of these monitors present minimal ergonomic discomfort for miners. However, a comprehensive ergonomic study is required to point out an optimum body part to attach the sensor for maximum ergonomic functionality.

6.2. TESTS

With no known applications of low-cost PM sensors in underground mines, important studies must be done to substantiate their use prior to the commercialization of such sensors for underground mines. First, laboratory and in-mine performance evaluation of low-cost PM sensors should be performed to assess the performance of the sensors under controlled and onsite environments. Low-cost PM sensors will further need to be calibrated to the underground ambient conditions to optimize their efficiency under those conditions. Periodic post deployment calibration is equally important for a successful long-term usage. It is normal for monitors to encounter errors over an extended period of use and a recalibration is sufficient to correct low-cost PM monitor outputs in this event. Moreover, it will be critical to perform an in-mine pilot study to explore whether and how a network of low-cost PM monitors can effectively monitor and improve PM levels in underground mines. The worthiness and usability of the low-cost sensor, when worn by miners performing their normal duties, will be known from the perspective of miners through this pilot study. For the purpose of these studies, various mines should be sampled to represent various geographical areas with various types of mines, ventilation systems, types of equipment, and mining methods in order to make these studies comprehensive.

6.3. DEPLOYMENT AND DATA RETRIEVAL

Low-cost PM monitors will be deployed in underground mines in a wireless sensor network (WSN) where every monitor can function autonomously to offer high flexibility and easy troubleshooting. When sensors are activated, each sensor

continuously monitors and displays real-time PM concentrations that the miner is exposed to. Data recorded are displayed on a display screen for miners to view their current exposure levels. Additionally, these sensors can be programmed to display color codes for PM concentration levels from a scale of green to red (safe to hazardous) to facilitate interpretation and easily alert miners of a dangerous PM concentration level [90]. An exposure alarm can also be installed to trigger immediately when a set level of PM exposure has been reached.

Using a Wi-Fi enabled microprocessor such as NodeMCU ESP8266, sensors can concurrently store monitoring data to a receiver computer in real-time which can be accessed by the mine ventilation engineer for onward planning. This real-time and cumulative data enable management to correlate PM levels to initiate timely proactive controls and for mine ventilation planning purposes. Furthermore, the data provide a good estimate of the average workplace dust levels at various locations. This will help miners and management to identify PM levels higher than normal and take immediate actions. For example, a defective dust control system or an insufficient ventilation rate in the mine can be identified quickly when dust real-time PM levels at a particular location reach an unusual level.

6.4. SPECIAL SAFETY REQUIREMENT FOR UNDERGROUND MINE USAGE

For the safety of the mine, MSHA requires electronic devices used in underground coal and other gassy mines to be intrinsically safe. This is due to the high risk of explosion presented by the buildup of methane and coal dust in underground mines which can be ignited by waves of electromagnetic energy within the radio

frequency spectrum. For low-cost PM sensors to be approved for use in underground mines, they must be certified by MSHA as intrinsically safe for use in underground mines. Low-cost PM sensors should therefore be modelled to meet this requirement before it can be applied in underground mines. The intrinsic safety of low-cost PM monitors can be enhanced by limiting the electrical energy within their circuits so that ignition is not possible but able to provide sufficient power to the sensor.

6.5. FLEXIBILITY

This novel technology presents the challenge of disengaging occasionally to change or charge batteries during operational hours when batteries are exhausted. The power consumed by these sensors are in the range of 0.45 to 1 W, which are substantially low. Connecting these sensors to commonly used 4000 mAh batteries can last between 27 and 33 h for a monitor whose current demand is 150 mA, lasting more than twice as much as Airtec's 12 h run and thrice as much as the PDM3700' 8 h run. In order to avoid abrupt shutdowns during operational hours, changing and charging of batteries can be done at the end of the shift or during breaks ahead of their expected run-out times. For stationary monitoring, the sensor may be connected to an AC power for uninterrupted power supply.

7. CONCLUSIONS

Mining-induced PM such as coal dust and DPM causes many respiratory diseases such as CWP and lung cancer. Current available underground PM monitoring devices

have disadvantages which limit their measuring capacity for compliance monitoring only. As a result, exposure levels for most miners remain unknown, leading to many unrealized overexposures. Recent research has shown that low-cost light scattering PM sensors offer the potential solution to this problem. This paper, therefore, investigates the feasibility of the application of low-cost PM sensors to achieve real-time high spatio-temporal PM measurement in underground mines.

Operated on optical principles, low-cost sensors are able to characterize both mass and number concentrations in real-time, which is critical for personal monitoring to achieve high spatio-temporal resolution. In spite of these promising potentials of low-cost PM sensors, they are affected by significant error sources that make their results erroneous and unreliable. Based on errors pointed out in previous studies, we categorized error sources into two forms: internal and external error sources. As elaborated in Section 3, internal error sources are due to preexisting sensor conditions and manufacturer errors whereas external sources of errors are often caused by changes in environmental conditions.

Accurate calibration has proven to be an effective tool for improving the low-cost PM sensor's data quality. As describes in Section 4, laboratory calibration chambers enable researchers to calibrate sensors under a variety of controlled environmental conditions, mainly PM concentration, relative humidity, and temperature through the application of univariate and multivariate calibration models. Governmental agencies such as EPA, EURAMET, and AQ-SPEC have proposed standardized sensor evaluation protocols with indices based on which sensors should be evaluated. Due to the many uncertainties and variabilities in evaluations done by private individual researchers, we

only discussed indices proposed by these agencies. We further propose that future studies adapt protocols established by these government agencies for accurate and uniform evaluation procedures.

This review has revealed the feasibility of low-cost sensors to achieve highly dense spatial coverage PM monitoring in underground mines. The potential application of low-cost PM sensors in underground mines has been demonstrated in Section 6. However, with no known underground mine application and study available, we suggest field and laboratory studies to sanction the potential application of low-cost PM sensors in underground mines. This review paper extends existing literature on low-cost PM sensor studies, and provides a framework on the development and application of the sensor for coal dust and DPM monitoring in underground mines. The outcomes of such endeavors will help protect the health of miners, enhance the safety of mining-related jobs, and inform industry and government about better management options for the cost-effective operation of underground mines.

REFERENCES

[1] D.E. Pollock, J.D. Potts, and G.J. Joy, Investigation into dust exposures and mining practices in mines in the southern appalachian region, *Min. Eng.*, 62(2010), No. 2, p. 44.

[2] D.J. Blackley, J.B. Crum, C.N. Halldin, E. Storey, and A.S. Laney, Resurgence of progressive massive fibrosis in coal miners – Eastern Kentucky, 2016, *MMWR Morb. Mortal. Week. Rep.*, 65(2016), No. 49, p. 1385.

[3] T. Moreno, P. Trechera, X. Querol, R. Lah, D. Johnson, A. Wrana, and B. Williamson, Trace element fractionation between PM_{10} and $PM_{2.5}$ in coal mine dust: Implications for occupational respiratory health, *Int. J. Coal Geol.*, 203(2019), p. 52.

[4] P. Chang, G. Xu, and J.X. Huang, Numerical study on DPM dispersion and distribution in an underground development face based on dynamic mesh, *Int. J. Min. Sci. Technol*., 30(2020), No. 4, p. 471.

[5] M. Thiruvengadam, Y. Zheng, and J.C. Tien, DPM simulation in an underground entry: Comparison between particle and species models, *Int. J. Min. Sci. Technol*., 26(2016), No. 3, p. 487.

[6] M.E. Birch and J.D. Noll, Submicrometer elemental carbon as a selective measure of diesel particulate matter in coal mines, *J. Environ. Monit*., 6(2004), No. 10, p. 799.

[7] Thermo Fisher Scientific, *Personal Dust Monitor Model PDM3700: Instruction Manual*, Franklin, MA, 2014.

[8] Flir Systems Inc, *Flir Airtec™ Diesel Particulate Monitor: Operators Manual*, Nashua, NH, 2015

[9] M. Badura, P. Batog, A. Drzeniecka-Osiadacz, and P. Modzel, Evaluation of low-cost sensors for ambient $PM_{2.5}$ monitoring, *J.* Sens., 2018(2018), art. No. 5096540.

[10] S. Collingwood, J. Zmoos, L. Pahler, B. Wong, D. Sleeth, and R. Handy, Investigating measurement variation of modified low-cost particle sensors, *J. Aerosol Sci*., 135(2019), p. 21.

[11] B. Feenstra, V. Papapostolou, S. Hasheminassab, H. Zhang, B.D. Boghossian, D. Cocker, and A. Polidori, Performance evaluation of twelve low-cost $PM_{2.5}$ sensors at an ambient air monitoring site, *Atmos. Environ*., 216(2019), art. No. 116946.

[12] X. Qiao, Q. Zhang, D. Wang, J. Hao, and J. Jiang, A quality control practice for low-cost PM2.5 sensor network, *Science of the Total Environment*, 779(2021), p. 146381.

[13] K.E. Kelly, J. Whitaker, A. Petty, C. Widmer, A. Dybwad, D. Sleeth, R. Martin, and A. Butterfield, Ambient and laboratory evaluation of a low-cost particulate matter sensor, *Environ. Pollut*., 221(2017), p. 491.

[14] D. Back, D. Theisen, W. Seo, C.S.J. Tsai, and D.B. Janes, Development of interdigitated capacitive sensor for real-time monitoring of sub-micron and nanoscale particulate matters in personal sampling device for mining environment, *IEEE Sens. J.*, 20(2020), No. 19, p. 11588.

[15] M. Alvarado, F. Gonzalez, A. Fletcher, and A. Doshi, Towards the development of a low cost airborne sensing system to monitor dust particles after blasting at open-pit mine sites, *Sensors*, 15(2015), No. 8, p. 19667.

[16] A. Leavey, Y. Fu, M. Sha, A. Kutta, C.Y. Lu, W.N. Wang, B. Drake, Y.X. Chen, and P. Biswas, Air quality metrics and wireless technology to maximize the energy efficiency of HVAC in a working auditorium, *Build. Environ*., 85(2015), p. 287.

[17] US-EPA, List of designated reference and equivalent methods, [in] *Water Environ. Federation Procedings*, North Carolina, 2005, p. 726.

[18] J.C. Volkwein, R.P. Vinson, S.J. Page, L.J. McWilliams, G.J. Joy, S.E. Mischler, and D.P. Tuchman, *Laboratory and Field Performance of A Continuously Measuring Personal Respirable Dust Monitor*, US Department of Health and Human Services, Public Health Service, Centers for Disease Control and Prevention, National Institute for Occupational Safety and Health, Cincinnati, OH, 2006.

[19] S.J. Page, J.C. Volkwein, R.P. Vinson, G.J. Joy, S.E. Mischler, D.P. Tuchman, and L.J. McWilliams, Equivalency of a personal dust monitor to the current United States coal mine respirable dust sampler, *J. Environ. Monit.*, 10(2008), No. 1, p. 96.

[20] J.C. Volkwein, E.D. Thimons, C. Yanak, D. Dunham, H. Patashnick, E. Rupprecht, Implementing a new coal dust monitor as an engineering tool, [in] *6th International Scientific Conference of the International Occupational Hygiene Association Procedings*, Pilanesberg, South Africa, 2005, p. 201

[21] J.C. Volkwein, R.P. Vinson, L.J. McWilliams, D.P. Tuchman, and S.E. Mischler, Performance of a new personal respirable dust monitor for mine use, *Report of Investigations*, 9663(2004), p. 25.

[22] National Institute of Occupational Safety and Health, *Diesel Particulate Matter* (*as Elemental Carbon*), 3rd ed., DHHS (NIOSH) Publication, Cincinnati, OH, 2003 [2020-06-10]. https://www.cdc.gov/niosh/docs/2003-154/pdfs/5040.pdf

[23] C. Barrett, E. Sarver, E. Cauda, J. Noll, S. Vanderslice, and J. Volkwein, Comparison of several DPM field monitors for use in underground mining applications, *Aerosol Air Qual. Res.*, 19(2019), No. 11, p. 2367.

[24] M.K. Mensah, K. Mensah-Darkwa, C. Drebenstedt, B.V. Annam, and E.K. Armah, Occupational respirable mine dust and diesel particulate matter hazard assessment in an underground gold mine in Ghana, *J. Heal. Pollut.*, 10(2020), No. 25,No. 200305.

[25] J.D. Noll and S. Janisko, Evaluation of a wearable monitor for measuring real-time diesel particulate matter concentrations in several underground mines, *J. Occup. Environ. Hyg*., 10(2013), No. 12, p. 716.

[26] Thermo Scientific, *Personal DATARAM Model pDR-1000AN/1200 Instruction Manual*, Thermo Fisher Scientific, Franklin, MA, 2013 [2020-08-20]. https://assets.thermofisher.com/TFS-Assets/LSG/manuals/EPM-manual-PDR1000an.pdf

[27] Thermo Scientific, *MIE pDR-1500 Instruction Manual*, Thermo Fisher Scientific, Franklin, MA, 2017 [2020-08-20]. https://assets.thermofisher.com/TFS-Assets/CAD/manuals/manual-pDR-1500.pdf

[28] G.J. Chekan, J.F. Colinet, F.N. Kissell, J.P. Rider, R.P. Vinson, and J.C. Volkwein, *Performance of a light-scattering dust monitor in underground mines*, US Department of Health and Human Services, Public Health Service, Centers for Disease Control and Prevention, National Institute for Occupational Safety and Health, Pittsburgh, PA 2005.

[29] H. Grimm and D.J. Eatough, Aerosol measurement: The use of optical light scattering for the determination of particulate size distribution, and particulate mass, including the semi-volatile fraction, *J. Air Waste Manag. Assoc.*, 59(2009), No. 1, p. 101.

[30] M. Kowalska, A. Mainka, and W. Mucha, The usefulness of an optical monitor for the assessment of human exposure to fine dust in indoor air, *Medycyna Pracy*, 70(2019), No. 2, p. 213.

[31] N. Masson, R. Piedrahita, and M. Hannigan, Approach for quantification of metal oxide type semiconductor gas sensors used for ambient air quality monitoring, *Sens. Actuators, B*, 208(2015), p. 339.

[32] M. Van Den Bossche, N.T. Rose, and S.F.J. De Wekker, Potential of a low-cost gas sensor for atmospheric methane monitoring, *Sens. Actuators, B*, 238(2017), p. 501.

[33] J.Y. Li, *Recent Advances in Low-cost Particulate Matter Sensor: Calibration and Application* [Dissertation], Washington University in St. Louis, St. Louis, 2019.

[34] J.Y. Li and P. Biswas, Optical characterization studies of a low-cost particle sensor, *Aerosol Air Qual. Res.*, 17(2017), No. 7, p. 1691.

[35] M. Budde, R. El Masri, T. Riedel, and M. Beigl, Enabling low-cost particulate matter measurement for participatory sensing scenarios, [in] *Proceedings of the 12th International Conference on Mobile and Ubiquitous Multimedia*, Karlsruhe, 2013, art. No. 19.

[36] S. Kelleher, C. Quinn, D. Miller-Lionberg, and J. Volckens, A low-cost particulate matter ($PM_{2.5}$) monitor for wildland fire smoke, *Atmos. Meas. Tech.*, 11(2018), No. 2, p. 1087.

[37] L.F. Weissert, K. Alberti, G. Miskell, W. Pattinson, J.A. Salmond, G. Henshaw, and D.E. Williams, Low-cost sensors and microscale land use regression: Data fusion to resolve air quality variations with high spatial and temporal resolution, *Atmos. Environ.*, 213(2019), p. 285.

[38] N. Zimmerman, A.A. Presto, S.P.N. Kumar, J. Gu, A. Hauryliuk, E.S. Robinson, A.L. Robinson, and R. Subramanian, A machine learning calibration model using random forests to improve sensor performance for lower-cost air quality monitoring, *Atmos. Meas. Tech.*, 11(2018), No. 1, p. 291.

[39] R. Piedrahita, Y. Xiang, N. Masson, J. Ortega, A. Collier, Y. Jiang, K. Li, R.P. Dick, Q. Lv, M. Hannigan, and L. Shang, The next generation of low-cost personal air quality sensors for quantitative exposure monitoring, *Atmos. Meas. Tech.,* 7(2014), No. 10, p. 3325.

[40] S.N. Sousan, K. Koehler, L. Hallett, and T.M. Peters, Evaluation of the Alphasense optical particle counter (OPC-N_2) and the Grimm portable aerosol spectrometer (PAS-1.108), *Aerosol Sci. Technol.,* 50(2016), No. 12, p. 1352.

[41] Y. Wang, J.Y. Li, H. Jing, Q. Zhang, J.K. Jiang, and P. Biswas, Laboratory evaluation and calibration of three low-cost particle sensors for particulate matter measurement, *Aerosol Sci. Technol.,* 49(2015), No. 11, p. 1063.

[42] A. Manikonda, N. Zíková, P.K. Hopke, and A.R. Ferro, Laboratory assessment of low-cost PM monitors, *J. Aerosol Sci.,* 102(2016), p. 29.

[43] S.N. Sousan, K. Koehler, G. Thomas, J.H. Park, M. Hillman, A. Halterman, and T.M. Peters, Inter-comparison of low-cost sensors for measuring the mass concentration of occupational aerosols, *Aerosol Sci. Technol.,* 50(2016), No. 5, p. 462.

[44] M. Budde, M. Busse, and M. Beigl, Investigating the use of commodity dust sensors for the embedded measurement of particulate matter, [in] *2012 Ninth International Conference Networked Sensng Systems*, Antwerp, 2012, p. 1.

[45] E. Austin, I. Novosselov, E. Seto, and M.G. Yost, Laboratory evaluation of the shinyei PPD42NS low-cost particulate matter sensor, *PLoS One,* 10(2015), No. 9, art. No. e0137789.

[46] S.N. Sousan, K. Koehler, L. Hallett, and T.M. Peters, Evaluation of consumer monitors to measure particulate matter, *J. Aerosol Sci.,* 107(2017), p. 123.

[47] C. Lin, J. Gillespie, M.D. Schuder, W. Duberstein, I.J. Beverland, and M.R. Heal, Evaluation and calibration of Aeroqual series 500 portable gas sensors for accurate measurement of ambient ozone and nitrogen dioxide, *Atmos. Environ.,* 100(2015), p. 111.

[48] M. Budde, M. Köpke, and M. Beigl, Robust in situ data reconstruction from poisson noise for low-cost, mobile, non-expert environmental sensing, [in] *Proceedings of the 2015 ACM International Symposium on Wearable Computers*, Osaka Japan, 2015, p. 179.

[49] A. Shrivastava and V.B. Gupta, Methods for the determination of limit of detection and limit of quantitation of the analytical methods, *Chron. Young Sci.,* 2(2011), No. 1, p. 21.

[50] A.C. Lewis, J.D. Lee, P.M. Edwards, M.D. Shaw, M.J. Evans, S.J. Moller, K.R. Smith, J.W. Buckley, M. Ellis, S.R. Gillot, and A. White, Evaluating the performance of low cost chemical sensors for air pollution research, *Faraday Discuss.*, 189(2016), p. 85.

[51] A.C. Rai, P. Kumar, F. Pilla, A.N. Skouloudis, S. Di Sabatino, C. Ratti, A. Yasar, and D. Rickerby, End-user perspective of low-cost sensors for outdoor air pollution monitoring, *Sci. Total. Environ.*, 607-608(2017), p. 691.

[52] H. Kaiser and H. Specker, Evaluation and comparison of analytical methods, *Fresenius' Z. Anal. Chem.*, 149(1956), p. 46.

[53] P. Schneider, N. Castell, M. Vogt, F.R. Dauge, W.A. Lahoz, and A. Bartonova, Mapping urban air quality in near real-time using observations from low-cost sensors and model information, *Environ. Int.*, 106(2017), p. 234.

[54] N. Castell, F.R. Dauge, P. Schneider, M. Vogt, U. Lerner, B. Fishbain, D. Broday, and A. Bartonova, Can commercial low-cost sensor platforms contribute to air quality monitoring and exposure estimates?, *Environ*. *Int.*, 99(2017), p. 293.

[55] B. Maag, Z.M. Zhou, and L. Thiele, A survey on sensor calibration in air pollution monitoring deployments, *IEEE Internet Things J.*, 5(2018), No. 6, p. 4857.

[56] M.B. Marinov, S. Hensel, B. Ganev, and G. Nikolov, Performance evaluation of low-cost particulate matter sensors, [in] *2017 XXVI International Scientific Conference Electronics (ET),* Sozopol, 2017, p. 1.

[57] R. Jayaratne, X.T. Liu, P. Thai, M. Dunbabin, and L. Morawska, The influence of humidity on the performance of a low-cost air particle mass sensor and the effect of atmospheric fog, *Atmos. Meas. Tech.*, 11(2018), No. 8, p. 4883.

[58] M.L. Gao, J.J. Cao, and E. Seto, A distributed network of low-cost continuous reading sensors to measure spatiotemporal variations of $PM_{2.5}$ in Xi'an, China, *Environ*. *Pollut.*, 199(2015), p. 56.

[59] M. Canu, B. Galvis, R. Morales, O. Ramírez, and M. Madelin, Understanding the Shinyei PPD24NS low-cost dust sensor, [in] *2018 IEEE International Conference on Environmental Engineering*, Milan, 2018, p. 1.

[60] M. Quinten, R. Friehmelt, and K.F. Ebert, Sizing of aggregates of spheres by a white-light optical particle counter with 90° scattering angle, *J. Aerosol Sci.*, 32(2001), No. 1, p. 63.

[61] J.Y. Kim, S.R. Magari, R.F. Herrick, T.J. Smith, D.C. Christiani, and D.C. Christiani, Comparison of fine particle measurements from a direct-reading instrument and a gravimetric sampling method, *J. Occup. Environ. Hyg.*, 1(2004), No. 11, p. 707.

[62] J.G. Liu, L.Z. Jin, J.Y. Wang, S.N. Ou, J.Z. Ghio, and T.Y. Wang, Micromorphology and physicochemical properties of hydrophobic blasting dust in iron mines, *Int. J. Miner. Metall. Mater.*, 26(2019), No. 6, p. 665.

[63] J.G. Liu, L.Z. Jin, J.Y. Wang, S.N. Ou, and T.Y. Wang, Co-influencing mechanisms of physicochemical properties of blasting dust in iron mines on its wettability, *Int. J. Miner. Metall. Mater.*, 26(2019), No. 9, p. 1080.

[64] O.A.M. Popoola, G.B. Stewart, M.I. Mead, and R.L. Jones, Development of a baseline-temperature correction methodology for electrochemical sensors and its implications for long-term stability, *Atmos. Environ.*, 147(2016), p. 330.

[65] D. Liu, Q. Zhang, J.K. Jiang, and D.R. Chen, Performance calibration of low-cost and portable particular matter (PM) sensors, *J. Aerosol Sci.*, 112(2017), p. 1.

[66] K.K. Johnson, M.H. Bergin, A.G. Russell, and G.S.W. Hagler, Field test of several low-cost particulate matter sensors in high and low concentration urban environments, *Aerosol Air Qual. Res.*, 18(2018), No. 3, p. 565.

[67] W.J. Chou, G.P. Yu, and J.H. Huang, Corrosion resistance of ZrN films on AISI 304 stainless steel substrate, *Surf. Coat. Technol.*, 167(2003), No. 1, p. 59.

[68] T. Sayahi, D. Kaufman, T. Becnel, K. Kaur, A.E. Butterfield, S. Collingwood, Y. Zhang, P.E. Gaillardon, and K.E. Kelly, Development of a calibration chamber to evaluate the performance of low-cost particulate matter sensors, *Environ. Pollut.*, 255(2019), art. No. 113131.

[69] L. Spinelle, M. Gerboles, M. Aleixandre, and F. Bonavitacola, Evaluation of metal oxides sensors for the monitoring of O_3 in ambient air at ppb level, *Chem. Eng. Trans.*, 54(2016), p. 319.

[70] L. Spinelle, M. Gerboles, and M. Aleixandre, Performance evaluation of amperometric sensors for the monitoring of O_3 and NO_2 in ambient air at ppb level, *Procedia Eng.*, 120(2015), p. 480.

[71] V. Papapostolou, H. Zhang, B.J. Feenstra, and A. Polidori, Development of an environmental chamber for evaluating the performance of low-cost air quality sensors under controlled conditions, *Atmos. Environ.*, 171(2017), p. 82.

[72] A. Polidori, V. Papapostolou, H. Zhang, *Laboratory Evaluation of Low-Cost Air Quality Sensors*, South Coast Air quality Management District, Diamondbar, CA, 2016, p. 1.

[73] A. Ankilov, A. Baklanov, M. Colhoun, K.H. Enderle, J. Gras, Y. Julanov, D. Kaller, A. Lindner, A.A. Lushnikov, R. Mavliev, F. McGovern, A. Mirme, T.C. O'Connor, J. Podzimek, O. Preining, G.P. Reischl, R. Rudolf, G.J. Sem, and V. Zagaynov, Intercomparison of number concentration measurements by various aerosol particle counters, *Atmos. Res*., 62(2002), No. 3-4, p. 177.

[74] A.D. Gillies and H.W. Wu, A new real time personal respirable dust monitor, [in] *Coal Operators' Conference Procedings*, Wollongong, 2006, p. 77.

[75] A.L. Northcross, R.J. Edwards, M.A. Johnson, Z.M. Wang, K. Zhu, T. Allen, and K.R. Smith, A low-cost particle counter as a realtime fine-particle mass monitor, *Environ. Sci. Process. Impacts*, 15(2013), No. 2, p. 433.

[76] J. Noll and S. Janisko, Using laser absorption techniques to monitor diesel particulate matter exposure in underground stone mines, *Int. Soc. Opt. Photonics*, 6759(2007), No. 47, art. No. 67590P.

[77] G. Olivares, I. Longley, and G. Coulson, Development of a low-cost device for observing indoor particle levels associated with source activities in the home, [in] *International Society of Eposure Science (ISES*), Seattle, WA, 2012, p. 2456.

[78] R. Williams, R. Long, M. Beaver, A. Kaufman, F. Zeiger, and M. Heimbinder, *EPA Sensor Evaluation Report*, U.S. Environmental Protection Agency, Washington, DC, 2014, p. 1.

[79] B.D. Grover, M.T. Kleinman, N.L. Eatough, D.J. Eataugh, and W.E. Qilson, Measurement of total $PM_{2.5}$mass (nonvolatile plus semivolatile) with the filter dynamic measurement system tapered element oscillating microbalance monitor, *J. Geophys. Res*., 110(2005), No. D7, art. No. D07S03.

[80] W. Zhu, F. Kapteijn, and J.A. Moulijn, Diffusion of linear and branched C6 alkanes in silicalite-1 studied by the tapered element oscillating microbalance, *Microporous Mesoporous Mater*., 47(2001), No. 2-3, p. 157.

[81] S.N. Sousan, A. Gray, C. Zuidema, L. Stebounova, G. Thomas, K. Koehler, and T. Peters, Sensor selection to improve estimates of particulate matter concentration from a low-cost network, *Sensors*, 18(2018), No. 9, art. No. 3008.

[82] Y. Jiang, X. Zhu, C. Chen, Y. Ge, W. Wang, Z. Zhao, J. Cai, and H. Kan, On-field and data calibration of low-cost sensor for fine partices exposure assessment, *Ecotoxicology and environmental safety*, 211(2021), p. 111958

[83] L. Spinelle, M. Gerboles, M.G. Villani, M. Aleixandre, and F. Bonavitacola, Field calibration of a cluster of low-cost available sensors for air quality monitoring. Part A: Ozone and nitrogen dioxide, *Sens. Actuators, B*, 215(2015), p. 249.

[84] X.L. Qin, L.J. Hou, J. Gao, and S.C. Si, The evaluation and optimization of calibration methods for low-cost particulate matter sensors: Inter-comparison between fixed and mobile methods, *Sci*. *Total*. *Environ*., 715(2020), art. No. 136791.

[85] T.S. Zheng, M.H. Bergin, K.K. Johnson, S.N. Tripathi, S. Shirodkar, M.S. Landis, R. Sutaria, and D.E. Carlson, Field evaluation of low-cost particulate matter sensors in high- and low-concentration environments, *Atmos. Meas. Tech*., 11(2018), No. 8, p. 4823.

[86] T. Watkins, *DRAFT Roadmap for Next Generation Air Monitoring*, United States Environmental Protection Agency, 2013 [2020]. https://www.epa.gov/sites/default/files/2014-09/documents/roadmap-20130308.pdf

[87] L. Spinelle, M. Aleixandre, and M. Gerboles, *Protocol of Evaluation and Calibration of Low-Cost Gas Sensors for the Monitoring of Air Pollution*, Publication of the European Union, Luxemburg, 2013.

[88] P. Thunis, A. Pederzoli, and D. Pernigotti, Performance criteria to evaluate air quality modeling applications, *Atmos*. *Environ*., 59(2012), p. 476.

[89] I.M. Spitzer, D.R. Marr, and M.N. Glauser, Impact of manikin motion on particle transport in the breathing zone, *J*. *Aerosol Sci*., 41(2010), No. 4, p. 373.

[90] M.D. Taylor, *Calibration and Characterization of Low-Cost Fine Particulate Monitors and their Effect on Individual Empowerment* [Dissertation], Carnegie Mellon University, Pittsburgh, PA, 2016.

II. CALIBRATION OF LOW-COST PARTICULATE MATTER SENSORS FOR COAL DUST MONITORING

ABSTRACT

Mining-induced coal dust causes various respiratory diseases to mine workers mainly coal workers' pneumoconiosis (CWP). Currently available underground monitors are expensive and bulky. These disadvantages limit them for regulatory sample monitoring purposes. Moreover, personal exposure levels for most miners remain unknown, risking them to potential overexposures. Low-cost light scattering particulate matter (PM) sensors offer a potential solution to this problem with the capability to characterize PM concentration with high spatio-temporal resolution. However, these sensors require precise calibration before they can be deployed in mining environments. No previous study has promulgated a standard protocol to assess these sensors for coal dust monitoring. The goal of this study was to calibrate Plantower PMS5003 sensors for coal dust monitoring using linear regression models. Two other commercially available PM sensors, the Airtrek and Gaslab CM-505 multi-gas sensors, were also evaluated and calibrated. They were evaluated for factors including linearity, precision, limit of detection, upper concentration limits, and the influence of temperature and relative humidity in a laboratory wind tunnel. The PMS5003 sensors were observed to be accurate below 3.0 mg/m^3 concentration levels with R-squared values of 0.70 to 0.90 which was the best among the sensors under with an acceptable precision below 1.5 mg/m^3. Moreover, this study shows that temperature and relative humidity have minimal influence on the efficacy of low-cost PM sensors' ability to monitor coal dust. This

investigation reveals the feasibility of low-cost sensors for real-time personal coal dust monitoring in underground coal mines if a robust calibration model is applied.

1. INTRODUCTION

Coal dust concentrations in underground mines can be considerably higher than surface mines due to limited ventilation to dilute the coal dust. This puts underground mine workers at a greater risk of coal dust overexposure. Overexposure to respirable coal mine dust (RCMD) has resulted in the onset of irreversible diseases, such as coal workers' pneumoconiosis (CWP), emphysema and chronic bronchitis collectively known as 'black lung" which can cause permanent disability and premature death [1]. Miners have also been diagnosed with silicosis due to exposure to coal dust with high silica contents [2], [3]. In recent times, there has been a resurgence of CWP among US coal miners [4] which is of great conern to the mining industry. Contrary to common understanding that CWP is only associated with long-term coal dust exposure, recent data indicates that advanced CWP has been found in younger coal miners [1].

Accurate real-time personal dust exposure monitoring is essential to alert mine workers to change behavior and apply mitigation methods to reduce their exposure when working. The Mine Safety and Health Administration (MSHA) requires the use of continuous personal dust monitors (CPDM) for measuring RCMD mass concentrations and determining compliance with the regulatory exposure limits. However, current CPDM devices are expensive and bulky [5]–[8]. For example, PDM3700 is the MSHA certified CPDM to be used in coal mines, but it costs ~$17,000 and weighs 2.0 kg [9].

These expensive PDMs are worn only by a few miners for regulatory compliance monitoring. These are mainly miners who are exposed to the highest coal dust concentrations at their work locations and those who have already been diagnosed with pneumoconiosis [1]. This practice has serious drawbacks, most notably is that the exposure levels for most miners are unknown. Besides, dust control effectiveness of modified engineering control strategies is not well understood by mining engineers due to lack of sufficient monitoring data. Finally, there is a lack of sufficient exposure information to accurately correlate coal dust exposure to its related-health data in epidemiology studies.

Light scattering low-cost particulate matter (PM) sensors have the potential to accurately monitor coal dust concentration in real time. The low cost, small size, and low power requirements of these sensors offer the promise of being widely worn by all coal mine workers. These could yield accurate concentration information if properly calibrated. Even though this technology has been significantly explored by researchers for other environmental applications [10]–[13], it remains a new technology for monitoring coal dust [14]. Because of questionable accuracy and long-term reliability of these sensors, it is critical to adopt a systematic approach to evaluate and effectively calibrate these sensors before they can be applied for coal dust monitoring. Many low-cost PM sensor calibration studies have demonstrated promising results in comparison with Federal Equivalent Methods (FEMs) or research-grade instruments for air quality PM monitoring [13], [15]–[18]. However, there are very few studies that investigate the performance and application of low-cost sensors for monitoring coal dust. Existing research by governmental agencies such as US Environmental Protection Agency (EPA)

[19] and European Metrology Research Program (EURAMET) [18], as well as research in the literature [13] have established standard protocols for calibrating low-cost PM sensors for environmental PM monitoring. However, there is still limited understanding of how these calibration models will perform with mining-induced coal dust.

The objective of this study was to evaluate and calibrate three types of lower cost PM sensors against a FEM reference monitor, Personal Dust Monitor (PDM) model 3700 and a research grade Aerodynamic Particle Sizer (APS) model 3321. A custom-built wind tunnel in the laboratory was used for the calibration experiments. Sensors and monitors were exposed to various levels of concentration within the tunnel to generate the linearity plots between the sensors and the reference monitors. Since several studies have established the linear relationship between light scattering low-cost PM sensors and reference monitors, univariate calibration models using linear regression were developed based on the linearity analysis to calibrate the sensors [17], [20]–[23]. The precision, limit of detection and upper concentration limits were evaluated to provide further understanding of the sensors' performance with coal dust. A 2^2 factorial design was used to determine the influence of temperature and relative humidity (RH) on the sensors' performance at low (~0.5 mg/m^3) and high (~1.5 mg/m^3) coal dust concentration levels. This method provides an understanding of the influence of each of the two levels of both temperature and RH on sensor outputs as well as the interaction of both conditions. The implementation of these sensors for coal dust monitoring will expand personal exposure monitoring in mines as every miner can wear one to detect timely overexposures to ensure timely controls are engineered to protect miners' health. On a broader scope, low-

cost PM sensors can greatly supplement more expensive research grade monitors used in other occupational environments.

2. EXPERIMENTAL METHODS

2.1. LOW-COST PM SENSORS AND REFERENCE MONITORS

Three low-cost PM sensors were evaluated in this study – the Plantower PMS50003 (PMS) low-cost PM sensor, the Airtrek PM sensor, and the Gaslab CM-505 multi-gas sensor. Two units of each sensor were evaluated. The Gaslab sensor, shown in Figure (a) measures PM 2.5 and PM 10 particle concentration together with oxygen, carbon dioxide and carbon monoxide concentrations. The Gaslab uses a combination of NDIR sensors, electrochemical sensors, and fluorescent sensors to measure gases and uses laser scattering technology to measure PM 2.5 and PM 10. The Airtrek sensors on the other hand, shown in Figure (b) use light scattering principles like that of the Plantower PMS5003 sensor to measure PM concentrations. The Airtrek sensors measure PM in four size bins of 1.0 µm, 2.5 µm, 4.0 µm, and 10.0 µm.

The Plantower PMS5003 (shown in Figure (d)) was used to assemble in-house made dust monitors. They are inexpensive light scattering PM sensors that are commercially available for about $ 30. This sensor employs a fan to draw ambient air into the light scattering measuring cavity through its inlet. As illustrated in Figure (c), the LED radiates laser-induced light into the sensing area to target particles within the measuring cavity. Light is scattered as it hits the particles. It is detected by the photo-diode detector, which is positioned at 180° with the LED light. The scattered light

received by the photo-diode detector sends pulses of electric signal to the in-built microprocessor. The number and intensity of electrical signals detected by the microprocessor are then converted to number and mass of particles respectively based on MIE theory [24].

These PMS sensors characterize PM by size into PM1, PM2.5, and PM10. The manufacturers of the PMS sensors state that PM1 is measured for particles in the size range of 0.3 µm to 1.0 µm, PM2.5 for particles in the size range of 1.0 µm to 2.5 µm and PM10 for particles in the size range of 2.5 µm to 10.0 µm. For each size category, the PMS reports two PM outputs, one without any form of correction factor, called standard PM concentration (or CF = 1) and the other with an atmospheric calibration factor, called environmental PM concentration. The manufacturers have not published any details about the calibration factor and how it was developed. Therefore, due to considerable uncertainties about manufacturer calibration, the standard PM concentrations were used for this study. Manufacturer specifications indicated high anti-interference performance using non-PM shielding technology. Previous studies have also shown that the Plantower sensors have superior performance as they have been integrated into PurpleAir air quality monitors [25]. These characteristics justify the reason the PMS sensors were used for this study.

Together with a DHT-22 temperature and relative humidity sensor, NodeMCU ESP8266 microcontroller and a 4 line by 20-character LCD screen, the PMS5003 was integrated into a prototype monitor (low-cost PM monitor) as displayed in Figure (e). This monitor was programmed with Arduino IDE to display real time concentrations of PM2.5 and PM10, temperature and relative humidity readings every 1.0 s onto the LCD

screen. To protect the low-cost PM sensor and its critical components from rainfall, sunlight, and physical damage, the sensor, and its components are housed in a 10.0 cm x 4.0 cm x 1.5 cm acrylic plastic box. This also allowed the team to see the screen readings in real time through the transparent acrylic case. The side of the acrylic case is strongly fastened but left uncovered to allow for normal operation of the PMS sensor without interference to the sensors' exposure. The low-cost PM monitor is continuously powered using a 5.0 V USB cable. For data analysis, the PM monitor is interfaced with a ThingSpeak Matlab based online IOT platform which serves as a cloud where all data is transmitted through Wi-Fi.

(a) Gaslab CM-505 multi-gas sensor

(b) Airtrek PM sensor

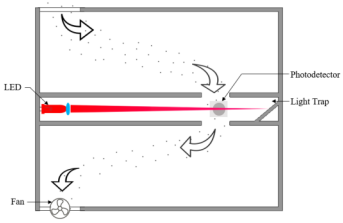

(c) Schematic PMS5003 sensor

(d) Plantower PMS5003 sensor

(e) PM monitor

Figure 1. Low-cost PM monitor: (a) schematic diagram of the plantower PMS5003, (b) a picture of the Plantower PMS5003 sensor, (c) the in house fabricated low-cost PM monitor

The primary reference monitor used in this study is the personal dust monitor model 3700 (PDM3700). This is a real time personal coal dust monitor which operates on the principle of tapered element oscillation microbalance (TEOM). It is capable of reporting concentrations at 1-minute intervals. The PDM3700 is equipped with a respirable size inlet installed near the inlet which ensures that the cut-off diameter for coal dust going through the mass sensor is 5.0 µm. This makes it capable of monitoring respirable size coal particles. It is used by miners by mounting the sample inlet, incorporated in the universal cap lamp, on the bill of a miner's hard hat to monitor dust within the miner's breathing zone [26]. The National Institute for Occupational Safety and Health (NIOSH) has validated PDM3700's accuracy, precision, and comfortability, and Mine Safety and Health Administration (MSHA) has approved this equipment as the regulatory compliance monitoring device [26]. This has also been designated as Federal Equivalent Method by the U.S. Environmental Protection Agency (EPA) for environmental air quality PM monitoring [27].

The APS measures PM mass and number concentration by particle aerodynamic sizes from 0.5 µm to 20.0 µm using the time-of-flight principles. To make it comparable with the PDM, PM concentration of particle size ranging from 0.00 to 4.37 µm from the APS was used for this study since it compares with the 4.37 µm D50 of the PDM cyclone. The APS draws ambient PM-laden air into the monitor through a nozzle at an accelerated flowrate of 5.0 liters per minute. Ideally, the APS needs to sample airflow at the same velocity as the air velocity at the sampling location. In this case, a 0.8 cm diameter nozzle was used to achieve a sampling velocity of 1.5 m/s to get as close as possible to airflow velocity in the wind tunnel. The accelerated airflow goes through the

sensing zone where the PM concentrations are measured using the time-of-flight principles. Particle size distribution is then reported every 15 seconds based on the settings used for this study [28].

2.2. WIND TUNNEL

The calibration chamber used in this study is a custom-built wind tunnel made with metal frames and acrylic glass panels (Figure 2). The wind tunnel has a U shape with cross-sectional dimension of the tunnel being 0.5 m x 0.5 m to simulate the airway bends in underground mines. The entire dimension of the U shape is 4.5 m long and 2.0 m wide.

The wind tunnel has a particle generator that is made up of a compressed air duct, dust reservoir with injector, and a concentration regulation valve installed at its inlet which dispenses dry coal dust into the wind tunnel. The injected coal dust goes through an aerosol dispersion system to ensure a homogenous distribution of coal dust particles across the cross section of the wind tunnel. The outlet of the wind tunnel is connected to a dust collector that also enables exhausting type airflow through the wind tunnel. The fan drives air through the wind tunnel at a velocity of 1.0 m/s which is the normal air velocity in underground mines [29]. The wind tunnel has a platform built at the monitoring location which is 25.0 cm from the top of the tunnel on which the sensors and the nozzles for the monitors are installed.

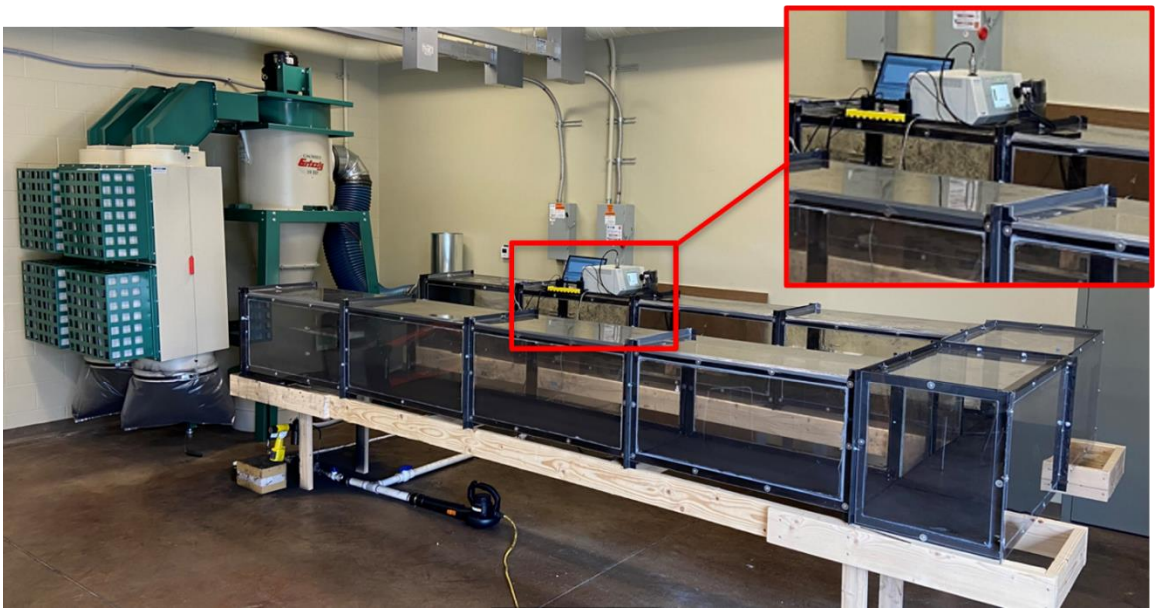

Figure 2. Calibration wind tunnel and the experimental set-up

2.3. CALIBRATION PROCEDURE

The coal dust used for this experiment is the Keystone mineral black 325 with a density of 1,220 kg/m3 with particle sizes in the range of 0.04 µm to 35.00 µm. Detailed characteristics and particle size distribution of this coal dust can be observed in Figure 3 [30]. Prior to the injection of coal dust particles, the two PMS sensors, APS, PDM, two Airtreks, and two Gaslabs were placed on the monitoring platform in the wind tunnel. The inlets to the sensors and monitors were placed very closely to one another to minimize spatial differences in particle concentration in such a way that did not cause interference with each other's exposure to airflow. Regarding the APS and PDM, the monitors were kept outside the wind tunnel and particles were sampled from the wind tunnel through nozzles which were positioned to face the flow in the tunnel. The remaining sensors and monitors were placed inside the wind tunnel with their inlets facing the flow. It was imperative to ensure that particle concentration at the sampling

locations stayed within 10% variation which was observed prior to the start of the experiments using the PDM. This was ensured by performing a preliminary test measuring and comparing the concentrations across the sampling location within the wind tunnel using the PDM. The uniform concentration maintained was the precaution used to ensure that variation in dust concentration between the sensors and monitors was insignificant.

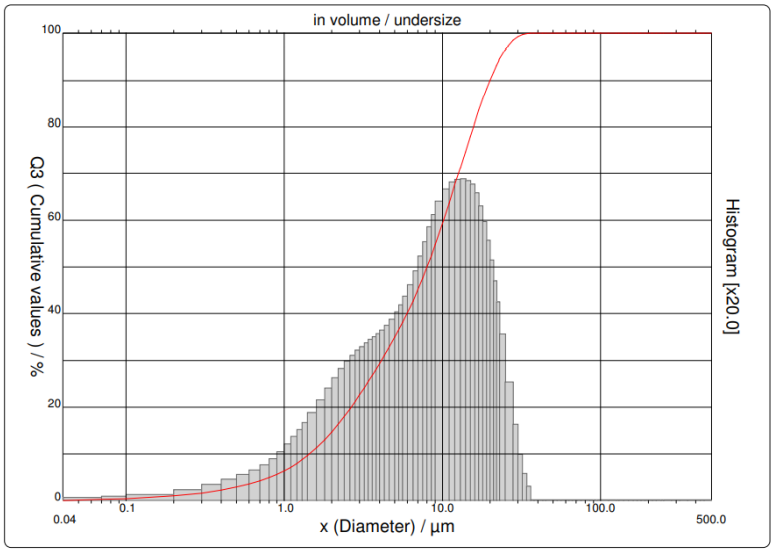

Figure 3. Particle size distribution for Keystone mineral black 325 coal dust

MSHA coal dust regulation is based on end-of-shift Time Weighted Average concentrations of 1.5 mg/m^3 [1]. The dust coal concentration in mines should typically fluctuate around this value, therefore we investigate the sensors' responses to different concentration levels ranging from 0 to 3.0. The coal dust injection rate was adjusted throughout the course of the experiments within that range depending on the test being performed.

The clock times on all sensors and monitors were reset to synchronize the time stamps. Although the APS and PMS sensors were programmed to record real time concentrations every 15.0 seconds, the Airtrek monitor reported concentrations every 30.0 seconds, while the Gaslab reports concentrations every 2.0 seconds. For these sensors and monitor that record their outputs multiple times within a minute, their readings were averaged to get minute-by-minute concentrations for all the sensors to be comparable with the PDM. This data is then used in the evaluation and calibration procedure. The PDM's reported time weighted average (TWA) concentration data were converted to minute-by-minute real-time concentrations using Equation to be consistent with all the other sensors' data. In this equation, TWAn is the time weighted average at each time step, C_n is the real time concentration measured, T is the time interval between successive measurement and Tn is the total number minutes at time n.

$$\mathrm{C} = \frac{TWAn \times Tn}{T} - (C_1 + C_2 + C_3 \ldots . C_{n-1}) \qquad \text{Equation 1}$$

2.4. CALIBRATION MATRICES

Low-cost PM monitors were evaluated and calibrated based on five calibration matrices: accuracy (linearity), precision, lower limit of detection, upper limit, and temperature and relative humidity influences. These matrices were adopted from the low-cost PM sensor evaluation protocol proposed and used by United States Environmental Protection Agency (US-EPA) [19], [31] the US Air quality sensor performance evaluation center (AQ-SPEC) [32], [33] and European Metrology Research Program

(EURAMET) [18] which have proven to be comprehensive and effective for low-cost PM sensors. These matrices are elaborated in the following sections.

2.4.1. Linearity. The accuracy of PM sensors is the closeness of sensor measurements to actual concentrations. In the linearity test, sensors and reference monitors were exposed to the same concentrations and environmental conditions within the wind tunnel. During the test, the coal dust injection rate was changed every 10.0 minutes between 0 and 3.0 mg/m^3. During this test, concentrations occasionally spiked above the target 3.0 mg/m^3 for a few seconds after which valves were quickly readjusted to the correct levels. This, however, allowed us to observe the characteristics of the sensors at peak concentrations beyond 3.0 mg/m^3. The linearity of the PMS sensors and the other monitors were assessed using the correlation coefficient from linear regression by plotting the output of monitors against PDM and APS. The concentrations measured by the reference monitors were used as the independent variable, while the concentrations measured by the sensors were reported as dependent variables. Using both the PDM and APS as reference monitors, each sensor is evaluated with both the PDM and APS. The linearity of each sensor and monitor, which is an indication of a monitor's accuracy, is evaluated by the R-squared value calculated using the ordinary least square (OLS) linear regression method. The accuracy of a sensor is lower for those with lower linearity values. The linear regression models generated from this evaluation was then used to derive the calibration equation to improve the accuracy of the PMS to the accuracy of the PDM.

2.4.2. Precision. The precision of the sensors was evaluated to understand the ability of the sensors to reproduce the same outputs at the same concentration level. Five

concentration levels were used for these experiments - 0.5 mg/m^3, 1.0 mg/m^3, 1.5 mg/m^3, 2.0 mg/m^3 and 3.0 mg/m^3. At each concentration level, coal dust concentration and other environmental conditions were kept constant within the wind tunnel and measurements were taken with sensors for 60 mins. The precision for each sensor was then measured using the EPA sensor evaluation protocol for low-cost PM sensors. This is determined by the coefficient of variation (CV) expressed as a percentage using the equation in Equation 2 where σ represents standard deviation, and μ is the mean value of measurements. A precision of less than 10% is required by EPA for sensor deployment. This would give us the understanding of the consistency and reliability of the PMS outputs in an extended use.

$$\mathrm{CV} = \frac{\sigma}{\mu} \qquad \text{Equation 2}$$

2.4.3. Limit of Detection. LOD describes the lowest concentration limit of sensors that significantly differentiates from sensor outputs at blank concentrations. This tells how the sensors will reliably differentiate concentration changes from instrument noise, which is the short-term deviations in measurements about the mean of a stable concentration which are not caused by changes in concentrations. Different from LOD, the lower limit of sensors was also evaluated as the average sensor output at zero coal dust concentration. The LOD for the low-cost sensors were evaluated by subjecting them to 0.0 mg/m^3 coal dust concentrations over a 60-minute period. This blank condition was generated by filling the chamber with clean air with no particles and completely shutting off the valves to the dust injection system. For this experiment, air is considered clean

when the PDM and APS reference monitors measures 0.0 mg/m^3. Based on outputs of sensors under these conditions, LOD is calculated using Equation 3 [34] where k is the slope from the fitted linear regression model, and σ_{blk} is the standard deviation. In this experiment, these parameters were calculated based on the 60 measurements taken over a testing period of 1 hour.

$$\text{LOD} = \frac{3\sigma_{blk}}{k} \qquad \text{Equation 3}$$

2.4.4. Upper Concentration Limits. The upper concentration limit is the concentration at which a 10 unit increase in reference monitors' measurements is unproportionally characterized by a 0.2 unit or an exponential increase in the outputs of low-cost sensors. This concentration serves as the maximum concentration that a sensor is capable of measuring with an acceptable degree of accuracy. Upper limits vary significantly among the various low-cost PM sensors. Even though manufacturers report certain values as the upper limits, usually 1.0 mg/m^3, it is important to evaluate the upper limit to determine if these limits differ for coal dust particles. The results from the linearity test described in Section 2.4.1 was analyzed to determine the operational range for the sensors and to determine the upper limits for each sensor. The inflection point of their response curves (also known as the knee of the curve) was determined as a sensor's upper limit using Equation 4. The maximum k value on the curve determines the inflection point at which the linearity of the sensor ends.

$$k(x) = \frac{|f''(x)|}{\left[1 + \left(f'(x)\right)^2\right]^{3/2}}$$ Equation 4

2.4.5. Influence of Temperature and Relative Humidity. A 2^2 factorial design was used to determine if the temperature and relative humidity changes have a significant impact on dust monitors' readings at low and high coal dust concentration levels. The temperature and relative humidity factors each had two levels, high (+) and low (-). For these tests, low temperatures ranged from 20 to 24oC whereas high temperatures ranged from 26 to 40oC which represents typical underground conditions as the temperature in most mines range from 15 and 35oC. Low RH ranged from 20 to 30% while high RH ranged from 35 to 45%. Even though RH in mines can exceed 45%, the challenge of simulating higher RH in the lab limited testing at higher RH values. At each concentration level, four tests were performed at different levels of temperature and relative humidity as shown in Table 1. The order of tests was randomized within each concentration. Each test lasted for 60 minutes with at least 5 minutes stabilization time between tests when the conditions are changed. All 0.5 mg/m^3 concentration tests were performed on 4/18/2022, and the 1.5 mg/m^3 concentration tests were performed on 4/19/2022. A 2 factorial ANOVA analysis of variance was used to evaluate the effect of temperature and relative humidity on the performance of the low-cost PM sensors.

The low temperature and relative humidity conditions were achieved using the lab ambient temperature and humidity regulated by the building HVAC system. The high temperature and humidity were achieved by operating a Honeywell heater and a

Honeywell cool moisture humidifier, which are displayed in Figure 4 installed at the inlet of the wind tunnel.

Figure 4. The Honeywell turbo force power heater and the Honeywell infrared cool moisture humidifier

Table 1. Experimental design for 0.5 and 1.5 mg/m^3 concentration at different temperature and humidity levels

Test Name	Temperature	Humidity
TLHL0.5	-	-
THHL0.5	+	-
TLHH0.5	-	+
THHH0.5	+	+
TLHL1.5	-	-
THHL1.5	+	-
TLHH1.5	-	+
THHH1.5	+	+

3. RESULTS

3.1. LINEARITY

Prior to the evaluation of the sensors, the two reference monitors were compared beforehand to determine their accuracy and to determine if any reference monitors had any errors which would eventually affect the sensors' calibration models. Figure 5 shows the correlation obtained from comparing the respirable particle size concentrations from the PDM with the APS. The PDM uses the BGI HD cyclone with precise D50 cut off point of 4.37 µm which has a proven significantly low bias relative to the International Standards Organization (ISO) respirable size selection curve. Since it is practically impossible for the APS to emulate the performance and behavior of the theoretical respirable particle size selection curve, the concentration of particles within the 4.37 µm size bin is used in this analysis [35]. When the data from PDM and APS were compared, a remarkably high linearity was observed between them. The R-squared value of 0.92 indicates a high correlation between them. In PM monitoring studies, an R-squared above 0.80 is generally considered as highly correlated, with R-squared values from 0.60 to 0.80 representing moderately correlated monitors, while a measure of R-squared below 0.60 is considered to have low correlation [22], [25]. A statistical test performed on these results gave a P-value of 0.00 indicating strong statistical significance of these results. It is apparent that despite the two monitors operating on different PM measurement principles, the difference in technologies had no significant impact on their correlation. Both monitors were seen to be highly accurate and appear to be equally responsive to coal dust particles. This explains why both monitors are recognized for their high

accuracies. As much as the APS is not recognized as a coal dust monitor, it has shown a high level of accuracy to be used as reference monitor for coal dust monitoring.

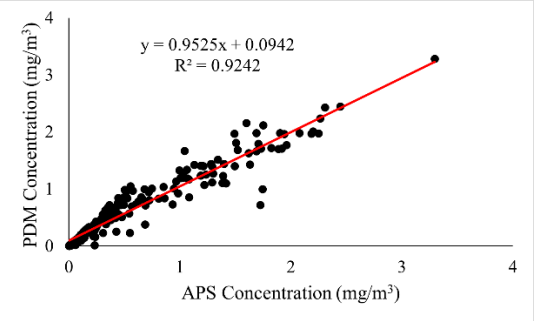

Figure 5. Correlation between PDM and the APS reference monitors

To calibrate the low-cost PM sensors, we evaluated the linearity of each sensor by analyzing the relationship of the output of the PDM and APS against each sensor. Figure 6 displays the statistical plots for the pairwise correlation between the sensors and reference monitors. Prior to the evaluation, the boxplot algorithm for outlier detection was used to filter out data points which were flagged as outliers. The PMS low-cost PM sensors had the best linear correlation among all the sensors under evaluation while the Airtreks and Gaslab monitors had progressively lower performance, respectively.

As can be seen from the plots, a considerably high linearity was recorded for both PMS sensors against both reference monitors. High R-squared values of 0.88 and 0.90 was recorded for PMS1 and PMS2 respectively with the PDM at P values of 0.00 for both sensors. These results agree with several previous studies which have obtained similar high linearity values for the PMS sensors [13], [25]. However, relatively lower R-squared values were observed for the same sensors using the APS as reference monitor

with R-squared values of 0.70 and 0.73 for PMS1 and PMS2 respectively. P-values generated for this statistical analysis were 0.01 and 0.02 for PMS1 and PMS2 respectively highlighting the statistical significance of the outputs. It should be noted that these results are only true for testing concentrations below 3.0 mg/m^3. While other studies have recorded relatively higher R-squared values for the same sensors, this was only achieved when NaCl or Arizona road dust are used for the testing. Coal dust on the other hand, has particle characteristics which are different from these particles and so the sensors could react to them.

The intra-model correlation between the two PMS sensors was found to be 0.97 with a P-value of 0.00 which makes them exceptionally agreeable with each other and can be calibrated using the same calibration model. The PMS can confidently measure coal dust concentrations provided the concentrations stay below 3.0 mg/m^3.

Although these results point to an acceptable level of accuracy for the PMS sensors, a striking characteristic was observed during the test when concentrations went above 3.0 mg/m^3. Beyond this concentration, the PMS sensors reported excessively high outputs which were unrealistic and disproportional with the actual concentration level. For example, the sensor concentrations reached as high as 60.0 mg/m^3 when concentration levels within the wind tunnel was below 5.0 mg/m^3 as indicated by the APS. These data points, as well as all other outliers for the other sensors' data were therefore eliminated from the statistical analysis as outliers using boxplot algorithms as keeping them on the plots would make the plots unreadable. This characteristic of the PMS sensors has not been observed in previous studies due to generally low testing

concentrations used. In those studies, PMS testing concentrations ranged between 0 and 1 mg/m^3.

Airtrek sensors had slightly lower linearity values as compared with the PMS sensors. As can be seen from the plots displayed in Figure 6, at concentrations below 2.0 mg/m^3 when the Airtrek sensors reported 1.5 mg/m^3, both Airtrek 1 and Airtrek 2 appeared to have a higher linear correlation with the reference monitors. This fairly agrees with manufacturer's datasheet stating that the Airtrek has a measurement range of up to 1.0 mg/m^3 even though it can report concentrations to 2.0 mg/m^3. However, when concentrations within the wind tunnel exceeded 2.0 mg/m^3 when the Airtrek sensors reported 1.5 mg/m^3, their outputs began to steeply approach 2.0 mg/m^3 giving the overall Airtrek response an exponential look. This was because the Airtrek sensors would still report concentrations beyond 1.5 mg/m^3 but with less accuracy, and report 2.0 mg/m^3 for all concentrations which are sensed by the sensors to be beyond 2.0 mg/m^3. A linear regression statistical analysis to determine the accuracy of the The Airtreks resulted in R-squared values of 0.58 and 0.60 for Airtrek1 and Airtrek2 respectively using the PDM as reference monitor. P-values generated from the statistical analysis were both 0.00 against the PDM emphasizing on its statistical significance. It was also found that Airtrek1 and Airtrek2 had R-squared values of 0.42 and 0.51 respectively using the APS as reference and P-values of 0.00 for each sensor. It can be seen from these results that these sensors can be reliable for concentrations below 1.0 mg/m^3. Between these sensors, there is an apparent high intra-model linearity with an R-squared of 0.73 with a P-value of 0.01. With a robust calibration model, individual calibration models are not required since a single calibration model can fit these sensors to achieve improved performance.

The Gaslab sensors had the lowest linearity among the three sensor models under evaluation. Gaslab1 reported R-squared values of 0.46 and 0.56 for PDM and APS respectively with P-values 0.00 each, whereas Gaslab2 reported linearity values of 0.66 and 0.52 for PDM and APS respectively with P-values of 0.00. The two Gaslab sensors recorded the lowest intra-model correlation of 0.23 among all the sensors while generating a P-value of 0.02. Much of the non-linearity between these sensors and the reference monitors was due to the limited range of the gaslab sensors which makes them report their maximum limit of 1.0 mg/m^3 even when the concentration exceeded that. As seen in Figure 6, it can be observed that these sensors reported no output beyond 1.0 mg/m^3 even when concentrations within the wind tunnel exceeded 1 mg/m^3. These results confirm the specifications of the Gaslab monitors by the manufacturers having a measurement range of 0.0 to 1.0 mg/m^3. These sensors may provide reliable monitoring information for environments with lower PM concentrations like indoor offices and home spaces.

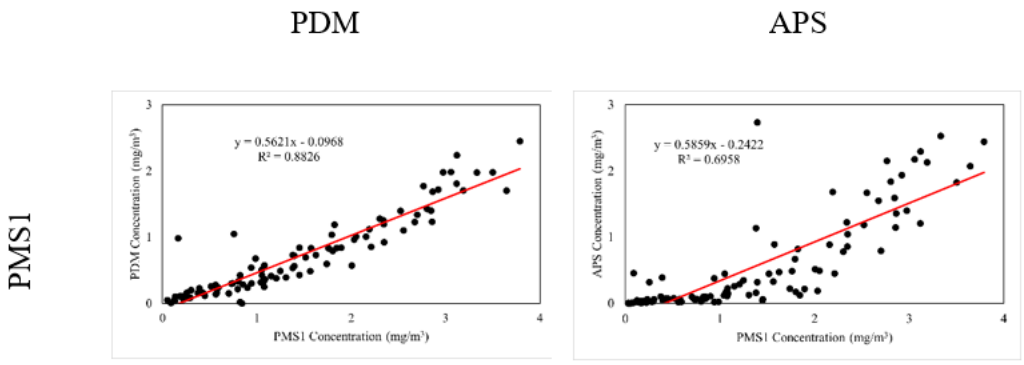

Figure 6. Pairwise correlation between the two PMS sensors, two Gaslab sensors and the two Airtrek sensors each against the two reference monitors PDM and APS

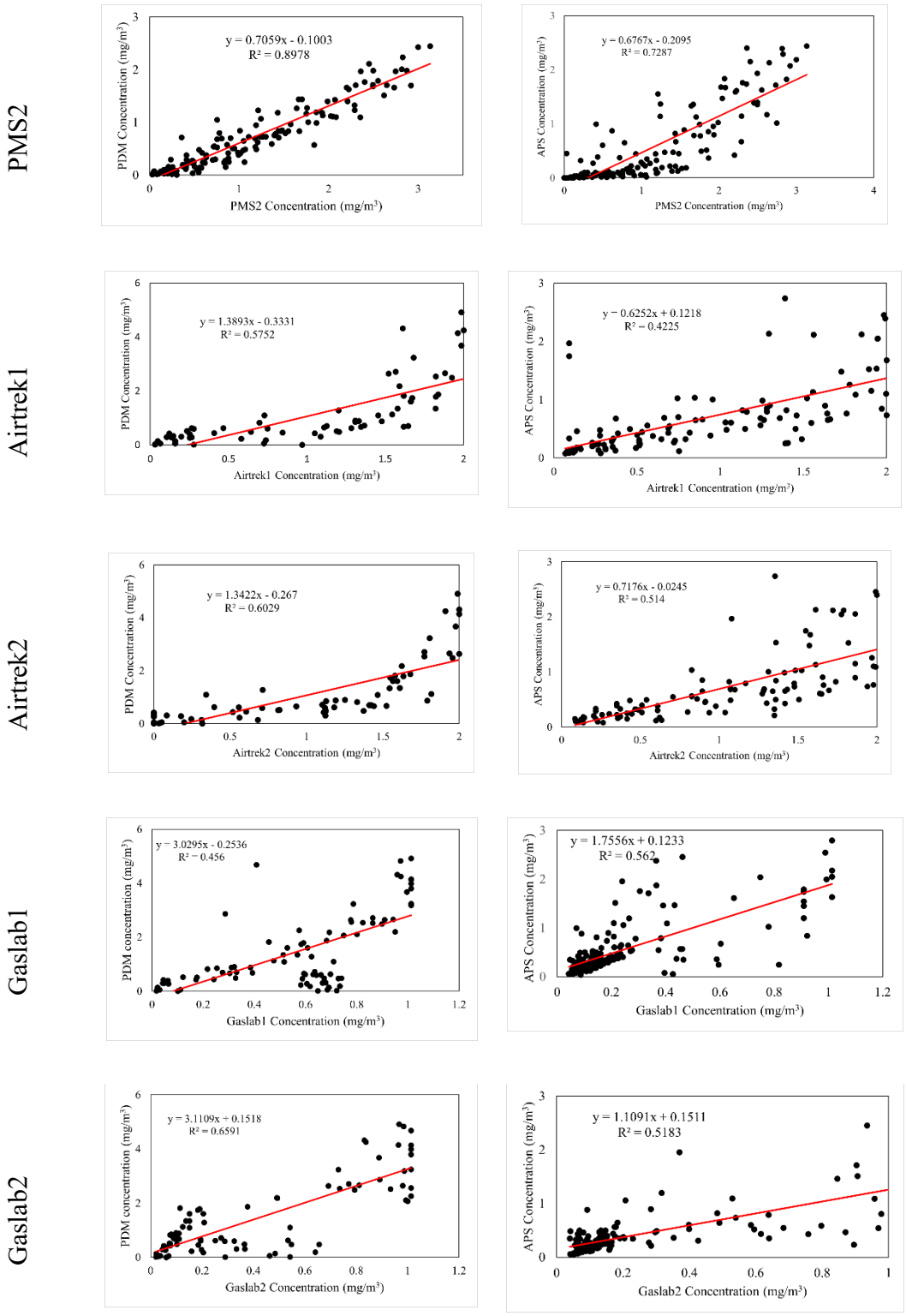

Figure 6. Pairwise correlation between the two PMS sensors, two Gaslab sensors and the two Airtrek sensors each against the two reference monitors PDM and APS (Cont.)

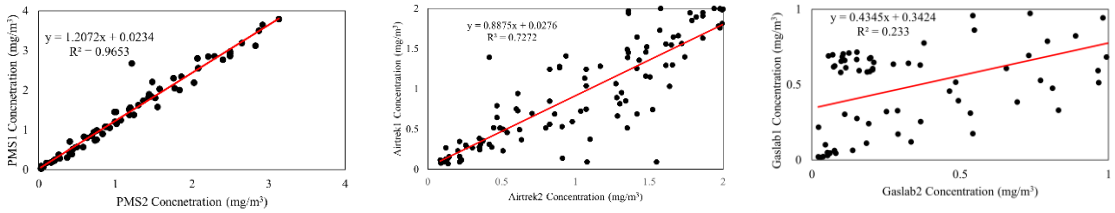

(a) (b) (c)

Figure 7. Intra-mode correlation between the two models of each sensor type (a) PMS5003 sensors (b) Airtrek sensors (c) Gaslab sensors

3.2. PRECISION

The results of the tests for precision are displayed in Figure 8, Table 2 and Figure 9. The true concentrations generated for these experiments are shown in Figure 8 while Table 2 and Figure 9 shows the variation of each sensor. It can be seen from the PDM and APS data that even though the concentrations were set to be constant throughout the testing period, there was some level of fluctutatuion in concentration within the wind tunnel resulting in concentrations occasionally exceeding and receeding the targeted cocncentrations. The spread of concentrations at each concentration level is represented by the boxplots shown in Figure 8. Because of this drawback in experiment, the precision of the sensors was measured using data points only when concentration was measured by the APS to be equal to the targeted concentration. All data points recorded when concentration was above and below the targeted concentration were eliminated.

In general, it was observed that CV for the sensors increased with increasing concentration indicating decreasing precision with increasing concentration. In the case of the PMS1 and PMS2 sensors, a CV of less than 10% was achieved at concentrations below 2.0 mg/m^3. At 2.0 mg/m^3 and above, the CV progressively increased from 27.56%

and 56.05% at 2.0 mg/m^3 to 47.83% and 70.34% at 3.0 mg/m^3. This shows the PMS sensors are only precise at lower concentratiosn below 2.0 mg/m^3. Even though they provide outputs at higher concentration levels, only low concentration outputs can be reliable. Therefore, the PMS sensors could be used for mine coal dust monitoring where concentrations are generally low such as inside operators' cabs and on miners underground as personal monitors. It should be noted, however, that the average concentration of coal dust in underground coal mines is 0.55 mg/m^3 [36]. Therefore, the limitation of imprecision at higher concentrations makes them capable of accurately measuring concentrations within an underground mine under normal operations.

Similarly, for Airtrek sensors, acceptable CV values were observed below 1.0 mg/m^3 where CV were 9.54% and 8.20% for Airtrek1 and Airtrek2 at 0.5 mg/m^3. CV noticeably increased above 1.0 mg/m^3 reaching 31.36% and 30.21 at 3.0 mg/m^3. A review of the manufacturers' datasheet for the Airtrek sensors reveals that the recommended upper limit for PM monitoring is 1.0 mg/m^3. Even though the sensors can measure and report concentrations higher than its recommended upper limit, these results indicate that those readings could be imprecise. Deploying these sensors for higher coal dust concentration environment can create misleading results to users.

The trend of decreased precision with increasing concentration appeared to be different with the Gaslab sensors. Even at low concentrations, these sensors had CV above the acceptable 10%. At 0.5 mg/m^3, a CV of 12.49% and 16.49% was measured for Gaslab1 and Gaslab2 respectively. These increased to 53.08% and 29.89% at 1.5 mg/m^3. Their limited upper concentration limits of 2.0 mg/m^3 made it impossible to evaluate their

precision at higher concentrations due to the sensors constantly reporting 2.0 mg/m^3 when the concentrations went beyond 2.0 mg/m^3.

These results confirm that even though these low-cost PM sensors can measure and report concentrations beyond their recommended upper limits, they begin to be imprecise and could report misleading results at higher concentrations. Nevertheless, if the imprecise readings from the sensors at higher concentrations appear to be consistent, a more robust calibration algorithm can correct this phenomenon. A more comprehensive experiment will have to be performed to determine a consistent trend if one exists. The EPA uses a slightly different method to evaluate sensor precision where a constant true concentration is achieved due to the smaller size and closed nature of their calibration chamber. This makes it much easier to achieve a near perfectly uniform dust concentration compared with a larger wind tunnel which has a more dynamic testing environment. It is worthwhile for future studies to evaluate sensors' precision in smaller calibration chamber at more constant concentrations.

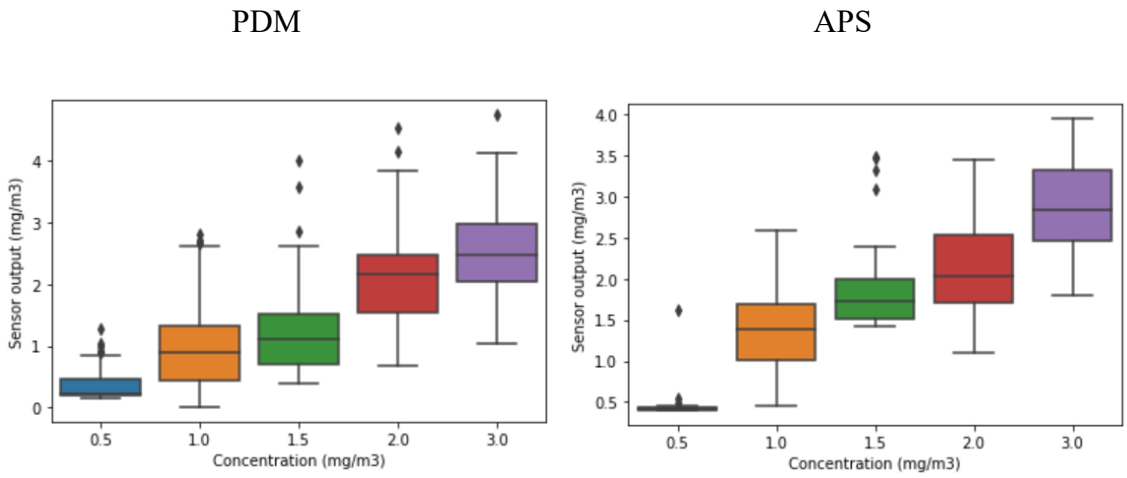

Figure 8. Precision results for reference monitors

Table 2. CV for all sensors at concentrations from 0.5 mg/m^3 to 3 mg/m^3

Sensors	Coefficient of variation (%)				
	0.5 mg/m^3	1.0 mg/m^3	1.5 mg/m^3	2.0 mg/m^3	3.0 mg/m^3
PMS1	7.95	7.52	10.08	27.56	47.83
PMS2	6.07	7.84	9.31	56.05	70.34
Airtrek1	9.54	7.54	41.09	37.66	31.36
Airtrek2	8.20	11.56	14.48	20.46	30.21
Gaslab1	12.49	48.42	53.08	-	-
Gaslab2	16.49	35.30	29.89	-	-

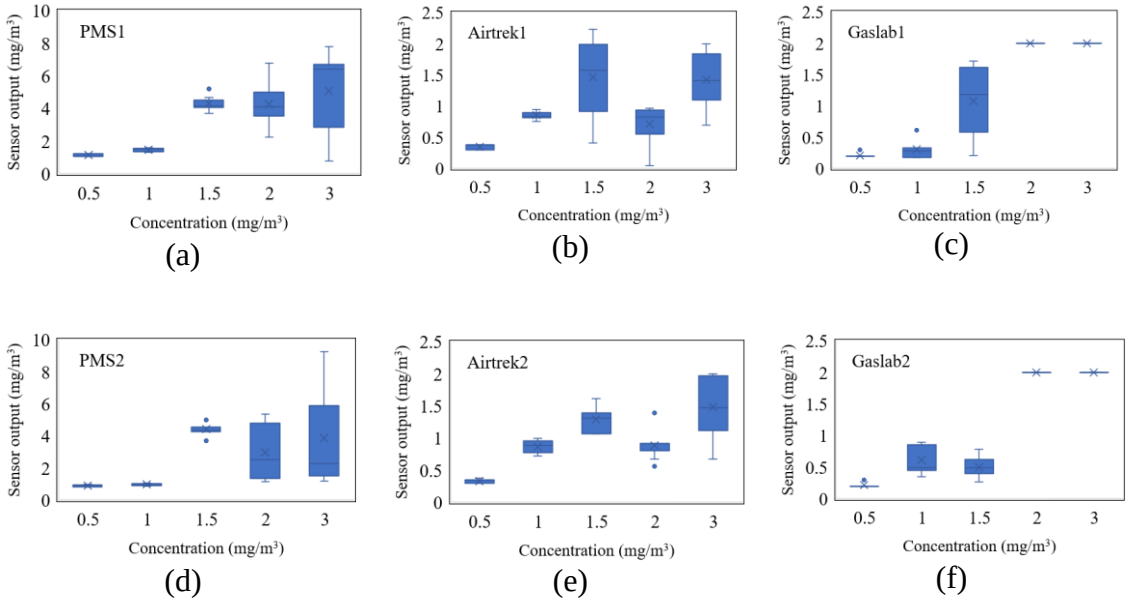

Figure 9. Variations for all sensors at concentrations from 0.5 mg/m^3 to 3 mg/m^3

3.3. LIMIT OF DETECTION

The results from this analysis are presented in Table 3. At 0.0 mg/m^3 dust injection concentration, the PDM recorded 0.00 mg/m^3 whereas the APS recorded 0.02 mg/m^3. Each of the PMS sensors recorded an average concentration of 0.01 mg/m^3 and

LOD values of 0.02 mg/m^3 each which was the lowest among the sensors being evaluated. The Airtrek sensors had slightly higher LOD values where they recorded 0.02 mg/m^3 and 0.89 mg/m^3 respectively. However, these Airtrek sensors had the best response to zero concentration giving an average concentration of 0.0 mg/m^3. With such accurate outputs at zero concentrations, these sensors would have had a significantly lower LOD if the linearity test obtained a high linearity for the airtrek sensors. The Gaslab sensors had the lowest lower limit values with an average concentration of 0.02 mg/m^3 at zero concentration and LOD values of 0.81 mg/m^3 and 0.94 mg/m^3. It should be noted that due to the absence of standard calibration curves for these sensors, the calibration curves generated using linear regression methods in Section 3.1 were used for this analysis.

Table 3. Lower limits of PMS, Airtrek and Gaslab sensors and their limit of detection

	PMS1	PMS2	Gaslab1	Gaslab2	Airtrek1	Airtrek2
Lower limit (mg/m^3)	0.01	0.01	0.02	0.02	0.00	0.00
LOD (mg/m^3)	0.02	0.02	0.81	0.94	0.02	0.89

3.4. UPPER CONCENTRATION LIMIT

In general, the low-cost PM sensors showed significantly lower upper limits as compared with the PDM and APS. This was expected since the APS and PDM are built with more advanced technology to operate in higher concentrations. By plotting the response of the reference monitors against the sensors, the nature of their response were observed and the concentration at which a sensor achieves its maximum value is

determined to be the upper limit using Equation 4. The results of this analysis are shown in Table 4. The two PMS sensors both demonstrated characteristics of their upper limits at 3.0 mg/m^3 of coal dust. Beyond 3 mg/m^3, a 10 unit increase in true concentration resulted in a corresponding sensor output of more than 200 % of the true concentration at which point the linearity of the sensor was discontinued. In principle, at higher concentrations when there are many particles within the sensing volume at the same time, these sensors suffer from coincidence errors. The multiple particles present in the sensing volume at the same time are recognized by the sensor as larger and heavier particles in which case the mass is overestimated resulting in such a high concentration compared with the reference monitors.

The airtrek sensors showed a slightly lower upper concentration limit of 1.5 mg/m^3 and 1.6 mg/m^3 for Airtrek1 and Airtrek2 respectively. It was observed in the linearity plots of the reference monitors against the Airtrek sensors in Section 3.1 that the change in slope from lower concentration to higher concentrations gave the response an exponential curve where the knee of that curve was calculated to be the upper concentration limits. Similar to the Airtrek sensors, the Gaslab sensors were characterized by an exponential curve even though they had a more linear relationship at lower concentrations. The two Gaslab sensors had upper concentration limits of 0.9 mg/m^3 which was the lowest among the three sensors and close enough to manufacturers specified upper limits. Considering the generally low upper limits of these low-cost PM sensors it is worthwhile to only apply them for lower concentration environments for optimum performances.

Table 4. Upper concentration limits

Sensor	PMS1	PMS2	Airtrek1	Airtrek2	Gaslab1	Gaslab2
Upper limit (mg/m^3)	3	3	1.5	1.6	0.9	0.9

3.5. TEMPERATURE AND RH INFLUENCE

Several studies have found that relative humidity results in a significant bias on the performance of low-cost PM sensors while others have also suggested no influence. It has been proven that the water droplets in the atmosphere can absorb infrared radiation which is emitted into the measuring cavity of the sensors [13]. Water vapor can also condense on aerosol particles, causing hygroscopic growth of particles making them seem as though they are larger particles and eventually causing overestimation of particle size and concentrations [37]. The influence of relative humidity on low-cost PM sensors is highly dependent on the surface properties and composition of the particles. This is the reason why many studies have found a significant influence of relative humidity on these sensors while many others have found little to no influence at all. In this study, both temperature and RH conditions had no significant effect on the performance of the low-cost PM sensors based on the 2k factorial ANOVA analysis of variance. The results of the temperature and RH conditions measured in the wind tunnel is displayed in Figure 10 and Figure 11. The temperature achieved within the wind tunnel ranged from 20 degrees Celsius to 31 degrees Celsius while RH was measured to be from 24 % to 44 %. While a wider range of temperature and RH conditions was targeted, it was challenging to control and maintain these conditions within the wind tunnel throughout the experiments.

Therefore, the results from this test are only valid for the temperature and RH range obtained in this test.

Using the ANOVA analysis, all sensors under all conditions of temperature and RH generated F ratios of more than 5.0 % in their respective models. This indicated no significant impact of temperature an RH on the sensors under these temperature and RH factor changes as shown in Figure 11. However, a more in-depth statistical analysis revealed that RH had marginal impact on the performance of the sensors as can be seen from Figure 10. Figure 10 shows boxplots integrated with dot plots of concentrations plotted against relative humidity while overlaying temperature conditions. Red plots represent elevated temperature and blue plots represent low temperature. These results suggest that high RH marginally overestimated the outputs of the Airtrek and Gaslab sensors at higher concentrations of 1.5 mg/m^3 especially at lower temperatures. However, this effect was not substantial enough to attribute it to the changes in RH conditions. Other factors such as a concentration fluctuation within the tunnel cause this phenomenon. If RH had significant impact on these sensors, a more robust calibration model would be applied to comprehensively calibrate the sensors to account for the influence of RH on the sensors. To fully understand why RH had no influence on these sensors measuring coal dust, further research is needed to study the surface properties and composition of coal dust particles in detail to substantiate why coal particles are unaffected by atmospheric RH.

Temperature, on the other hand, had no impact on the performance on the PMS, Airtrek and Gaslab sensors. Figure 10 shows that there was influence of the temperature

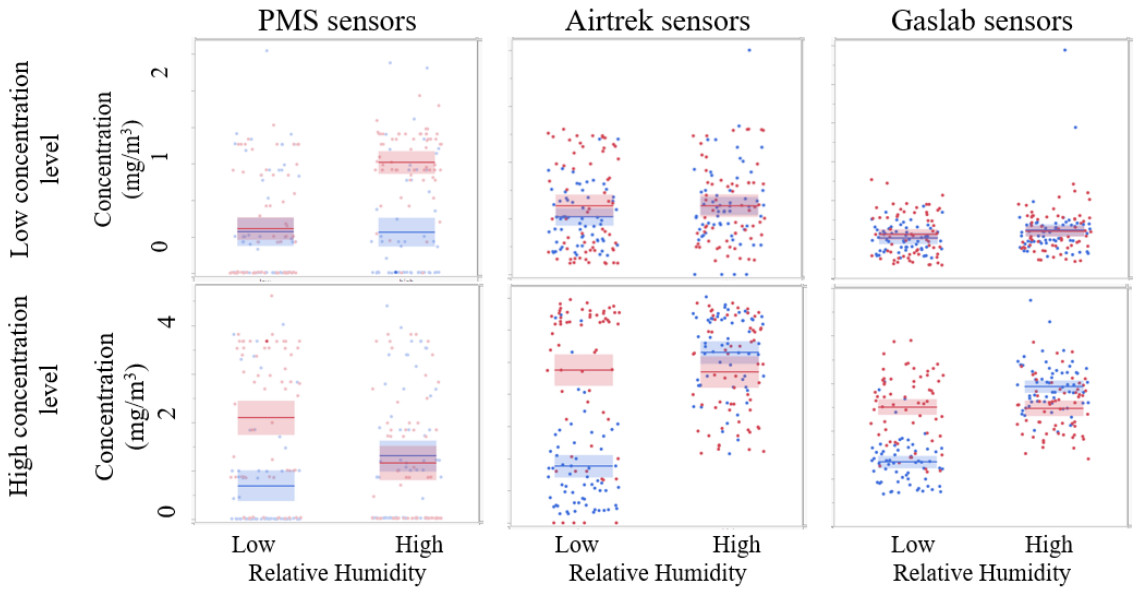

Figure 10. Concentrations reported by PMS, Airtrek and Gaslab sensors under different temperature and relative humidity conditions. Results are further elaborated with boxplots.

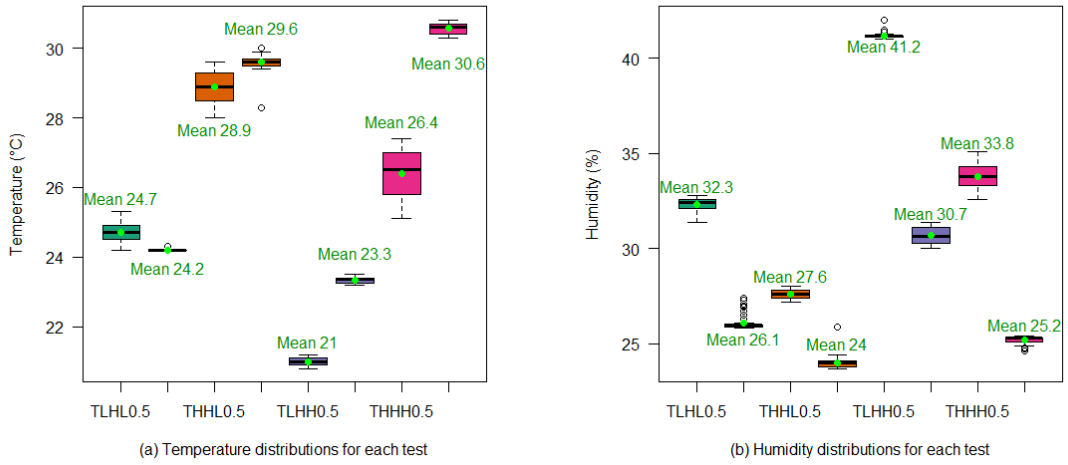

Figure 11. temperature and relative humidity distribution for the tests

rise and fall had on the sensor outputs. These results are consistent with several studies, many of which have established that there is no theoretical dependency of the light

scattering principle on temperature. However, some low-cost PM sensors are affected by temperature due to the use of thermal resistors in their operation. In that case, the temperature difference between the outside environment and the thermal resistor could affect the intake flowrate and sensor outputs. In this study, none of the sensors evaluated have that technology. The reference monitors had no impact from the temperature changes since they have temperature and RH control technology in-built. It should be noted that the challenge of difficulty in controlling and maintaining temperature and RH conditions within the wind tunnel could have impacted the findings of this study.

4. CONCLUSION

Accurate personal monitoring is essential to detect overexposures of the miners working underground in coal mines. This is also critical for recommendations of suitable controls. However, the high cost and size limitations of the PDM limits its usage to only a few miners risking most miners to unknown overexposures. Low-cost PM sensors can measure personal exposure levels for all miners in real time due to their low cost, small size, and light weight. Prior studies have established the potentials for low-cost PM sensors to be used as PM monitors. However, their application for mining-induced PM and underground conditions remained unexplored. Therefore, this study developed a coal dust monitor using the Plantower PMS5003 sensors, evaluated their performance in laboratory experiments together with Airtrek and Gaslab sensors, and calibrated them using linear regression calibration algorithms.

It was found that all three sensors under evaluation had different degrees of linearity with the APS and PDM. The PMS sensors had the best linearity with both PDM and APS among all the other sensors under evaluation, with R2 values ranging from 0.70 to 0.90 and an excellent intra-model linearity of 0.97 for concentrations levels below 3.0 mg/m^3. The Airtrek sensors had slightly lower linearity between 0.0 and 2.0 mg/m^3, but had lost its linearity at concentration beyond 2.0 mg/m^3 giving them an exponential response with the reference monitors. The Gaslab sensors had the least linearity among the sensors with R2 values ranging from 0.40 to 0.52. All three sensors had precision levels identical to that of the reference monitors at concentration levels below 1.5 mg/m^3. It was found that beyond 1.5 mg/m^3, the sensors experienced a decrease in precision with increasing concentration. PMS sensors demonstrated the highest measurement range with the lowest lower limit of 0.0 mg/m^3 and highest upper limits of 3.0 mg/m^3. Airtreks generated a closer range of 2.0 mg/m^3 while the gaslabs had a range of 1.0 mg/m^3. Statistical tests gave P-values of less than 0.05 for all linearity results indicating that these results are reliable beyond the testing results. At concentrations above these limits, the sensors all show challenges reading those concentrations which would potentially give misleading outputs. However, since the upper limit for the PMS sensors are above the PEL for coal dust, the wearer would already be notified. It was also observed that temperature and relative humidity had no significant influence on the performance of these sensors even though an observation of the results show minimal overestimation of sensors' performance at higher RH. The concentration change, however, was not significant enough to attribute it to RH changes.

These results provide compelling evidence that the PMS5003 low-cost PM sensor has the potential to monitor coal dust concentrations up to 3.0 mg/m^3. Underground coal miners could widely wear this to ensure early overexposure detection and timely control to protect the health of miners. This will eliminate the high expenditure incurred by mines and the federal government associated with treatment of CWP, as well as compensations. This technology is also expected to facilitate improved underground structure and ventilation designs and provide high quality "big data" to facilitates the health studies related to respiratory diseases caused by PM. However, it will be worthwhile to note some limitations that still need to be investigated. During the tests, the research team had the limitation of achieving RH conditions higher than 45%. While RH conditions in underground mines could reach as high as 70%, future studies will need to consider testing at RH of 45% to ~70%. Although the study revealed that the influence of temperature and RH were minimal, these factors should be accounted for in a calibration model in a multiple variable algorithm to make the performance more robust. Future studies should therefore apply models such as multiple linear regression and machine learning algorithms to cover temperature and RH in the calibration models.

REFERENCES

[1] MSHA, "Major Provisions and Effective Dates MSHA ' s Final Rule to Lower Miners ' Exposure to Respirable Coal Mine Dust," vol. 2014, pp. 1–2, 2014.

[2] D. Knight, R. Ehrlich, A. Cois, K. Fielding, A. D. Grant, and G. Churchyard, "Predictors of silicosis and variation in prevalence across mines among employed gold miners in South Africa," *BMC Public Health*, vol. 20, no. 1, pp. 1–12, 2020, doi: 10.1186/s12889-020-08876-2.

[3] D. Wang *et al.*, “Comparison of Risk of Silicosis in Metal Mines and Pottery Factories: A 44-Year Cohort Study,” *Chest*, vol. 158, no. 3, pp. 1050–1059, 2020, doi: 10.1016/j.chest.2020.03.054.

[4] D. J. Blackley, C. N. Halldin, and A. Scott Laney, “Continued increase in prevalence of coal workers’ pneumoconiosis in the United States, 1970-2017,” *American Journal of Public Health*, vol. 108, no. 9. American Public Health Association Inc., pp. 1220–1222, Sep. 01, 2018. doi: 10.2105/AJPH.2018.304517.

[5] M. Badura, P. Batog, A. Drzeniecka-Osiadacz, and P. Modzel, “Evaluation of low-cost sensors for ambient PM2.5 monitoring,” *J Sens*, vol. 2018, 2018, doi: 10.1155/2018/5096540.

[6] Z. Al Barakeh, P. Breuil, N. Redon, C. Pijolat, N. Locoge, and J. P. Viricelle, “Development of a normalized multi-sensors system for low cost on-line atmospheric pollution detection,” *Sens Actuators B Chem*, vol. 241, pp. 1235–1243, 2017, doi: 10.1016/j.snb.2016.10.006.

[7] S. Kelleher, C. Quinn, D. Miller-Lionberg, and J. Volckens, “A low-cost particulate matter (PM2.5) monitor for wildland fire smoke,” *Atmos Meas Tech*, vol. 11, no. 2, pp. 1087–1097, 2018, doi: 10.5194/amt-11-1087-2018.

[8] P. Kumar *et al.*, “The rise of low-cost sensing for managing air pollution in cities,” *Environ Int*, vol. 75, pp. 199–205, 2015, doi: 10.1016/j.envint.2014.11.019.

[9] A. Halterman, S. Sousan, and T. M. Peters, “Comparison of respirable mass concentrations measured by a personal dust monitor and a personal DataRAM to gravimetric measurements,” *Ann Work Expo Health*, vol. 62, no. 1, pp. 62–71, 2018, doi: 10.1093/annweh/wxx083.

[10] J. Li, “Recent advances in low-cost particulate matter sensor : calibration and application,” Washington University in St. Louis, 2019.

[11] S. Sousan, K. Koehler, L. Hallett, and T. M. Peters, “Evaluation of the Alphasense optical particle counter (OPC-N2) and the Grimm portable aerosol spectrometer (PAS-1.108),” *Aerosol Science and Technology*, vol. 50, no. 12, pp. 1352–1365, 2016, doi: 10.1080/02786826.2016.1232859.

[12] K. E. Kelly *et al.*, “Ambient and laboratory evaluation of a low-cost particulate matter sensor,” *Environmental Pollution*, vol. 221, pp. 491–500, 2017, doi: 10.1016/j.envpol.2016.12.039.

[13] Y. Wang *et al.*, “Laboratory evaluation and calibration of three low-cost particle sensors for particulate matter measurement,” vol. 6826, 2015, doi: 10.1080/02786826.2015.1100710.

[14] N. A. Amoah, G. Xu, Y. Wang, J. Li, Y. Zou, and B. Nie, “Application of low-cost particulate matter sensors for air quality monitoring and exposure assessment in underground mines: A review,” *International Journal of Minerals, Metallurgy and Materials*, vol. 29, no. 8, pp. 1475–1490, 2022.

[15] C. C. Chen *et al.*, “Calibration of Low-Cost Particle Sensors by Using Machine-Learning Method,” in *2018 IEEE Asia Pacific Conference on Circuits and Systems, APCCAS 2018*, Institute of Electrical and Electronics Engineers Inc., Jan. 2019, pp. 111–114. doi: 10.1109/APCCAS.2018.8605619.

[16] S. De Vito, E. Massera, M. Piga, L. Martinotto, and G. Di Francia, “On field calibration of an electronic nose for benzene estimation in an urban pollution monitoring scenario,” *Sens Actuators B Chem*, vol. 129, no. 2, pp. 750–757, 2008, doi: 10.1016/j.snb.2007.09.060.

[17] D. Liu, Q. Zhang, J. Jiang, and D. Chen, “Performance calibration of low-cost and portable particular matter (PM) sensors,” *J Aerosol Sci*, vol. 112, no. May, pp. 1–10, 2017, doi: 10.1016/j.jaerosci.2017.05.011.

[18] L. Spinelle, M. Aleixandre, and M. Gerboles, *Protocol of evaluation and calibration of low-cost gas sensors for the monitoring of air pollution*, vol. 68. 2013. doi: 10.2788/9916.

[19] R. Williams *et al.*, “EPA Sensor Evaluation Report,” no. May, p. 40, 2014, [Online]. Available: http://www.epa.gov/research/airscience/docs/sensor-evaluation-report.pdf%5Cnhttp://cfpub.epa.gov/si/si_public_record_report.cfm?dirEntryId=277270

[20] A. Polidori, V. Papapostolou, and H. Zhang, “Laboratory Evaluation of Low-Cost Air Quality Sensors,” no. August, 2016, [Online]. Available: http://www.aqmd.gov/docs/default-source/aq-spec/protocols/sensors-lab-testing-protocol6087afefc2b66f27bf6fff00004a91a9.pdf?sfvrsn=2

[21] E. Austin, I. Novosselov, E. Seto, and M. G. Yost, “Laboratory Evaluation of the Shinyei PPD42NS Low-Cost Particulate Matter Sensor,” pp. 1–17, 2015, doi: 10.1371/journal.pone.0137789.

[22] K. E. Kelly *et al.*, “Ambient and laboratory evaluation of a low-cost particulate matter sensor,” *Environmental Pollution*, vol. 221, pp. 491–500, 2017, doi: 10.1016/j.envpol.2016.12.039.

[23] M. Ghamari, C. Soltanpur, P. Rangel, W. A. Groves, and V. Kecojevic, “Laboratory and field evaluation of three low-cost particulate matter sensors,” *IET Wireless Sensor Systems*, vol. 12, no. 1, pp. 21–32, 2022, doi: 10.1049/wss2.12034.

[24] Z. Yong and Z. Haoxin, “PMS5003 series data manual,” 2016.

[25] T. Sayahi, A. Butterfield, and K. E. Kelly, “Long-term field evaluation of the Plantower PMS low-cost particulate matter sensors,” *Environmental Pollution*, vol. 245, pp. 932–940, 2019, doi: 10.1016/j.envpol.2018.11.065.

[26] J. C. Volkwein *et al.*, “Laboratory and Field Performance of a Continuously Measuring Personal Respirable Dust Monitor,” *US Department of Health and Human Services, Public Health Service, Centers for Disease Control and Prevention, National Institute for Occupational Safety and Health, Cincinnati, OH*, pp. 1–55, 2006.

[27] US-EPA, “List of designated reference and equivalent methods,” *Proceedings of the Water Environment Federation*, vol. 2005, no. 16, pp. 726–737, 2012, doi: 10.2175/193864705783867675.

[28] TSI Inc., “AERODYNAMIC PARTICLE SIZER MODEL 3321,” 2017. [Online]. Available: www.tsi.com

[29] P. Roghanchi, K. C. Kocsis, and M. Sunkpal, “Sensitivity analysis of the effect of airflow velocity on the thermal comfort in underground mines,” *Journal of Sustainable Mining*, vol. 15, no. 4, pp. 175–180, Jan. 2016, doi: 10.1016/j.jsm.2017.03.005.

[30] U. Uknowledge and A. R. Kumar, “Dust Control Examination using Computational Fluid Dynamics Dust Control Examination using Computational Fluid Dynamics Modeling and Laboratory Testing of Vortecone and Impingement Modeling and Laboratory Testing of Vortecone and Impingement Screen Filters Screen Filters”, doi: 10.13023/etd.2018.383.

[31] US-EPA, “DRAFT Roadmap for Next Generation Air Monitoring,” no. March, p. 27, 2013.

[32] A. Polidori, V. Papapostolou, B. Feenstra, and H. Zhang, “Field Evaluation of Low-Cost Air Quality Sensors Field Setup and Testing Protocol,” no. January, 2017, [Online]. Available: http://www.aqmd.gov/aq-spec/evaluations/field

[33] V. Papapostolou, H. Zhang, B. J. Feenstra, and A. Polidori, “Development of an environmental chamber for evaluating the performance of low-cost air quality sensors under controlled conditions,” *Atmos Environ*, vol. 171, pp. 82–90, 2017, doi: 10.1016/j.atmosenv.2017.10.003.

[34] H. Kaiser and H. Specker, “Evaluation and comparison of analytical methods,” *Fresenius ’Journal for Analytical Chemistry*, vol. 149, no. 1–2, pp. 46–66, 1956, doi: 10.1007/BF00454145.

[35] B. Belle, “Pairwise evaluation of PDM3700 and traditional gravimetric sampler for personal dust exposure assessment,” *Mine Ventilation Conference, Brisbone*, no. August, pp. 28–30, 2017.

[36] B. C. Doney *et al.*, “Respirable coal mine dust in underground mines, UnitedStates, 1982-2017.pdf,” *American journal of Insustrial Medicine*, vol. 62, pp. 478–485, 2019.

[37] R. Jayaratne, X. Liu, P. Thai, M. Dunbabin, and L. Morawska, “The influence of humidity on the performance of a low-cost air particle mass sensor and the effect of atmospheric fog,” *Atmos Meas Tech*, vol. 11, no. 8, pp. 4883–4890, 2018, doi: 10.5194/amt-11-4883-2018.

III. CALIBRATION OF LOW-COST PM SENSORS FOR COAL DUST MONITORING USING MACHINE LEARNING ALGORITHMS

ABSTRACT

The recent resurgence of coal workers' pneumoconiosis among coal miners in the United States has been linked to the exposure to excessive levels of coal dust. To control miners' overexposure, the PDM3700 monitors were adopted in the mining industry to measure each miner's coal dust exposure levels. However, the high cost of the PDM3700 hinders its purpose of measuring all miners' exposure levels. The Plantower PMS5003 low-cost PM sensors have demonstrated the ability to measure coal dust concentrations with high spatial resolution in real time due to their low cost and small size. These sensors, however, require extensive calibration to ensure they maintain a high accuracy over long periods of deployment. Since they have only been calibrated for mining induced PM monitoring using linear regression models in the past, the objective of this study is to leverage machine learning algorithms for coal dust monitoring sensor calibration. A laboratory collocation experiment was performed using the PDM and APS as reference monitors in a wind tunnel under a wide range of concentrations, temperatures and relative humidities. The results revealed that nonlinear machine learning techniques significantly outperformed traditional linear regression models for low-cost sensor calibration. With artificial neural network being the strongest calibration model, the Pearson correlation of the PMS5003 sensors reached 0.98 and 0.97 with the Airtrek sensors reaching Pearson correlation of 0.91 while the Gaslab sensors reached correlations of 0.93 and 0.92. This shows a 2% to 11% improvement in model

performance over the linear regression model through artificial neural network calibration. The success of machine learning algorithms in this work has demonstrated the feasibility of deploying low-cost PM sensors for coal dust monitoring in mines.

1. INTRODUCTION

Overexposure to respirable coal mine dust has been associated with the coal workers' pneumoconiosis (CWP), also known as "black lung" [1-2]. Miners have also been diagnosed with silicosis in mines where the respirable coal mine dust has at least 5% silica dust content [3]. There has been an increase in CWP prevalence among the US coal miners since 2000 and this recent resurgence has been considered the most serious in history with the recent prevalence at 11% for long term coal miners [4-5]. Coal miners are currently at an increased risk of contracting CWP and silicosis which potentially causes long term permanent disability premature death. Contrary to common belief that CWP and silicosis are only associated with long-term respirable coal dust exposure, recent data indicates that it has also been diagnosed in younger coal miners [6].

Effective personal dust monitoring is essential for controlling overexposure and preventing CWP. Personal real time monitoring units are capable of detecting overexposures in a timely manner to provide alert for early control measures. The National Ambient Air Quality Standards (NAAQS) and the Mine Safety and Health Administration (MSHA), who regulate particulate matter (PM) concentrations in ambient and mining environments respectively have implemented various PM monitoring guidelines [7–9]. To protect miners from respirable coal mine dust (RCMD)

overexposure, MSHA has promulgated regulations requiring underground mines to keep RCMD end-of-shift concentrations at a time weighted average of 1.5 mg/m^3 in underground mines [6]. These compliance agencies, however, only approve the use of Federal Equivalent Methods (FEMs) and Federal Reference Methods (FRMs) for the PM monitoring. The Personal Dust Monitor (PDM) model 3700 remains the only MSHA certified coal dust monitoring unit. However, the PDM is too expensive and bulky [10–12]. A unit of the PDM costs ~$19,000 and weighs 2.0 kg [12-13]. The result of these drawbacks is that only a few miners are able to use the PDM primarily for regulatory compliance monitoring purposes. These are mainly miners who are exposed to the highest coal dust concentrations at their work locations and those who have already been diagnosed with pneumoconiosis [6]. Therefore, the exposure levels for most miners are not measured.

The limitations of the PDM have warranted the need for more affordable coal dust monitors in mines. The use of low-cost PM sensors for real time PM exposure monitoring has gained much attention in recent times. These sensors have the capacity to characterize PM with high spatial and temporal resolution due to fast response, low cost, small size and light weight [14–16]. Several studies have been performed on these sensors which have achieved impressive performances in comparison with FEMs [17-18], FRMs [15], [19], and research grade PM monitors [20–22]. Due to the promising potential of the low-cost PM sensors, regulatory agencies such as the EPA have developed calibration guidelines to improve their accuracies and have designed a roadmap for their adaptation [8]. The South Coast Air Quality Management District (SCAQMD) have also looked into ways of incorporating them into local communities [23], [24]. Even though these sensors

have been widely studied for ambient PM monitoring, they still remain a new technology for mining-induced PM monitoring and possess questionable accuracies that leaves room for more powerful calibration methods. The simple linear regression (SLR) model remains the only calibration model that has been applied to calibrate low-cost PM sensors for coal dust monitoring [14].

The SLR calibration methods are unable to account for other environmental factors such as temperature and relative humidity. This affects their transferability into environments different from their calibration environments which challenges their accuracy for ambient deployment [22], [25]. The more advanced multiple linear regression (MLR) model has been developed to account for the influence of temperature and relative humidity on the low-cost PM sensors. However, the MLR algorithm is more dependent on random variations in sensors' outputs making it more sensitive to the conditions of the length of the testing period [26]. The limitations on these calibration models have therefore warranted the use of more advanced calibration models using machine learning algorithms to evaluate and calibrate low-cost PM sensors [27–30]. A recent study evaluated and calibrated the Plantower PMS5003 low-cost sensor with reference to the Synchronized Hybrid Ambient Real Time Particulate (SHARP) monitor [31]. They compared the simple linear regression, multiple linear regression and two machine learning calibration algorithms – XGBoost and the feedforward neural network which revealed feedforward neural network (FNN) as the most accurate calibration algorithm with a root mean squared error (RMSE) of 3.91 [31]. Another study applied the same FNN model to calibrate the Plantower PMS7003 low-cost sensors which improved their accuracies from 0.618 to 0.905 using R-squared as an indicator using the Beta

Attenuation Monitor (BAM-1020) [27]. Random Forest and Support Vector Machine (SVM) have been found to additional algorithms that have superior performance over other machine learning algorithms [28], [30], [32]. Despite these promising potentials of machine learning algorithms, no study has applied these methods to calibrate low-cost PM sensors for coal dust monitoring and in underground mine conditions.

This study therefore aims to calibrate low-cost PM sensors for coal dust monitoring using machine learning algorithms. Laboratory evaluation experiments were performed under varying levels of coal dust concentrations, temperatures and relative humidity conditions. The MSHA FEM Personal Dust Monitor (PDM) model 3700 and the research grade Aerodynamic particle Sizer (APS) model 3321 were used as the two reference monitors. Based on the data from this experiment, the sensors were calibrated using 5 machine learning algorithms and compared to determine the most accurate calibration method. The widely used simple and multiple linear regression models together with three other machine learning algorithms: artificial neural network (ANN), support vector machine (SVM) and random forest regressor (RFR) were used in this study.

2. EXPERIMENTAL SET UP

The experimental set up used for the calibration experiment has been described in a previously published study by the authors [14]. The setup is made of a 0.5 m × 0.5 m U shaped wind tunnel designed to simulate underground mine airways. It is equipped with a

dust injection system which allows the control of coal dust concentrations within the wind tunnel as well as temperature and relative humidity controls.

2.1. REFERENCE MONITORS

The Environmental Protection Agency (EPA) FRM PDM model 3700 developed by the National Institute of Occupational Safety and Health (NIOSH), and the research grade Aerodynamic Particle Sizer (APS) were the reference monitors used in this study. The PDM is a real time personal coal dust monitor which operates based on the principle of tapered element oscillation microbalance (TEOM). Its accuracy, precision, comfortability is validated by NIOSH and has been approved for regulatory monitoring by the MSHA. NIOSH laboratory tests have demonstrated that there is 95% confidence that PDM measurements are within ±25% of true concentrations. Their field precision tests also show that the PDM monitors have a 0.078% standard deviation [33]. The PDM is equipped with a respirable size coal dust cyclone with a cut-off size modelled to closely simulate the human respiratory system respirable curve. Therefore, only respirable size particles go through to the mass transducer where the mass concentration is determined using the tapered element oscillation microbalance (TEOM) method.

The APS measures PM mass and number concentration by particle aerodynamic sizes from 0.5 µm to 20.0 µm using the time-of-flight principles. To make it comparable with the PDM, PM concentration of particle size below 4.37 µm from the APS was used for this study since it compares with the 4.37 µm D50 of the PDM cyclone. The APS draws ambient PM-laden air into the monitor through a nozzle at an accelerated flowrate of 5.0 liters per minute. The accelerated airflow goes through the sensing zone where the

PM concentrations are measured. Particle size distribution is then reported every 15 seconds based on the settings used for this study [34].

2.2. LOW-COST SENSORS

Three low-cost PM sensors were calibrated in this study – the Plantower PMS50003 (PMS) low-cost PM sensor, the Airtrek PM sensor, and the Gaslab CM-505 multi-gas sensor. Two units of each monitor were evaluated to compare their intra-model precisions. The Gaslab sensor, shown in Figure (a) measures PM 2.5 and PM 10 particle concentration together with oxygen, carbon dioxide and carbon monoxide concentrations. The Gaslab uses a combination of NDIR sensors, electrochemical sensors, and fluorescent sensors to measure the concentrations of PM and other gases. The Airtrek sensors on the other hand, shown in Figure (b) use light scattering principles like that of the Plantower PMS5003 sensor. The Airtrek sensors measure PM in four size bins of 1.0 µm, 2.5 µm, 4.0 µm, and 10.0 µm.

The PMS sensors are inexpensive PM detection and measurement sensors that operate on light scattering principles. These sensors are commercially available for ~$30 per unit. It draws ambient airflow through an inlet into the sensing area using a fan. As illustrated in Figure (c), the LED radiates laser-induced light into the sensing area to target particles within the measuring cavity. The light scattered by the particles is detected by the photodetector which sends pulses of electric signal to the in-built microprocessor. The number and intensity of electrical signals measured by the microprocessor are then converted to number and mass concentrations respectively based on MIE theory.

These PMS sensors characterize PM by size into PM1, PM2.5, and PM10. The manufacturers of the PMS sensors state that PM1 is measured for particles in the size range of 0.3 µm to 1.0 µm, PM2.5 for particles in the size range of 1.0 µm to 2.5 µm and PM10 for particles in the size range of 2.5 µm to 10.0 µm. For each size category, the PMS reports two PM outputs, one without any form of correction factor, called standard PM concentration (or CF = 1) and the other with an atmospheric calibration factor, called environmental PM concentration. The manufacturers have not published any details about the calibration factor and how it was developed. Therefore, due to considerable uncertainties about manufacturer calibration, the standard PM concentrations were used for this study. Manufacturer specifications indicates the performance of these sensors are not affected by non-PM aerosols due to an inbuilt shielding technology.

Together with a DHT-22 temperature and relative humidity sensor, NodeMCU ESP8266 and a 4 line by 20-character LCD screen, the PMS was integrated into a prototype monitor (low-cost PM monitor) as displayed in Figure (e). This monitor was programmed with Arduino IDE to display real time concentrations of PM2.5 and PM10, temperature and relative humidity readings every 1.0 s onto the LCD screen. To protect the low-cost PM sensor and its critical components from rainfall, sunlight, and physical damage, the sensor, and its components are housed in a 10.0 cm x 4.0 cm x 1.5 cm acrylic plastic box. This also allowed the team to see the screen readings in real time through the transparent acrylic case. The side of the acrylic case is strongly fastened but left uncovered to allow for normal operation of the PMS sensor without interference to the sensors' exposure. The low-cost PM monitor is continuously powered using a 5.0 V USB cable. For data analysis, the PM monitor is interfaced with a ThingSpeak MATLAB

based online IOT platform which serves as a cloud where all data is transmitted through Wi-Fi.

(a) Gaslab CM-505 multi-gas sensor

(b) Airtrek PM sensor

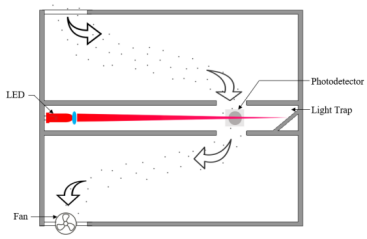

(c) Schematic PMS5003 sensor

(d) Plantower PMS5003 sensor

(e) PM monitor

Figure 1. Sensors and reference monitors used in the experiments

2.3. DATA COLLECTION

A custom-built air-tight wind tunnel was built with acrylic glass for the monitoring experiment. The wind tunnel was equipped with a particle generator which was used to control the coal dust concentrations within the tunnel. A heater and humidifier were also installed to control the temperature and relative humidity conditions respectively. A constant air velocity of 1.0 m/s was maintained in the wind tunnel

throughout the experiment while coal dust concentrations were constantly varied between 0 and 3 mg/m^3. Temperatures within the wind tunnel varied from 20^{o}C to 32^{o}C using the wind tunnel's heating system and the lab building's HVAC system. Relative humidity ranging from 23% to 43% was generated within the wind tunnel using the humidifier. The sensors and reference monitors were exposed to the combination of these conditions and the coal dust concentrations.

While the PDM records concentrations every minute, all other sensors and monitors were programmed to record data every 15 seconds. The experiment lasted about 6 hours a day for 8 days. It was ensured that the clock times on all these sensors and monitors were reset to synchronize the time stamps on all the sensors and monitors.

2.4. DATA PROCESSING

To clean up the data from these sensors for analysis, the PDM's reported time weighted average (TWA) concentration data were converted to minute-by-minute real-time concentrations using Equation to be consistent with all the other sensors' concentration units. In this equation, TWA is the time weighted average at each time step, C_n is the real time concentration measured, T is the time interval between successive measurement and Tn is the total number minutes at time n.

$$\mathrm{C} = (TWA \times n) - (C_1 + C_2 + C_3 \ldots . C_{n-1}) \qquad \text{Equation 1}$$

Further processing required the four 15-second concentrations reported each minute by the sensors to be averaged to obtain minute by minute concentrations and make them comparable with the PDM data. The boxplot method of outlier detection was

used to detect outliers. It was observed that the PMS sensors were the only sensors to record outlier concentrations in its data. Since the number of outliers detected were significantly small, these data points were deleted with no effect on the analysis.

3. DATA ANALYSIS

3.1. SIMPLE LINEAR REGRESSION

The performances of these low-cost PM sensors were evaluated using the simple linear regression (SLR) method to establish a calibration curve for these sensors. It is desired for light scattering low-cost PM sensors to establish a linear relationship with PM concentrations. In this study, this relationship was determined by establishing the correlations between sensor output and true concentrations determined by the PDM. The concentrations measured by the reference monitors were used as the independent variable, while the concentrations measured by the sensors were reported as dependent variables. Each sensor is evaluated against each sensor and monitor to obtain a calibration curve. The least-squares method was used to fit the calibration curve through the data points to determine the calibration equation as displayed in Equation 2 where y is the reference monitor concentration, α is the y intercept, β is the slope if the calibration curve, and x is the sensor outputs. This method used the sum of squared method to establish the curve with the least sum of squares as the curve of best fit to calibrate the sensors. Using the ordinary least square (OLS) linear regression method, R-squared were calculated to quantify the relationship between sensor outputs and true concentrations and to show the percentage of true concentration that can confidently be predicted using these

sensors. Pearson correlations were determined to determine the strength of the linear relationship.

In order to make the results of this evaluation comparable with other methods used in this study, the Mean Squared Error (MSE) is determined using the test dataset to evaluate the performance of the model. It is important to note, however, that a major downside to this method of calibration is that it is only able to estimate the relationship between two variables. However, low-cost PM sensors are affected by other factors such as temperature and relative humidity which cannot be accounted for in simple linear regression models.

$$y = \alpha + \beta x \qquad \text{Equation 2}$$

3.2. MULTIPLE LINEAR REGRESSION

Since simple linear regression models are limited to single variables for dependent and independent variables, the multiple linear regression (MLR) models are used in this section to account for the influence of temperature and relative humidity. These factors, together with the sensor outputs are then considered as the multiple independent variables while the true concentration determined by the reference monitor is remains the dependent variable. Similar to the simple linear regression, the least squares approach was used to estimate the values of the model coefficients needed to establish the MLR calibration model. The coefficients are then used to determine the minimum sum of squared deviations between data points and the plane which establishes the plane of best fit. The nature of the equation for the plane which was considered the calibration model is

shown in Equation 3 where y represents the true concentration, β_0 represents the constant term, β_1 to β_3 represent the slope coefficient for each independent variable and C is the model error term. The correlation values for each sensor were calculated to demonstrate the strength of the correlation between the sensor outputs and independent variables.

Using the 70-30 train test split, the model is trained using the training dataset. R-squared and Pearson correlation values were calculated to measure how much true concentration can be correctly determined by the low-cost sensors. P-values were measured in statistical tests to determine the statistical significance of the regression model. The test dataset was then used to evaluate the performance of the model. The performance was evaluated using the MSE.

$$y = \beta_0 + \beta_1 \times Conc + \beta_2 \times temp + \beta_3 \times RH + C \qquad \text{Equation 3}$$

3.3. ARTIFICIAL NEURAL NETWORK

Low-cost PM sensor response to concentration and the influence of temperature and relative humidity may not always be linear. A more comprehensive algorithm such as the Artificial Neural Network (ANN) is important for the non-linear relations within the dataset. The ANN algorithm is inspired by the biological neural network within the brains of humans. The neural network within the ANN trains data by matching samples' inputs to their corresponding outputs. This matchmaking is used to generate and optimize the probability-weighted relationship between the inputs and outputs. A schematic representation of this algorithm is demonstrated in Figure 2 and showing the structure of the ANN architecture. As can be seen in Figure 2, the input layer brings the data of input

variables into the model for further processing. In this application, the input layer consists of the sensor outputs, temperature and relative humidity. Two hidden layers were used in this algorithm. These layers are responsible for assigning and optimizing weights to each connection and adding a bias term to its sum resulting in an equation demonstrated in Equation 4 where W_1 represents the assigned weights, X_n represents input variables, B represents the added bias and $f(x)$ represents the ReLU activation function. In a two-layer hidden layer in the case of this model, this process is carried over to the second hidden layer where a new set of weights are assigned, and a new set of biases added. An activation function is then applied to the resulting linear equation before moving on to the next hidden layer. A rectifier linear unit (ReLU) activation function was used in this model and programmed in these hidden layers. The result of these computations is sent to the output layer of the model.

True concentrations determined by the PDM is used as the node on the output layer. The dataset was randomized and split into training and testing datasets. The 70-30 train split method was used. Thus, 70% of the dataset was used as training set which trains the algorithm on prediction and 30% was used as testing dataset which evaluates the performance of the algorithm. The mean squared error (MSE) was used as the measure of the model performance.

$$\mathrm{Z} = f(W_1X_1 + W_2X_2 + W_3X_3 \ldots . W_nX_n + B) \qquad \text{Equation 4}$$

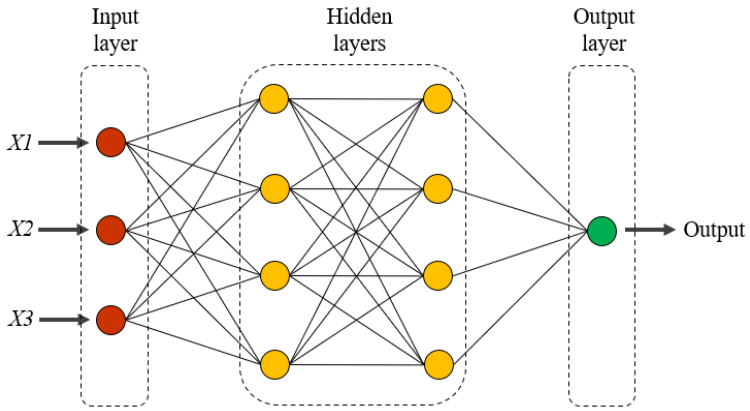

Figure 2. Structure of the Artificial Neural Network architecture

3.4. RANDOM FOREST

The random forest regressor algorithm is a supervised machine learning model that uses an ensemble of decision trees to solve regression problems. Random forest models combine the multitude of decision trees each of which train inputs to their respective outputs to predict the outputs. Each decision tree begins with the root node which splits into internal nodes through a set of branches repeatedly until a leaf node is obtained and a decision made.

A sample decision tree regressor is shown in Figure 3 to demonstrate the sequence of this algorithm. The 70-30 train test split is applied in this algorithm and a bootstrapped dataset is created from the training dataset. This method involves randomly sampling a given number of variables from the dataset for each decision tree to obtain a multitude of trees. As can be seen in the sample calibration tree in Figure 3 (a), the tree starts with root node assigned with coal dust concentration being the strongest predictor. This node is split in to branches with the condition that the concentration is greater than 2.0 mg/m^3. If this condition is satisfied, the algorithm follows the path of determining the

concentration to be 2.5 mg/m^3. On the other hand, the algorithm follows the path to the next node if concentration is below 2.0 mg/m^3. While this explains the sequence of the decision tree, these steps are repeated in several interior nodes until the algorithm reaches the leaf node when a decision is made on the concentration prediction considering temperature and RH variables.

An ensemble of decision tree is developed based on this algorithm, trained using the same data, and the results of all models combined in an ensemble learning process. To determine the final random forest prediction, the results of all the trees used in the model are combined as can be seen in Figure 3 (b). This model makes concentration predictions based on the outputs of all decision trees involved in the training and ultimately determines the predicted concentration as the mean concentration from all the trees. The mean squared error (MSE) criterion is calculated to evaluate the model performance.

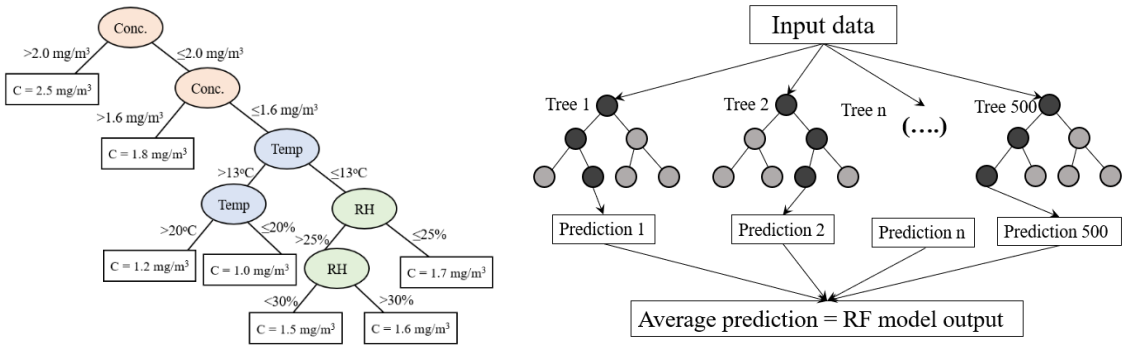

(a) Random forest decision tree structure

(b) Random forest architecture

Figure 3. Random forest regressor algorithm representation

3.5. SUPPORT VECTOR MACHINES

This algorithm is a supervised method that predicts discrete values similar in principle to the categorical SVM. Similar to linear regression principles, the support vector regressor finds the line of best fit through the datapoints, and in the case of a higher dimension data, hyperplane of best fit. However, unlike linear regression which minimizes the sum of squared errors between datapoints and the plane of best fit, the objective of the SVR is to establish the line of best fit within a threshold error value.

The SVR algorithm does this by minimizing the objective function shown in Equation 5 which minimizes the error between the line of best fit and the margins. The corresponding error term in this case is then considered as constraints shown in Equation 6 where the absolute error is set to less than or equal to the acceptable error for our model. However, there is the likelihood of some datapoints falling outside the constraint margins. To account for these points in the generation of the optimum hyperplane, a slack variable seen as the second term in Equation 5 is added to reduce the error margin as much as possible.

It should be noted that the difference between the hyperplane of best fit and datapoints outside the error margins introduces errors to the algorithm. As a result, the deviations are added to the new objective function and are minimized to account for these data points and reduce error margins as much as possible. This algorithm maximizes the prediction of coal dust concentration within an acceptable margin of error of 5%. The 70-30 train test split is applied for training and testing the model which is evaluated using MSE to measure the model performance.

$$\text{MIN} = \frac{1}{2}\left|\left|w\right|\right|^2 + C\sum_{i=1}^{n}|\xi_i| \qquad \text{Equation 5}$$

$$|y_i - w_i x_i| \leq \varepsilon + |\xi_i| \qquad \text{Equation 6}$$

4. RESULTS

The results of the sensors' evaluation and the performance of calibration models were discussed to compare the performance of the five calibration models used in this study. The performance of the sensors involved were also evaluated to determine the feasibility of the use of these low-cost PM sensors for coal dust monitoring using the calibration models discussed in this study.

4.1. PRELIMINARY DATA ANALYSIS

The raw data obtained from the experiments are presented in Figure 4 (a) and (b). These figures show the time series data of the raw sensor outputs recorded over the testing period for all 6 low-cost sensors and the 2 reference monitors. The corresponding time series for relative humidity and temperature conditions are shown on separate plots in Figure 4 (b) to visualize the trend of RH and temperature conditions over the testing period. The outputs of these sensors would be later corrected using calibration models developed in this study. It should be noted that the data shown here represent the results from several days of monitoring stitched together. Changes in outputs and the presence of spikes in this data are the results of changes in concentration within the wind tunnel

throughout the testing period. The performance of the calibration models on these data are discussed in subsequent sections.

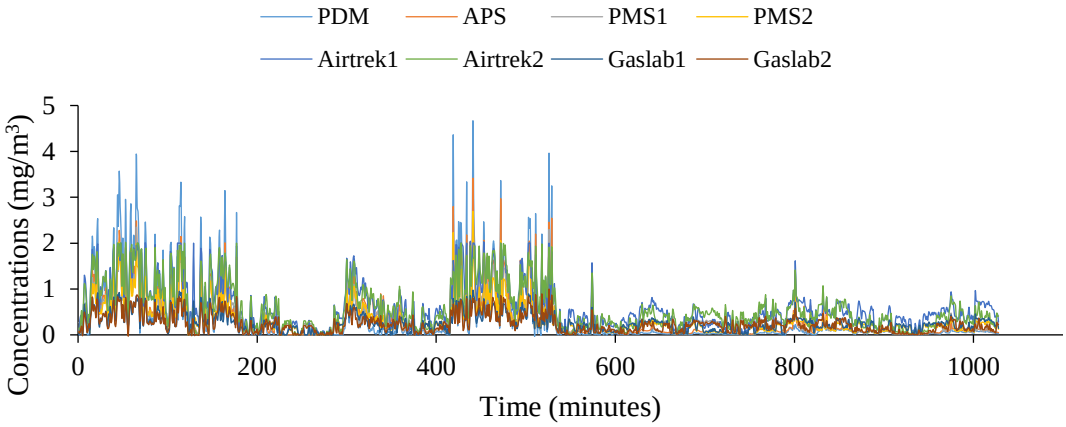

(a)

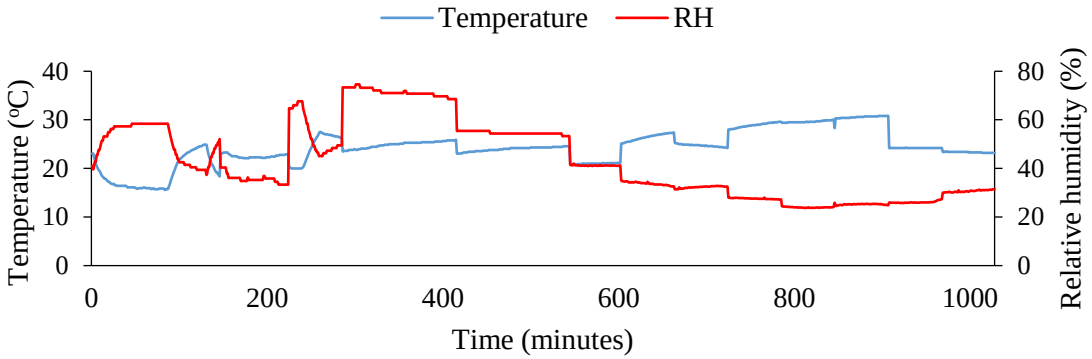

(b)

Figure 4. Time data series results of coal dust concentrations, temperature and relative humidity over time. (a) time data series comparing the responses of the reference monitors and low-cost PM sensors. This figure shows 1028 total minutes (17.2 hours) of monitoring data (b) Time series data of relative humidity and temperature conditions over the testing period

4.2. SIMPLE LINEAR REGRESSION

The results of the simple linear regression calibration models are shown in Figure 5 and Figure 6. Figure 5 shows a pairwise correlation of between all the sensors and monitors involved in this study using scatter plots with correlation coefficient for each scatter plot displayed. These plots were generated using the uncalibrated data from the sensors to understand the nature of outputs generated by the sensors relative to the reference monitors. It is understood from these results that all the sensors involved have a positive response to concentration changes with correlation values ranging from 0.84 to 0.95. In general, the response of the sensors agreed better with the reference monitors as compared with results from a previous study [35]. This strong performance is linked to the considerably higher number of datapoints used in this study. Higher number of datapoints for regression has been demonstrated to statistically increase model performance. It was, however, observed that while the two PMS sensors had an entirely linear response with 0.95 correlation coefficients, the Airtrek and Gaslab sensors had significantly lower correlation with the PDM. The lower correlation was caused by their limited upper concentration limits of 2.0 mg/m^3 and 1.0 mg/m^3 respectively for the Airtrek and Gaslab sensors giving their data an exponential appearance. These results agree with previous a previous study which pointed out the measurement limitations of the Gaslab and Airtrek sensors [35].

The simple linear regression calibration model developed to correct the sensors' response was trained with 70% of the dataset and tested using the remaining 30%. The model was trained using the ordinary least square regression method to generate the simple linear regression model. Each model built for each sensor is of the format

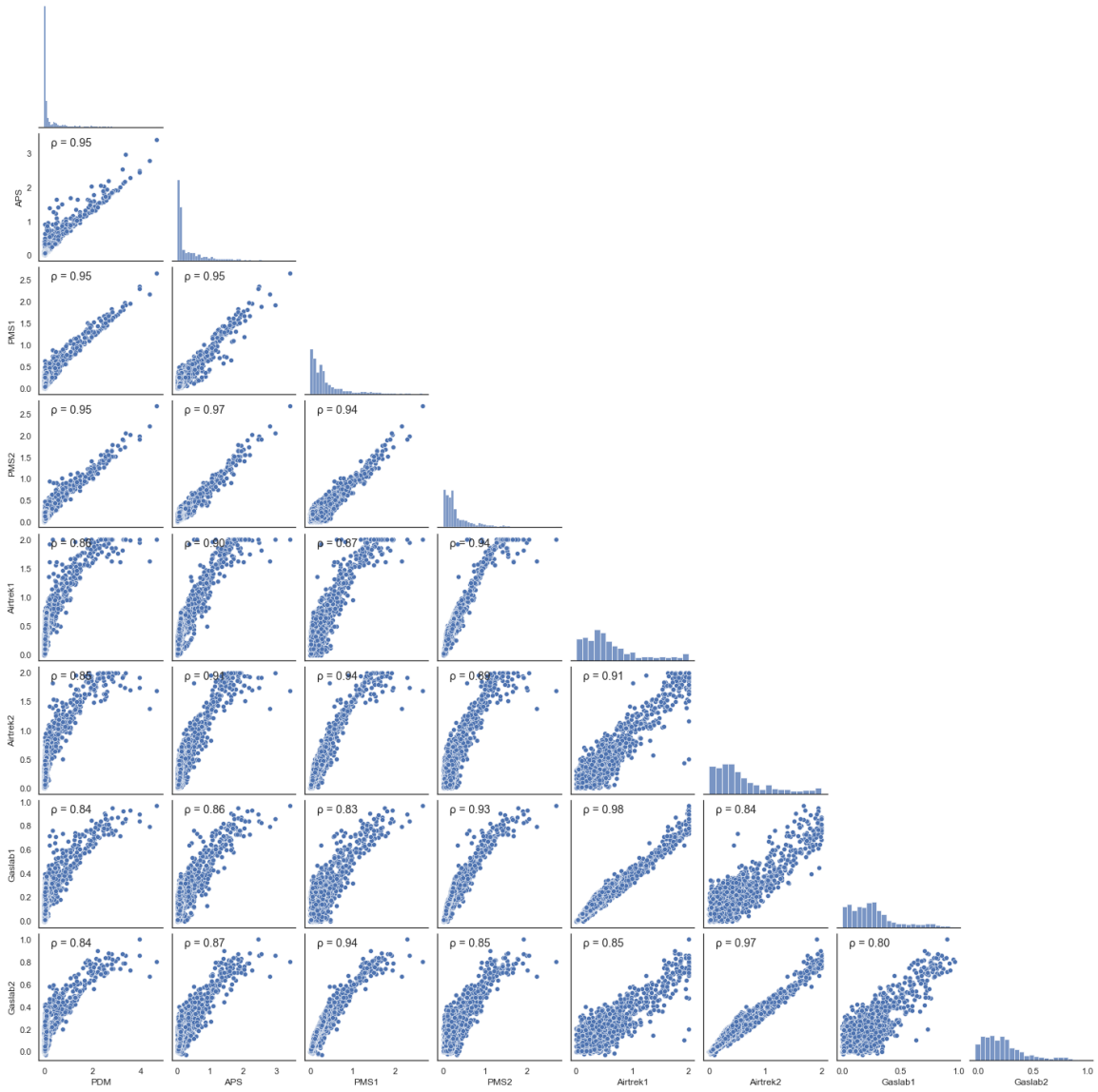

Figure 5. Pairwise correlation among the six sensors and PDM and APS using the 70% training dataset. Both x and y axes represent sensors' and monitors' concentration outputs in mg/m^3

discussed in Section 3.1 using coefficients of the sensor outputs, slope of the calibration curve and the intercept. The results shown in Figure 6 compares the actual and predicted values generated from this model using the testing dataset with the correlation coefficient for each model shown on the plots. These were compared with the uncalibrated responses

from the sensors. In these results, the actual values are represented by the PDM concentrations shown on the x axes while the predicted values are indicated by the sensor corrected concentrations shown on the y axes. The Pearson correlation coefficient was used to evaluate these models over coefficient of determination because while the later is used to determine the correlation of the model, the Pearson correlation determines the strength and direction of the linear relationship. These results show little improvement in the sensors' performance with little to no improvement in correlation values compared to the uncalibrated performance.

A striking drawback observed in these models is that for models whose y-intercept happened to be negative, as in Figure 6 (b), (c), (e) and (f), the model predicted negative concentrations for PDM concentrations lower than the x-intercept. Another important limitation to using the simple linear regression model is its inability to account for multiple independent variables.

4.3. MULTIPLE LINEAR REGRESSION

The influence of relative humidity and temperature was analyzed and accounted for in this multiple linear regression model developed to calibrate the low-cost PM sensors. This was expected to yield better performance compared with the simple linear regression method since temperature and relative humidity have shown a level of influence on optical PM sensors' outputs. The results from these models are shown in Figure 7 comparing the performance of the MLR calibration model to the SLR model. An MLR calibration model was generated for each sensor in the format shown in Section 3.2,

Equation 3. This model is trained using 70% of the sensors' dataset and tested using the remaining 30% of the dataset.

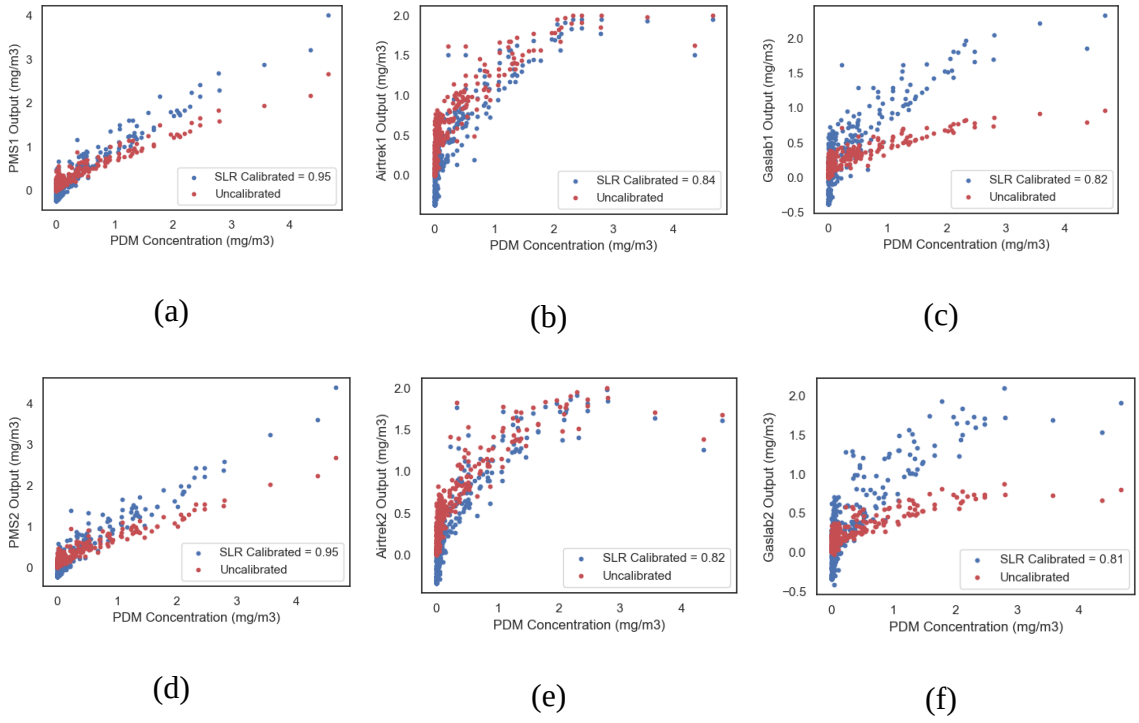

Figure 6. Simple linear regression calibration model showing predicted calibrated sensor outputs against PDM concentration. The sensors represented in this figure are (a) PMS1 (b)Airtrek1 (d) Gaslab2 (a) PMS2 (e)Airtrek2 (f) Gaslab2

After accounting for relative humidity and temperature, the multiple linear regression models calibrated the low-cost PM sensors slightly better than the simple linear regression models. Evaluating the performance of the model on the 30% data unseen by the model revealed an increase in Pearson correlation coefficient negligibly by 0 to 3% among the sensors as compared with the SLR models and obtained moderate MSE values from 0.20 to 0.33 mg/m^3. This evaluation compared the actual concentrations read by the PDM against predicted concentrations based on sensor raw

output which have been corrected by the MLR model. These results suggest that accounting for temperature and relative humidity correction in linear regression models to calibrate low-cost sensors can improve the performance of the sensors depending on how much influence temperature and RH has on the sensor's performance. This confirms the influence of temperature and RH on the performance on the low-cost PM sensors making them necessary to be included in sensor calibration models even though the performance increase is just marginal using MLR models. However in this case, it was found that temperature and RH has minimal impact on the PMS sensors' performance which explains why the performance only increased slightly accounting for temperature and RH. It can be seen from the results that the performance increase was relatively higher for the Airtrek and Gaslab sensors which had exponential responses suggesting that those sensors are influenced more by temperature and RH. The results also showed that the exponential response in the Airtrek and Gaslab data was unable to be corrected by the MLR model. Moreover, the model predicted negative concentrations for concentrations lower than the x-intercept of the plane of best fit.

4.4. RANDOM FOREST REGRESSOR

The random forest regressor (RFR) calibration model significantly outperformed both the simple and multiple linear regression models for all six sensors. The results of the RFR prediction model are shown in Figure 8 comparing prediction performance to the multiple linear regression model. This model emerged as one of the best performing calibration models explored in this study showing an improved Pearson correlation of 0.97 for both PMS1 and PMS2 with MSE of 0.02 mg/m^3. The Airtrek sensors had

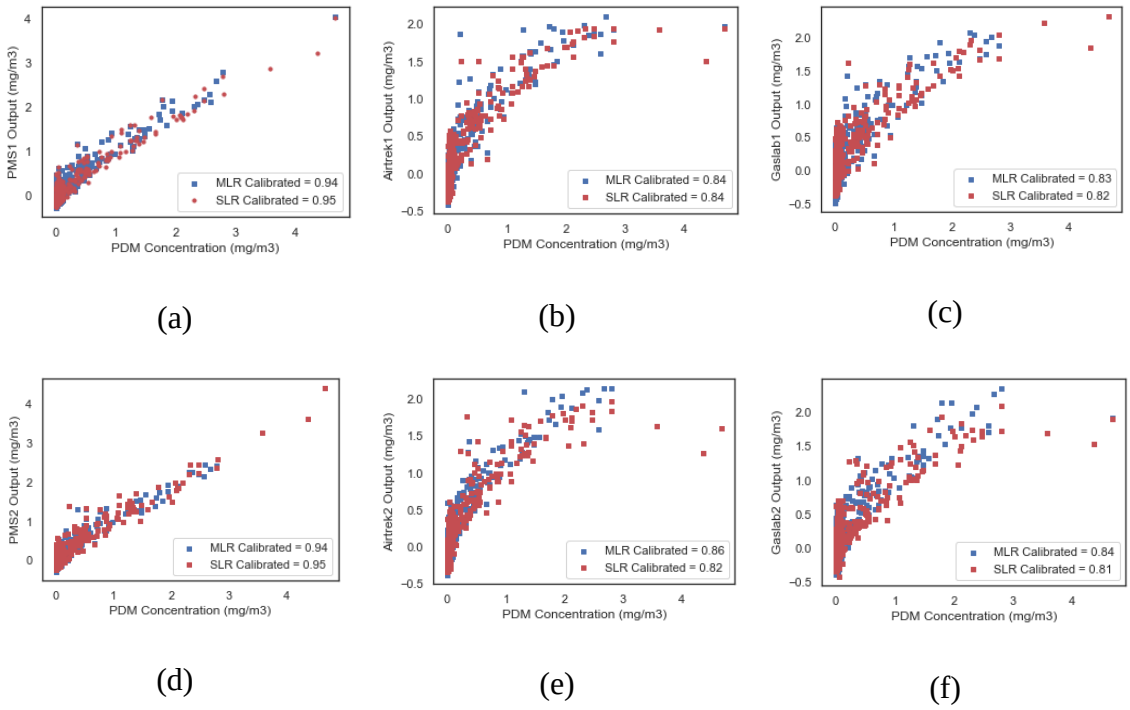

Figure 7. MLR results showing its comparison with the SLR model

improved correlations of 0.89 and 0.91 for Airtrek1 and Airtrek2 respectively with MSE of 0.07 mg/m^3 for both sensors. The Gaslab sensors also had improved correlations of 0.93 and 0.92 for Gaslab1 and Gaslab2 respectively with MSE values of 0.04 mg/m^3 and 0.06 mg/m^3. As can be seen from Figure 8, the poor performance of the regression models at lower concentrations leading to the prediction of negative concentrations was remarkably corrected by the RFR model showing a remarkable improvement in correction performance for all 6 sensors indicated by the Pearson correlations shown on the plots. Moreover, a near perfect 1:1 linear relationship was developed even for sensors which initially had exponential curves. In the results of this model, it was observed that the RFR calibration values were more condensed around the calibration curve, indicating a better fitting than the regression models. This is even more significant in the Gaslab and

Airtrek sensors which initially have exponential looking data. These findings agree with other studies which demonstrated the potential of the RF models to outperform regression models. For example, a study improved the correlation between HK-B3 PM sensor and the MicroPEM monitor from 0.87 using linear regression to 0.98 using the RFR model (Y. Wang et al., 2019). This was not surprising due to the random forest model's known ability to balance datasets with numerous variables and variations making it suitable for complicated models.

The random forest can potentially be used as the calibration model of choice for low-cost PM sensors for coal dust monitoring as demonstrated in these results. However, the model can be complicated by the multiple parameters that need to be considered in building the model. If incorrect values are used, it will have a direct impact on the model performance. In this study, the hyperparameters were tuned using Scikit-Learn's RandomizedSearchCV method performing a 5-Fold cross validation with each iteration. In each iteration, a different combination of model settings was used in search of the optimum hyperparameters. The optimum combination of hyperparameters obtained from this search was then used to train the training dataset to obtain these results. It was realized in this study that optimum hyperparameters included 500 number of trees, 'auto' number of features in consideration at every split, a maximum number of levels allowed at each decision tree of 100, minimum sample number to split at a node to be 3, a minimum sample leaf of 3 and a 'true' bootstrapped method to be used to sample data points.

The random forest calibration model structure threw more light on the relative importance of the explanatory variables evaluated in this study. For these low-cost PM

sensors, the coal dust concentration response from the sensors emerged as the most important predictor variable in the calibration followed by the RH condition. The factor that least affects the decision tree was the temperature variables. This was determined in the model by examining the rate of change of MSE when each variable is permuted in a decision tree. The decision trees in this model were built based on the importance of each explanatory variable to the prediction of the true concentration. Mean square error was then calculated each time an explanatory variable is included in the bootstrapped dataset. The importance of each parameter was determined by calculating the rate of increase in mean squared error during bootstrapping. For a variable that has strong influence in the prediction of the true concentration, permuting those variables in the model increases the MSE significantly.

4.5. ARTIFICIAL NEURAL NETWORK

The ANN model used in this study to calibrate the sensors compared well with the RF model achieving similar results. Similar to the RF model, the ANN model significantly outperformed the simple and multiple linear regression models. The model was able to correct the negative concentrations predicted by the regression models while also optimizing the 1:1 relationship between the PDM and sensors. In the results shown in Figure 9, the prediction performance of the ANN model is compared with the RFR model side by side. Together these two models were the best performing models among all the models used in this study having similar Pearson correlation. Even though the ANN model slightly outperformed the RF model by 1% and 2% respectively for PMS1

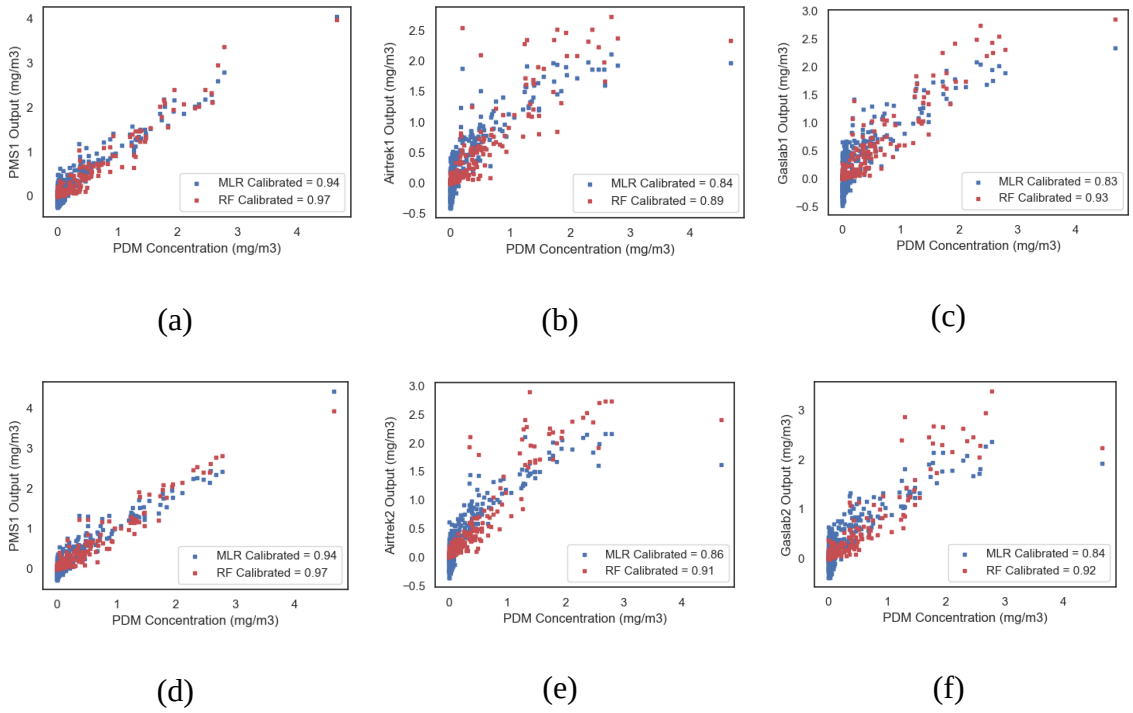

Figure 8. RFR model performance for low-cost PM sensors using the testing dataset. Correlation plots show actual data values (PDM concentration) against predicted values which is considered sensor corrected outputs (Sensor outputs) for all six sensors. Each plot shows model performances of each model using pearson correlation coefficient. The sensors represented in this figure are (a) PMS1 (b)Airtrek1 (d) Gaslab2 (a) PMS2 (e)Airtrek2 (f) Gaslab2

and Airtrek1, the Pearson correlation for the remaining 4 sensors remained the same for both models. It is therefore possible to consider ANN as the best performing model for low-cost PM sensor calibration for coal dust monitoring even though it can be interchanged with RF model due to the closeness of their performance.

The parameters used in this ANN model determined the results of this model. Tuning the hyperparameters of the layers involved in the ANN model revealed the optimum learning rate to be 0.1 and a batch size of 30 with 60 epochs using mean squared error as the loss function. With three input values at the input layer, the values were passed to an optimum two-layer hidden layer each with 10 neurons. Finally, the

output layer contained one neuron which contained the predicted coal dust concentration output. These parameters are essential to be properly deployed as it ensures model accuracy as well as avoiding suboptimal model performance. For example, running the ANN model used in this calibration application for more than 60 epochs only becomes computationally expensive but offers insignificant improvement in model performance.

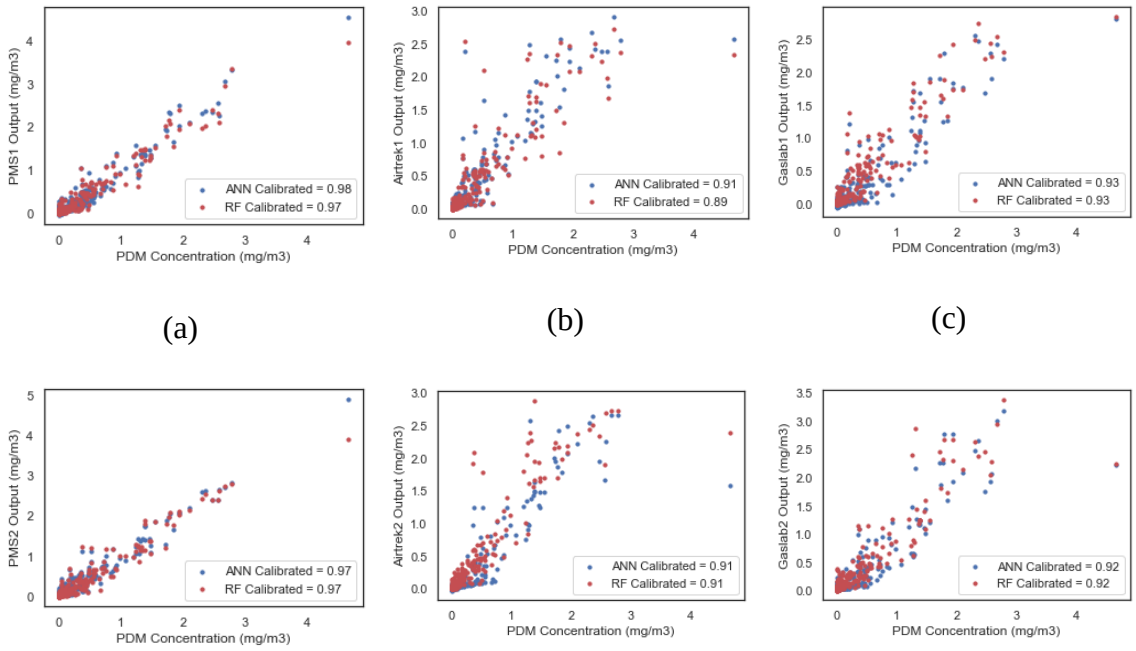

Figure 9. Results of ANN models showing calibrated sensor outputs against PDM concentration comparing the ANN and RFR models. The sensors represented in this figure are (a) PMS1 (b)Airtrek1 (d) Gaslab2 (a) PMS2 (e)Airtrek2 (f) Gaslab2

The results discussed in this section were as a result of applying the optimum hyperparameters in training the training dataset and tested using the testing dataset which made up 30% of the entire data. The model was evaluated using the Pearson correlation coefficient which showed values of 0.98 ad 0.97 for PMS1 and PMS2 respectively. These

results closely compared with similar studies which applied ANN to calibrate the Plantower PMS7003 sensor improving its R^2 from 0.86 to 0.97 [27].

4.6. SUPPORT VECTOR MACHINES

The support vector machine model had the worst calibration performance among models tested beside the simple and multiple linear regression models. Since the linear regression models have the drawback of not fitting no-so-linear dataset with high accuracy, the SVM model was expected to significantly correct the outputs of the sensors. However, traits of inaccuracies still remained in the predictive evaluation. The results for the SVM model are displayed in Figure 10 showing scatter plots of PDM concentrations against predicted calibrated sensors outputs compared with the ANN model results to highlight the significant difference in performance of these two models. Even the SVM model results showed minimal improvement in sensor performance for the Airtrek and Gaslab sensors, it could not perform better than any other model tested for the PMS sensors after they were calibrated. The Airtrek sensors' correlation increased from 0.84 and 0.82 to 0.86 and 0.89 respectively for Airtre1 and Airtrek2 corresponding with MSE of 0.30 mg/m^3 and 0.29 mg/m^3. The gaslab sensors on the other hand, recorded an increase in correlations from 0.82 and 0.81 to 0.85 and 0.88 with MSE of 0.32 mg/m^3 and 0.30 mg/m^3. However, the Pearson correlation for both PMS1 and PMS2 had no improvement having a Pearson correlation of 0.95 with MSE value of 0.20 mg/m^3. Aside from the correlations, the MSE values generated by this model were significantly higher as compared with the RFR and ANN models.

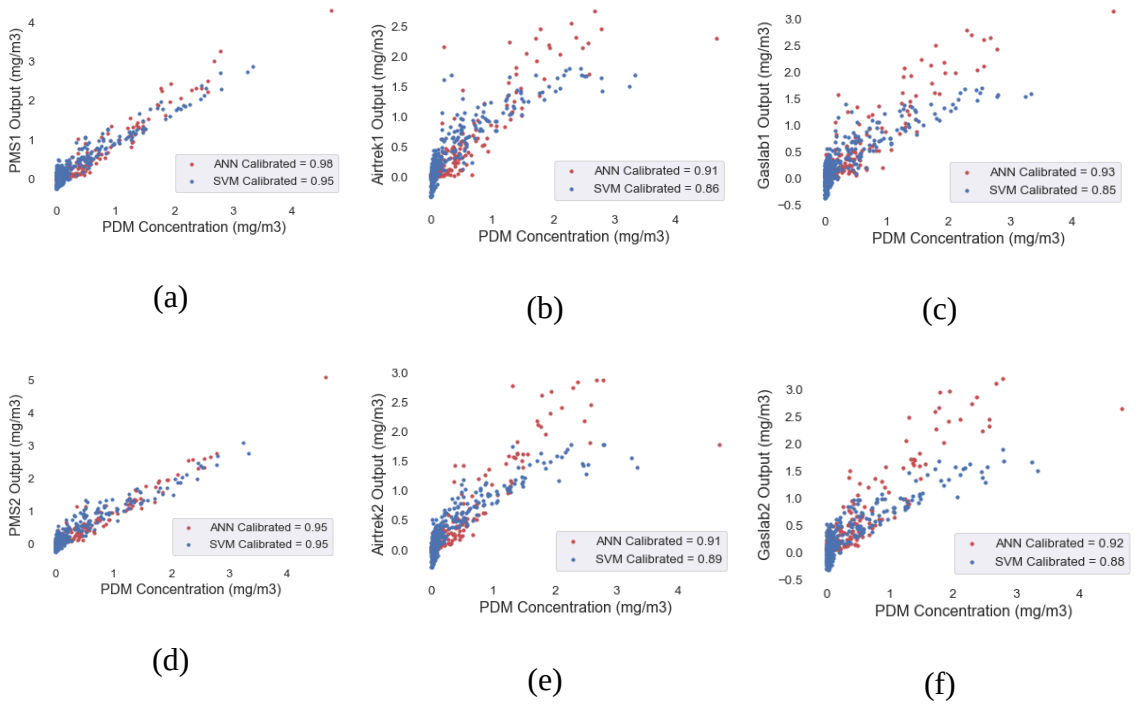

Figure 10. Model performance of SVM model compared with ANN model testing datasest comparing PDM concentrations with predicted sensor calibration outputs. The sensors represented in this figure are (a) PMS1 (b)Airtrek1 (d) Gaslab2 (a) PMS2 (e)Airtrek2 (f) Gaslab2

A detailed analysis of the results showed the existence of all the drawbacks of the linear regression models. First, it was observed that even after tuning the model hyperparameters and applying the optimum parameters, the SVM model predicted a significant number of negative concentrations for most of the sensors. This is due to the SVM model's plane of best fit having a negative intercept on the PDM concentration. When this happens, lower concentrations are predicted to be negative which can be misleading. In our case, this phenomenon was caused primarily by the nature of the raw dataset having negative y-intercept values. Secondly, a level of exponential relationship was observed over the desired linear relationship between the predicted sensor outputs and the PDM concentrations for the Airtrek and Gaslab sensors. These results suggest the

SVM model's inability to correct the portions of the sensors' dataset that were oddly correlated even though better performances have been observed in other studies [32].

5. CONCLUSION

Overexposure to respirable coal mine dust in underground coal mines has been linked to the recent resurgence of coal workers' pneumoconiosis. Effective real time personal coal dust monitoring in underground coal mines will inform timely overexposure detection to allow control measures to be implemented. However, the currently used PDM3700 personal coal dust monitor is too expensive for all miners to wear which hinders most miners from knowing their exposure levels. Low-cost PM sensors present the technology to measure personal exposure levels with high special and temporal resolution due to their low cost, small size and light weight. Nevertheless, these sensors require powerful calibration to ensure their accuracy over long term deployments. Even though these sensors have been previously calibrated with simple linear regression models, a more accurate calibration model is required for improved accuracy. This study therefore compared the performance of five machine learning algorithms on calibrating the low-cost PM sensors for coal dust monitoring.

Sensor evaluation experiments were performed within a wind tunnel. Two PMS5003 low-cost PM sensors, two Airtrek sensors and two Gaslab sensors were positioned in close proximity within the wind tunnel while the coal dust concentration varied between 0 and 4 mg/m^3. These tests were performed using the PDM and APS monitors as reference monitors. Temperatures during this period ranged from 20 degrees

Celsius to 31 degrees Celsius while the RH ranged from 24 % to 44 %. The data collected from this experiment was used to train the machine learning models to correct sensor outputs to depict accurate coal dust concentrations. The models used include the simple linear regression, multiple linear regression, random forest regressor, artificial neural network, and support vector machine.

Based on the results from this study, linear regression models significantly underperformed the other models, with ANN being the best performing model used. After the sensors were calibrated using the simple linear regression model, the correlations for the sensors ranged from 0.81 to 0.95 with the PMS sensors being the best performing sensors having Pearson correlation of 0.95 each. The MLR model surprisingly only improved the performance of the sensors slightly with a 0 to 3% increase in correlation among the sensors. The application of the RFR, ANN and SVM models showed significant levels of sensor performance improvement. The SVM model improved the linearity of the sensors with respect to the PDM achieving correlation of 0.85 to 0.95 between the sensors. However, it maintained a high MSE of 0.20 mg/m^3 to 0.32 mg/m^3 which were about 10 times higher than the MSE from the RFR and ANN models. The RFR model achieved an impressive performance with improved correlation of 0.97 for both PMS1 and PMS2, and 0.89 and 0.91 signifying a 5% and 9% improvement by Airtrek1 and Airtrek2 respectively. The Gaslab sensors also had an 11% increase in their correlation with the PDM to 0.93 and 0.92. Finally, the ANN model showed similar performance with the RFR model in terms of correlation between calibrated outputs and PDM concentrations. The ANN had similar correlation values but outperformed the RFR model in two sensors where the PMS1 showed a correlation of

0.98 and the Airtrek1 had a correlation of 0.91 indicating a 1% and 2% improvement over the RFR model.

These machine learning algorithms have demonstrated excellent calibration potentials for low-cost PM sensors in coal dust monitoring. This study has reiterated the potentials for low-cost PM sensors to be used for personal coal dust monitoring in mines supplementing the PDM. When deployed, timely interventions to coal dust overexposure in mines will be feasible at all locations within the mine which will contribute to protecting the health of miners. While these potentials have been extensively studied, a framework for the application of low-cost PM sensors in mines is needed to direct the application and regulation of this technology in mines.

REFERENCES

[1] A. S. Laney and M. D. Attfield, "Coal workers' pneumoconiosis and progressive massive fibrosis are increasingly more prevalent among workers in small underground coal mines in the United States," *Occup Environ Med*, vol. 67, no. 6, pp. 428–431, 2010, doi: 10.1136/oem.2009.050757.

[2] H. Liu *et al.*, "Identification and classification of high risk groups for Coal Workers' Pneumoconiosis using an artificial neural network based on occupational histories: A retrospective cohort study," *BMC Public Health*, vol. 9, pp. 1–8, 2009, doi: 10.1186/1471-2458-9-366.

[3] R. A. Cohen *et al.*, "Lung pathology in U.S. coal workers with rapidly progressive pneumoconiosis implicates silica and silicates," *Am J Respir Crit Care Med*, vol. 193, no. 6, pp. 673–680, 2016, doi: 10.1164/rccm.201505-1014OC.

[4] D. J. Blackley, C. N. Halldin, and A. Scott Laney, "Continued increase in prevalence of coal workers' pneumoconiosis in the United States, 1970-2017," *American Journal of Public Health*, vol. 108, no. 9. American Public Health Association Inc., pp. 1220–1222, Sep. 01, 2018. doi: 10.2105/AJPH.2018.304517.

[5] B. C. Doney *et al.*, “Respirable coal mine dust in underground mines, UnitedStates, 1982-2017.pdf,” *American journal of Insustrial Medicine*, vol. 62, pp. 478–485, 2019.

[6] MSHA, “Major Provisions and Effective Dates MSHA ’ s Final Rule to Lower Miners ’ Exposure to Respirable Coal Mine Dust,” vol. 2014, pp. 1–2, 2014.

[7] U. States and E. Protection, “Consultation on EPA’s Draft Integrated Rev Plan for the NAAQS for PM (EPA-CASAC-10-004),” 2009.

[8] US-EPA, “DRAFT Roadmap for Next Generation Air Monitoring,” no. March, p. 27, 2013.

[9] R. Williams *et al.*, “EPA Sensor Evaluation Report,” no. May, p. 40, 2014, [Online]. Available: http://www.epa.gov/research/airscience/docs/sensor-evaluation-report.pdf%5Cnhttp://cfpub.epa.gov/si/si_public_record_report.cfm?dirEntryId=277270

[10] M. Badura, P. Batog, A. Drzeniecka-Osiadacz, and P. Modzel, “Evaluation of low-cost sensors for ambient PM2.5 monitoring,” *J Sens*, vol. 2018, 2018, doi: 10.1155/2018/5096540.

[11] Z. Al Barakeh, P. Breuil, N. Redon, C. Pijolat, N. Locoge, and J. P. Viricelle, “Development of a normalized multi-sensors system for low cost on-line atmospheric pollution detection,” *Sens Actuators B Chem*, vol. 241, pp. 1235–1243, 2017, doi: 10.1016/j.snb.2016.10.006.

[12] L. J. M. Jon C. Volkwein, Robert P. Vinson and and S. E. Mischler. Donald P. Tuchman, “Performance of a New Personal Respirable Dust Monitor for Mine Use,” *Report of Investigations 9663, National Institute for Occupational Safety and Health, Pittsburgh Research Laboratory*, pp. 1–25, 2004, [Online]. Available: papers://d0b7ba82-564e-41a5-892d-096be28ddf10/Paper/p192

[13] M. Usman, A. Douglas, and S. Gillies, “Real-time monitoring of DPM , airborne Dust and correlating Elemental Carbon measured by two methods in underground mines in USA,” in *15th North American Mine Ventilation Symposium*, 2015, pp. 1–7.

[14] N. A. Amoah, G. Xu, Y. Wang, J. Li, Y. Zou, and B. Nie, “Application of low-cost particulate matter sensors for air quality monitoring and exposure assessment in underground mines: A review,” *International Journal of Minerals, Metallurgy and Materials*, vol. 29, no. 8, pp. 1475–1490, 2022.

[15] K. E. Kelly *et al.*, “Ambient and laboratory evaluation of a low-cost particulate matter sensor,” *Environmental Pollution*, vol. 221, pp. 491–500, 2017, doi: 10.1016/j.envpol.2016.12.039.

[16] L. Spinelle, M. Aleixandre, and M. Gerboles, *Protocol of evaluation and calibration of low-cost gas sensors for the monitoring of air pollution*, vol. 68. 2013. doi: 10.2788/9916.

[17] D. M. Holstius, A. Pillarisetti, K. R. Smith, and E. Seto, "Field calibrations of a low-cost aerosol sensor at a regulatory monitoring site in California," *Atmos Meas Tech*, vol. 7, no. 4, pp. 1121–1131, 2014, doi: 10.5194/amt-7-1121-2014.

[18] S. Kelleher, C. Quinn, D. Miller-Lionberg, and J. Volckens, "A low-cost particulate matter (PM2.5) monitor for wildland fire smoke," *Atmos Meas Tech*, vol. 11, no. 2, pp. 1087–1097, 2018, doi: 10.5194/amt-11-1087-2018.

[19] A. Polidori, V. Papapostolou, and H. Zhang, "Laboratory Evaluation of Low-Cost Air Quality Sensors," no. August, 2016, [Online]. Available: http://www.aqmd.gov/docs/default-source/aq-spec/protocols/sensors-lab-testing-protocol6087afefc2b66f27bf6fff00004a91a9.pdf?sfvrsn=2

[20] T. Sayahi, A. Butterfield, and K. E. Kelly, "Long-term field evaluation of the Plantower PMS low-cost particulate matter sensors," *Environmental Pollution*, vol. 245, pp. 932–940, 2019, doi: 10.1016/j.envpol.2018.11.065.

[21] Y. Wang *et al.*, "Calibration of a low-cost PM2.5 monitor using a random forest model," vol. 6826, 2015, doi: 10.1080/02786826.2015.1100710.

[22] T. Zheng *et al.*, "Field evaluation of low-cost particulate matter sensors in high- and low-concentration environments," *Atmos Meas Tech*, vol. 11, no. 8, pp. 4823–4846, 2018.

[23] B. Feenstra *et al.*, "Performance evaluation of twelve low-cost PM2.5 sensors at an ambient air monitoring site," *Atmos Environ*, vol. 216, no. February, p. 116946, 2019, doi: 10.1016/j.atmosenv.2019.116946.

[24] A. Polidori, V. Papapostolou, B. Feenstra, and H. Zhang, "Field Evaluation of Low-Cost Air Quality Sensors Field Setup and Testing Protocol," no. January, 2017, [Online]. Available: http://www.aqmd.gov/aq-spec/evaluations/field

[25] A. Cavaliere *et al.*, "Development of low-cost air quality stations for next generation monitoring networks: Calibration and validation of PM2.5 and PM10 sensors," *Sensors (Switzerland)*, vol. 18, no. 9, pp. 1–20, 2018, doi: 10.3390/s18092843.

[26] P. Nowack, L. Konstantinovskiy, H. Gardiner, and J. Cant, "Machine learning calibration of low-cost NO2 and PM10 sensors: Non-linear algorithms and their impact on site transferability," *Atmos Meas Tech*, vol. 14, no. 8, pp. 5637–5655, Aug. 2021, doi: 10.5194/amt-14-5637-2021.

[27] C. C. Chen *et al.*, “Calibration of Low-Cost Particle Sensors by Using Machine-Learning Method,” in *2018 IEEE Asia Pacific Conference on Circuits and Systems, APCCAS 2018*, Jan. 2019, pp. 111–114. doi: 10.1109/APCCAS.2018.8605619.

[28] Y. Wang, Y. Du, J. Wang, and T. Li, “Calibration of a low-cost PM2.5 monitor using a random forest model,” *Environ Int*, vol. 133, Dec. 2019, doi: 10.1016/j.envint.2019.105161.

[29] L. O. H. Wijeratne, D. R. Kiv, A. R. Aker, S. Talebi, and D. J. Lary, “Using machine learning for the calibration of airborne particulate sensors,” *Sensors (Switzerland)*, vol. 20, no. 1, Jan. 2020, doi: 10.3390/s20010099.

[30] N. Zimmerman *et al.*, “A machine learning calibration model using random forests to improve sensor performance for lower-cost air quality monitoring,” *Atmos Meas Tech*, vol. 11, no. 1, pp. 291–313, 2018, doi: 10.5194/amt-11-291-2018.

[31] M. Si, Y. Xiong, S. Du, and K. Du, “Evaluation and calibration of a low-cost particle sensor in ambient conditions using machine-learning methods,” *Atmos Meas Tech*, vol. 13, no. 4, pp. 1693–1707, Apr. 2020, doi: 10.5194/amt-13-1693-2020.

[32] W. C. V. Wang, S. C. C. Lung, and C. H. Liu, “Application of machine learning for the in-field correction of a PM2.5 low-cost sensor network,” *Sensors (Switzerland)*, vol. 20, no. 17, pp. 1–19, Sep. 2020, doi: 10.3390/s20175002.

[33] J. C. Volkwein *et al.*, “Laboratory and Field Performance of a Continuously Measuring Personal Respirable Dust Monitor,” *US Department of Health and Human Services, Public Health Service, Centers for Disease Control and Prevention, National Institute for Occupational Safety and Health, Cincinnati, OH*, pp. 1–55, 2006.

[34] TSI Inc., “AERODYNAMIC PARTICLE SIZER MODEL 3321,” 2017. [Online]. Available: www.tsi.com

[35] N. A. Amoah, G. Xu, A. Kumar, and Y. Wang, “Calibration of low-cost particulate matter sensors for coal dust monitoring,” *Science of The Total Environment*, 2023.

IV. OPTIMIZED CANOPY AIR CURTAIN DUST PROTECTION USING A TWO-LEVEL MANIFOLD AND COMPUTATIONAL FLUID DYNAMICS

ABSTRACT

Prolonged exposure to high concentrations of respirable coal mine dust causes coal workers' pneumoconiosis and silicosis. Underground coal mine roof bolter operators are more prone to elevated exposure to coal and silica dust. The canopy air curtain (CAC) was developed by NIOSH to protect roof bolter operators from the exposure. The CAC supplies filtered air over the breathing zone of the operator. This dilutes the high coal dust concentrations and provides for an impenetrable air curtain. Many studies have been carried out to improve CAC efficiency. However, field test has shown variable dust control efficiencies indicating rooms to further improve due to the non-uniform airflow distribution across the plenum and ineffective perimeter flow. This study therefore redesigns the CAC with optimized flow distribution that effectively protects roof bolters from coal dust exposures. The Simplex Evolutionary Operational (EVOP) optimization algorithm was applied to optimize the configuration of the new CAC. Computational fluid dynamics (CFD) simulations are run at each iteration of the algorithm. The combination of these methodologies led to the optimization of the uniformity of airflow distribution across the plenum to achieve the best possible uniformity. A lab experiment using a physical model of the optimized CAC was used to validate the CFD model and confirm the ability of this design to protect roof bolter operators from excessive coal dust.

1. INTRODUCTION

Exposure to high concentrations of respirable coal mine dust causes coal workers' pneumoconiosis (CWP), a potentially fatal lung disease with no known conclusive cure[1]–[3]. Overexposure to respirable coal mine dust exposure has also been linked to the onset of silicosis if the silica content in the coal dust is high [4], [5]. Underground coal mine roof bolter operators are known to have a higher risk of both excessive coal dust and silica exposure [3], [6], [7]. This is due to reasons such as miners' position downwind of the continuous miner, improper and inadequate ventilation, and dust from the bolting operations due to faulty or unmaintained dust collector. Typically, roof bolting downwind to the continuous miner can substantially increase bolter operators' coal dust exposure level up to 7.0 mg/m^3 [8]. These levels exceed the maximum concentrations allowed by MSHA outlined in the New Dust Rules of 2014 [9]. According to this rule, mines are required to maintain respirable coal dust concentrations at or below 1.5 mg/m^3 time weighted average (TWA) end of shift concentration, and if the mine's respirable coal mine dust contains more than 5% silica, then the permissible limit is reduced and calculated by 10 divided by the percentage of quartz present in the dust.

To reduce dust exposure levels of coal mine roof bolters, a canopy air curtain (CAC) was developed by the National Institute of Occupational Safety and Health (NIOSH). The CAC is mounted below the roof bolter's protective canopy under which the bolter performs the bolting operations. The CAC uses a blower fan to draw air from the mine atmosphere through a HEPA filter to provide clean air. The filtered air is then delivered through tubing to the plenums which are located underneath the canopy of the

bolting machine. While bolting operations are ongoing with the operator working underneath the CAC, the plenums supply filtered air over the breathing zone of the operator. This offers a level of coal dust protection without affecting operator safety, comfort, and mobility [8].

Since its invention, many improvements have been made in the design of the CAC. Laboratory assessment carried out by NIOSH on their initial CAC design yielded an efficiency of 62% [10]. A new prototype with improved design covered the entire operating area of the canopy [8]. This design was then optimized to provide uniform airflow over the entire plenum using CFD simulations and trial-and-error process. It achieved dust reduction of more than 67 % for entry velocities up to 0.61 m/s (120 fpm). A new design was made based on the NIOSH design with a much thinner profile with slotted openings to provide perimeter airflow [11]. This design only yielded an efficiency of 24 % based on the NIOSH gallery test. Later, a 3rd generation CAC was designed with a higher perimeter airflow to prevent contaminated airflow from infiltrating the protected zone. Although the third generation CAC lab test dust reduction has improved up to 49.3% [12], the field test has shown variable dust control efficiencies necessitating rooms to further improve the design [7].

It has been established by NIOSH that the efficiency of the CAC depends on the uniformity of air flowing over the breathing zone of the operator. Therefore, it is important to ensure an even distribution of airflow across the plenum at a velocity higher than 0.51 m/s (100 fpm) in order to provide protection beneath the entire canopy area. To achieve a uniform airflow distribution across the plenum, we propose the use of a two-level manifold system. A manifold system consists of the main flow header, and several

outlets. However, it is challenging for a typical manifold with a constant cross-sectional area header to achieve uniform flow distribution due to the static pressure build up toward the end of the header causing a higher efflux through the downstream outflows. Studies have shown that the manifold with a tapered longitudinal section can achieve nearly uniform flow distribution because the pressure distribution is more uniform in the header. To apply it to the CAC, we used CFD modeling technique to design a two-level manifold system: air is firstly evenly distributed horizontally using the main manifold, and the outlet of the main manifold will be connected to a series of sub-manifolds that uniformly distribute air downward.

The objective of this research is to optimize the design of the CAC using a two-level manifold system with improved airflow distribution that effectively protects roof bolters from coal dust exposures. To achieve this objective, CFD simulations are carried out using the existing peripheral design used in a previous NIOSH study but a redesigned internal structure to incorporate the two-level manifold system. A CFD based parametric study is performed with the aim of determining the optimum manifold designs. The Simplex Evolutionary Operation (EVOP) optimization algorithm was executed to optimize this design of the CAC with each iteration in the optimization process requiring a CFD simulation. A laboratory-made CAC model was then built based on this optimum design configuration and tested in laboratory experiments to validate the CFD models. The CFD results show a near perfectly uniform distribution of airflow over the plenum of the CAC. The CFD model resulted in a non-uniformity coefficient of 0.004907 compared with 0.003617 from laboratory experiments validating the accuracy of the CFD model.

2. MODEL DESCRIPTION

The design of a CAC is critical to ensure an optimal discharge of air through the outlets towards the operator's breathing zone. The structure of the CAC must allow for an elevated and uniform air velocity at the outlets resulting in an air-curtain formation that protects the operator from exposure to particulate matter. The following sections describe the geometry and associate CFD models to simulate the airflow patterns.

2.1. GEOMETRY

Figure illustrates the peripheral geometry of the CAC design incorporated into the roof bolter canopy as part of the machine by J.H Fletcher and Co. [8], and this peripheral geometry is used in this study. Previous designs have added various designs of baffles, inflow vanes and flow straighteners to the CAC internal structure. In the existing design, a single angled plate with an adjustable louver is installed inside the plenum to regulate the airflow distribution. This current design has an uneven flow of air beneath the plenum with approximately 30% of the plenum area being unprotected. Areas with low to no airflow are the trapezoidal region as well as the transition zone between the square and the trapezoidal region. The currently used third generation CAC only reduces coal dust exposure by 34.6 % to 49.3 % [12].

The internal design of our model consists of a two-level manifold system as shown in Figure 2. The schematic of the manifold structure used in this study is demonstrated in Figure 3. Manifolds are industrial devices that distribute a large fluid stream into several parallel streams. In this application, a uniform distribution is desired

among all the outlets to ensure ultimate dust protection. The outlets of the first level manifolds serve as the inlets to the second level manifolds generating a two-level manifold system.

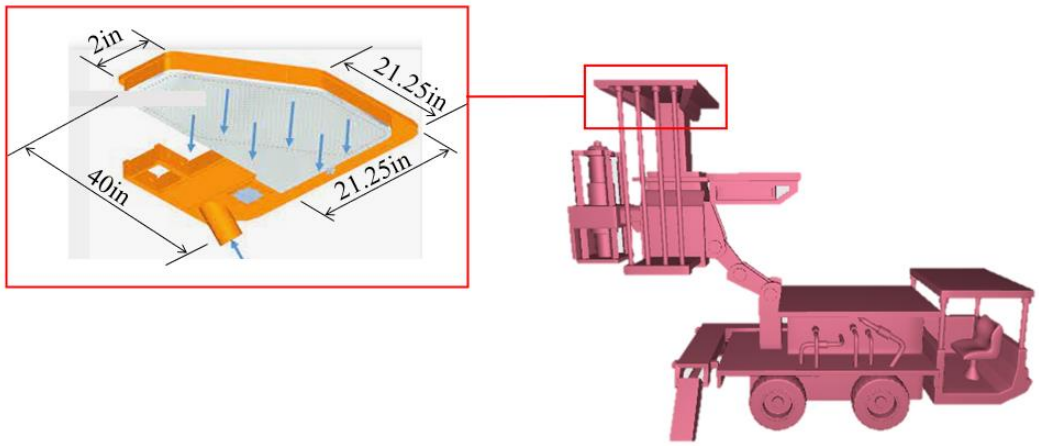

Figure 1. CAD drawing of a typical roof bolter equipment showing the structure of the canopy air curtain mounted on its canopy

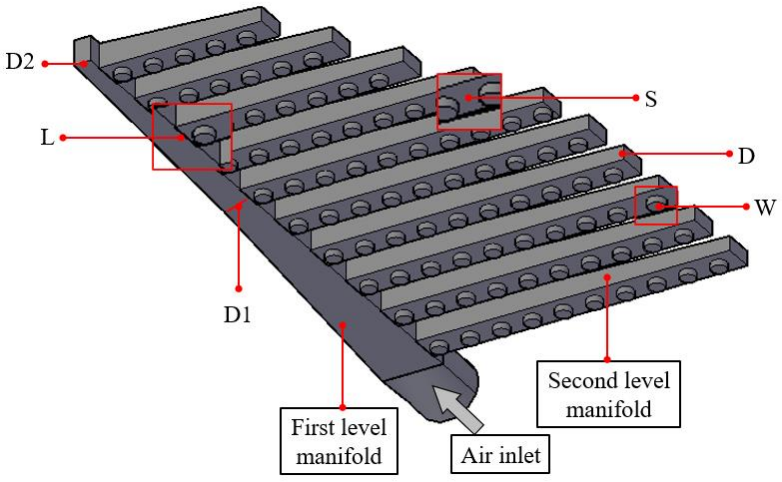

Figure 2. Two-level manifold CAC

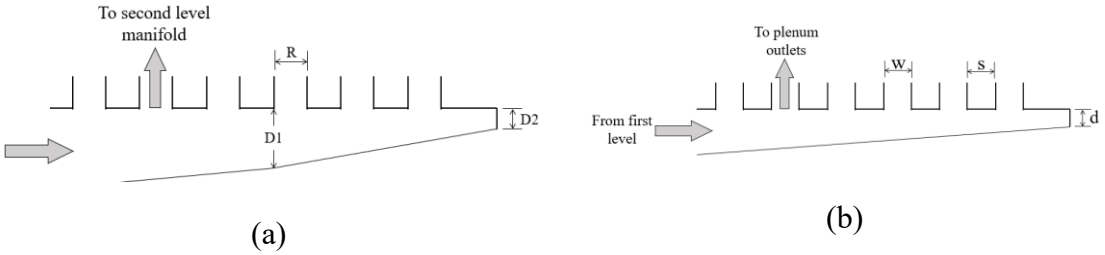

Figure 3. Schematic of (a) first level manifold and (b) second level manifold with labels of parameters to be optimized

The first level manifold which receives airflow from the fan has a cross-sectional dimension of 10.2 cm × 4.0 cm at its entry and tapered at an angle at two points along its length. These dimensions are integrated into the design to be able to fit the 10.2 cm diameter of the fan duct without taking up additional area of space. The CAC is required to have a height restriction of 5.1 cm (2 in.) to provide head clearance for operators. This restricts the overall height of the CAC to approximately 5 cm which is why the entry of the first level manifold is designed to have a height of 5.0 cm. Air is delivered to this manifold through the 10.2 cm diameter duct which is considered as the inlet for CFD analysis. Air flows through the first level manifold and distributes into the plenum area containing the second level manifolds. Internally, the plenum area is made up of branches whose parameters are designed in this study. However, the heights of these manifolds are chosen to be a fixed value of 4.0 cm but tapered along its header. The 4.0 cm dimension is chosen due to the height restrictions for the CAC and the desire to maximize the use of the available space. The widths (R in Table 1) of these second level manifolds are however, included in the optimization process to be determined. The design constraints restricted the number of second level manifolds in the CAC to be 10 with separation distance between second level manifold outlets (s) also a variable to be optimized in this

study. These manifolds are linearly tapered at an angle along the header for controlled airflow distribution in the manifolds. The dimension of the end of the second level manifolds (D) are to be optimized to generate the optimum tapering angle for the optimum uniformity. The use of the two-level manifold system gives a significantly higher control over airflow distribution across the plenum by controlling the quantity of air being sent into each branch.

2.2. OPTIMIZATION METHOD

Most optimization models available in literature have the limitation of being entrapped in a local optimum solution leaving the global optimum solution unidentified or requiring a large number of experiments to adequately cover all decision variables to be optimized. Gradient descent and evolutionary operation algorithms were, therefore, the candidate algorithms considered for their ability to identify global optimum solution with relatively smaller number of iterations. The Simplex Evolutionary Operation (EVOP) algorithm was chosen for this study because of its established ability to find global optimum solutions with high probability without the need for information regarding the gradient or sub-gradient of the objective function [13]. An advantage to this this algorithm is that it is computationally inexpensive for problems with a relatively small number of decision variables such as the one in this study especially since the optimization iterations are interfaced computationally expensive CFD simulations [14],[15]. EVOP algorithms are known to identify global optimum solution typically within iterations 5 -10 times the number of decision variables [16].

This algorithm first defined the parameters to be optimized, their initial conditions, and their parametric boundaries as defined in Table 1. Ten second level manifolds are designed for practical considerations when fabricating the CAC. The constraints for each of the parameters are determined based on geometry limitations and the parameter in relation with other parameters. As can be seen, there are k=6 variables to be optimized. The Simplex EVOP method first leads us to determine the initial k+1=7 designs cases (vertex) to be simulated. The parameters for the initial 7 simulation cases are determined based on Table 2, where the value of p and q are defined in Equation 7 and Equation 8. Thus, 7 CFD simulations were performed at the initial stage of the optimization process.

Once the above seven modeling cases are completed, the dimensionless nonuniformity coefficient is calculated for each case and are ranked in decreasing order. As we want to find the case with the lowest non-uniformity (elaborated in Section 2.3),

Table 1. CAC design parameters

Parameters	Initial Value (cm)	Constraints	Comments
D1	5	2<D1<10	First level manifold middle size
D2	2	0<D2<D1	First level manifold end size
R	5	1<R<10	First level manifold rectangular outlet width (height is fixed as 5 cm)
d	2.5	0=<d<=5	Second level manifold end size
w	5	1<w<10	Second level manifold hole size
s	5	1<s<15	Second level manifold hole space

$$p = dx\frac{\sqrt{k+1}+k-1}{k\sqrt{2}} \quad \text{Equation 7}$$

$$q = dx\frac{\sqrt{k+1}-1}{k\sqrt{2}} \quad \text{Equation 8}$$

Table 2. Initial conditions

Vertex	D1 cm	D2 cm	L cm	d cm	w cm	s cm
1	$x_1 = 5$	$x_1 = 2$	$x_1 = 5$	$x_1 = 2.5$	$x_1 = 5$	$x_1 = 5$
2	$x_1 + p$	$x_1 + q$	$x_1 + q$	$x_1 + q$	$x_1 + q$	$x_1 + q$
3	$x_1 + q$	$x_1 + p$	$x_1 + q$	$x_1 + q$	$x_1 + q$	$x_1 + q$
4	$x_1 + q$	$x_1 + q$	$x_1 + p$	$x_1 + q$	$x_1 + q$	$x_1 + q$
5	$x_1 + q$	$x_1 + q$	$x_1 + q$	$x_1 + p$	$x_1 + q$	$x_1 + q$
6	$x_1 + q$	$x_1 + q$	$x_1 + q$	$x_1 + q$	$x_1 + p$	$x_1 + q$
7	$x_1 + q$	$x_1 + q$	$x_1 + q$	$x_1 + q$	$x_1 + q$	$x_1 + p$

$$r = \left(\frac{2}{k}\right) \cdot \left(\sum c\right) - w \quad \text{Equation 9}$$

the case with the highest non-uniformity is the one we want to avoid. Label the coordinates of this worst response as *w*, the next to worst as *n* and denote the coordinate matrix of all responses that are better than *w* by *c*. The reflection point r is calculated using Equation 9. *r* is the next model needed to be simulated which moves to the opposite direction from the one with the worst non-uniformity. This case will replace the previous

worst case, and the procedure is repeated. If the reflection point is outside the constraints of feasible dimensions of any parameter, it is treated as having the worst non-uniformity, which will force the procedure to reflect back to cases with feasible parameters.

2.3. OBJECTIVE FUNCTION OF NON-UNIFORMITY COEFFICIENT

The objective function of the optimization process is the dimensionless non-uniformity coefficient, defined in Equation 10 which was calculated for every CAC design considered in this study at each iteration of the optimization process. In the equation, β_i is a dimensionless parameter defined in Equation 11 which represents the flow ratio in the i_{th} outlet, $\bar{\beta}$ represents the average flow ratio for all outlets defined in Equation 12 and N denotes the total number of parallel pipes (outlets) in the manifold. In Equation 11, Q_i denotes volume flowrate for the i_{th} outlet in m^3/s and Q represents total flowrate in m^3/s. A higher value of the nonuniformity coefficient indicates a high nonuniformity in the flow distribution. Therefore, the smaller value of the nonuniformity coefficient will imply a high uniformity in the flow distribution across the outlets. This optimization therefore aims to achieve the CAC design with the lowest possible non-uniformity value as the optimum design.

The optimization problem is therefore formulated as follows: Find decision (design) variables *D1*, *D2*, *L*, *d*, *w* and *s*, to minimize objective function:

$$\Phi(D1, D2, L, D, W, S) = \sqrt{\frac{\sum_{i=1}^{n}\left(\beta_i - \bar{\beta}\right)^2}{N}} \qquad \text{Equation 10}$$

Where Φ is the non-uniformity coefficient as a function of (*D1, D2, L, D, W* and *S*), β_i and $\bar{\beta}$ are defined in Equation 11 and Equation 12.

$$\beta_i = \frac{Q_i}{Q} \quad \text{Equation 11}$$

$$\bar{\beta} = \frac{\sum_{i=1}^{n} \beta_i}{N} \quad \text{Equation 12}$$

Q_i = volume flowrate for the i_{th} outlet in m^3/s and Q = total flowrate in m^3/s

Subject to constraints:

$$2 < D1 < 10 \quad \text{Equation 13}$$

$$0 < D2 < D1 \quad \text{Equation 14}$$

$$1 < R < 10 \quad \text{Equation 15}$$

$$0 \leq d \leq 5 \quad \text{Equation 16}$$

$$1 < w < 10 \quad \text{Equation 17}$$

$$1 < s < 15 \quad \text{Equation 18}$$

$$P(D1, D2, L, d, w, \mathrm{s}) \leq 3000$$ Equation 19

Where $P(D1, D2, L, d, w, s)$ is the pressure drop in the CAC.

2.4. BOUNDARY CONDITIONS AND NUMERICAL SCHEMES

The simulations were developed using Ansys Fluent CFD software. The airflow through the domain was simulated with an inlet velocity of 29.5 m/s until a steady-state condition was achieved. The outlet of the plenum was assigned as 0 Pa. static pressure boundary condition. All other impermeable surfaces within the domain were assigned a stationary wall condition. The solver used to run the simulation is a steady-state solver for incompressible, turbulent flow, using the semi-implicit algorithm (SIMPLE) algorithm. The standard k – ε turbulence model was implemented for this simulation, which is a common model used in mining turbulent flow applications including NIOSH CAC studies [17]. This is a two-equation model that solves Reynold's stresses by solving two additional transport equations (PDEs) for turbulence kinetic energy (k) and dissipation rate of turbulence (ε) [18]. For this simulation, the second-order discretization numerical scheme was used.

2.5. GOVERNING EQUATIONS

Airflow within the domain was considered incompressible and turbulent with no heat transfer. The Navier-Stokes's equations were solved to compute this simulation. Navier-stokes equations are vector equations obtained by applying Newton's law of motion to characterize the motion of a fluid element. The equations that form the Navier-

Stokes's equation are the conservation of mass (Equation 20), momentum (Equation 21), and energy (Equation 23). These equations were solved iteratively using the FLUENT solver until convergence was achieved. A threshold residual value of 0.0001 in velocity components and mass flow rate was set. All simulations were run in iterations until convergence was achieved.

$$\frac{\partial \rho}{\partial t} + \vec{\nabla} \cdot \rho \vec{v} = 0 \qquad \text{Equation 20}$$

where ρ is the density of the simulation fluid (kg/m^3), t is the time (seconds), and $\vec{v}$ is the velocity vector.

$$\frac{\partial (\rho \vec{v})}{\partial t} + \vec{\nabla} \cdot (\rho \vec{v} \vec{v}) = \vec{\nabla} \cdot p + \vec{\nabla} \cdot \vec{\bar{\tau}} + \rho \vec{b} \qquad \text{Equation 21}$$

where $\vec{\bar{\tau}}$ is the viscous stress tensor (Newton) given by Equation 22 below for a Newtonian fluid, $\vec{b}$ is body force and μ is molecular viscosity coefficient

$$\vec{\bar{\tau}} = \mu \left(\vec{\nabla} \vec{v} + \left(\vec{\nabla} \vec{v} \right)^T \right) - \frac{2}{3} \mu \left(\vec{\nabla} \vec{v} \right) \vec{\bar{I}} \qquad \text{Equation 22}$$

$$\frac{\partial \rho e}{\partial t} + \vec{\nabla} \cdot (\rho e \vec{v}) = \rho \dot{q} + \vec{\nabla} \cdot \left(k \vec{\nabla} T \right) - \vec{\nabla} \cdot \left(\vec{\bar{\tau}} \cdot \vec{v} \right) + \rho \vec{b} \cdot \vec{v} \qquad \text{Equation 23}$$

where $\dot{q}$ is the volumetric heat addition per unit mass, T is the temperature and e is the internal energy per unit mass.

2.6. MESH INDEPENDENCE

Using the developed model geometry, a high-quality computational mesh was constructed in the flow domain. Due to complexity of this model and turbulence of the flow, an unstructured mesh was generated as can be seen in Figure 4. Five layers of prism cells were generated along the walls to capture the boundary layer phenomenon with a first mesh layer thickness of 0.0005 m. Mesh and boundary condition parameters were derived to satisfy a y+ of 30 since that is the maximum acceptable y+ value for meshes to be considered accurate. These mesh parameters generated a mesh quality of 0.9 which is recognized as an acceptable mesh quality. The accuracy of the mesh parameters is verified using mesh independence study.

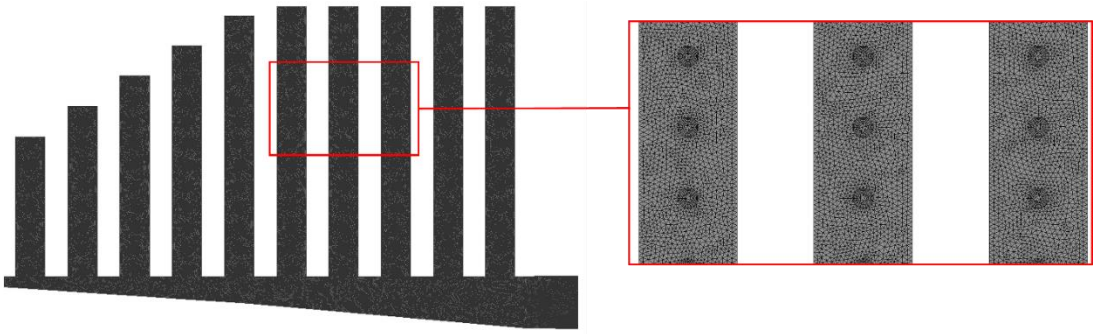

Figure 4. Computational Mesh for the CFD simulations

Mesh independence study was carried out to ensure that the results did not depend on the computational mesh and to ensure that both accuracy and computational cost are within acceptable levels. The mesh independence study was performed by generating three meshes; each of them was designed with a progressively lower characteristic dimension to generate a coarse mesh, medium mesh and fine mesh.

Table 3. Grid parameters for mesh independence studies

Parameters	Coarse Mesh	Medium Mesh	Fine Mesh
Volume (cubic m)	0.0188	0.0188	0.0188
Number of elements, N (million)	3.25	7.07	14.77
Average cell size (mm)	1.81	1.40	1.09
Cell size ratio	-	1.3	1.28

Table 4. Calculation of mesh convergence indices

Parameters	Coarse Mesh	Medium Mesh	Fine Mesh
Static pressure at inlet (Pa)	2623.15	2695.61	2774.3
Average static pressure at inlet (Pa)	2697.69		
Deviation from mean pressure (%)	2.76	0.08	2.84
Average deviation from mean pressure (%)	1.89		

Richardson's method of uncertainty quantification in CFD was used for the mesh independence study [19]. It was ensured that the average height of cells in the meshes were progressively reduced from coarse mesh to fine mesh. The simulations were run until convergence and the variation in the total pressure on the inlet was computed across all three meshes. It is expected that for an accurate simulation whereby the mesh quality has no significant effect on the results, the relative standard deviation between the total pressure values monitored at the inlet on all three meshes should be within 5%. The measured percentage deviations are reported in Table 4. The results obtained from the mesh independence study falls within the criteria set out in the Richardson's method indicating that the mash quality has no significant effect on the CFD results. Therefore, these mesh parameters are adopted for all other simulations carried out in this study.

2.7. MODEL VALIDATION

To ensure the simulation results are accurate and a representation of reality, they were compared with laboratory results for validation. A prototype model of the optimized CAC design, shown in Figure 5, was constructed in the laboratory based on the optimum configuration. The model was built using acrylic materials precisely cut with water jet technology to ensure construction accuracy with the dimensions. It was ensured that the model was air-tight to prevent air loss during operation. A forcing fan was connected to the CAC model through a 10.2 cm diameter circular duct. Due to the unavailability of the Howden AF-10 to the authors of this paper, the Chicago fan was then used.

Figure 5. Laboratory built CAC based on optimum design from CFD simulations

The airflow uniformity of this prototype model was evaluated to validate the CFD model. The operating point of the forcing fan during this experiment was 0.23 m^3/s at 2485.80 Pa static pressure Compared with the CFD model, its operating point was 0.23 m^3/s at a static pressure of 2695.61 Pa. The velocity distribution across the outlets was measured using a pitot tube connected to a manometer to measure flow velocity of each

individual outlet. These data were then used to determine airflow uniformity for the CAC unit.

3. RESULTS

There are 6 design factors covering both the primary and secondary level manifolds of the CAC. The results obtained from the simulations carried out in this research were used in combination with the Simplex EVOP optimization algorithm to determine the optimum configuration of these design factors. These results from this study are discussed in the sections that follow.

3.1. DESIGN OPTIMIZATION

The results of the CAC optimization using the simplex EVOP is shown in Figure 6. In general, the optimization resulted in a progressively more uniform configuration with each iteration. The trend of this result was expected since the nature of the EVOP algorithm is to generate a better configuration with each iteration. As a result, the non-uniformity coefficient generally decreased throughout the iterations. The optimum configuration for the CAC determined with this algorithm was modeled at the 22^{nd} iteration. This decision was based on the satisfaction of the termination criteria established in the EVOP algorithm used in this study. As can be seen from Figure 6, the nonuniformity of the cases continued to decrease beyond the 22^{nd} iteration. However, the solutions after the 22^{nd} iteration violated the constraints in Equation 19 generating static pressure drops exceeding the 3000 Pa limit for fans used in this application. As a result,

all designs generated after the 22nd iteration were infeasible to manufacture even though they resulted in better uniformity.

The high uniformity generated in this model is partly linked to its careful design. Since the canopy of the roof bolter has a trapezoidal shape, the first level manifold needed a careful design to ensure that the optimum uniformity is achieved since the lengths of the branches decrease towards the trapezoidal end of the plenum. Distributing equal quantities of air into each branch would mean there would be more air quantities delivered to the area under the trapezoidal part of the plenum as compared to the squared region. To achieve the desired uniformity across both regions, the first-level manifold was tapered at two sections along its length. This method is established as one of the most effective manifold uniformity techniques as demonstrated in [20], [21]. Applying this technique to the first level manifold caused different rates of air quantity distribution along these two adjoining headers which made it possible to adjust the airflow distribution within the trapezoidal region separately from the airflow distribution within the squared region. The goal was to send progressively lesser quantities of air towards the shorter branches to achieve a uniform quantity per unit area across all branches that make up the second level manifold. A combination of two linearly tapering angles were put along the length of the first level manifold and simulated to determine the optimum combination of tapering angles to uniformly distribute the airflow exiting the outlets across all the branches. This technique greatly enhanced the uniformity of our designs.

As illustrated in Figure 7, the detailed configuration of the optimized CAC design is shown which summarizes the dimensions of this model. The dimension of this model

fits the existing design of the roof bolter's canopy while meeting the head clearance requirement. Therefore, this design required no equipment redesign to be mounted.

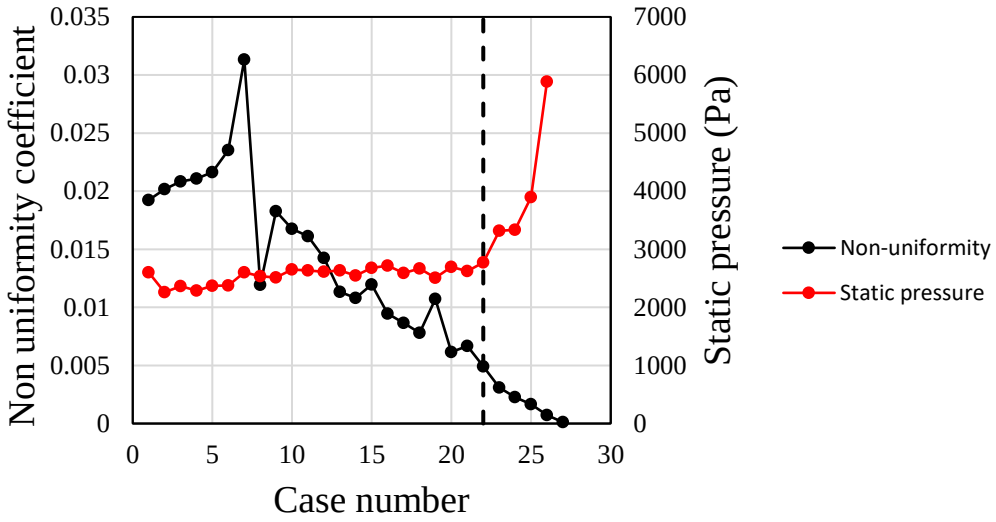

Figure 6. Optimization results

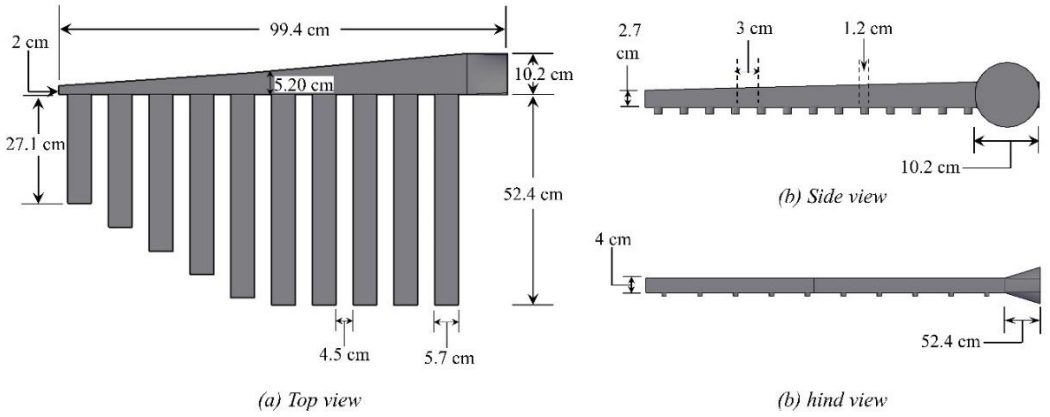

Figure 7. Optimum CAC configuration

3.2. CFD RESULTS

The airflow contours for the steady state of the simulation for the CAC and the outlets are shown in Figure 8 and Figure 9. As can be seen on the legend, the red portion represents areas with relatively higher velocity of greater than 40 m/s while the blue areas represent areas with relatively lower air quantities below 1 m/s. As can be seen from Figure 8, airflow from the fan forces its way into the first level manifold of the CAC which is uniformly distributed among the second level manifolds with progressively lesser airflow going into the shorter branches. It has been established in literature that having a manifold with a tapered longitudinal section can achieve near perfect uniform flow distribution if optimized because the pressure distribution is more uniform along the header. The optimized tapered design of the first level manifold in this study confirms that the optimum taper design generated nearly no static pressure build-up within any part of the manifold causing a perfectly uniform efflux throughout the second level manifolds.

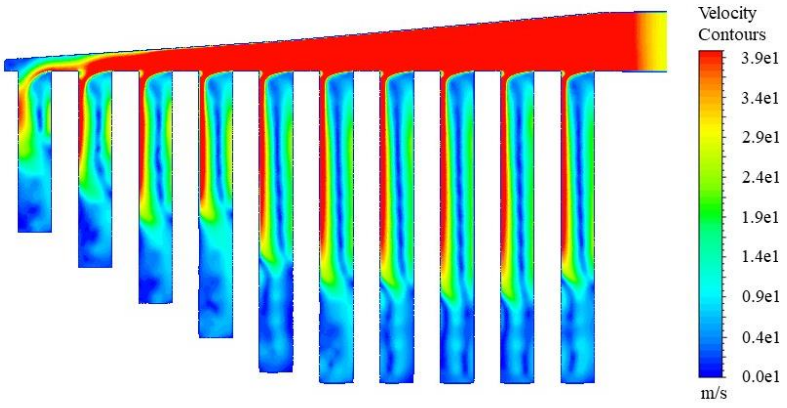

Figure 8. Contour of internal airflow pattern in CAC

Visualizing the airflow contours of the CAC outlets shown in Figure 9 moreover shows that there is a high degree of improved outflow uniformity across the plenum. This shows a significant improvement on the existing third generation CAC model. However, a small region of relatively lower flow quantities can be observed towards the center of the CAC. This, however, did not prove to affect the uniformity of the overall plenum area considering the minimal non-uniformity coefficient calculated from these results.

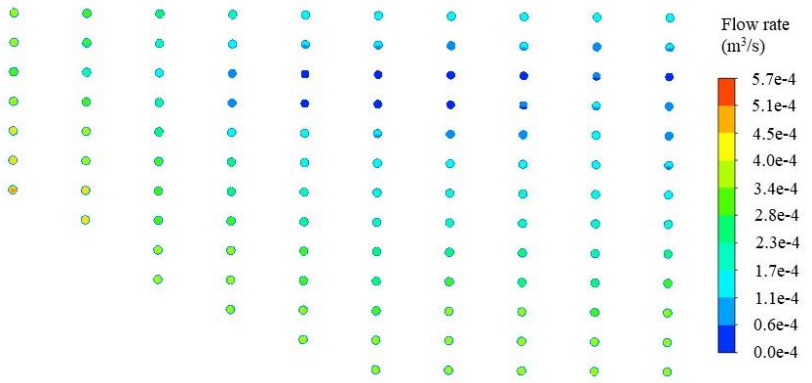

Figure 9. Contours for the CAC outlets

3.3. MODEL VALIDATION

The laboratory-built unit of the CAC was mounted 2.07 m (6.8 inches) from the ground. Outlet velocity for each outlet was measured using a pitot tube measuring the center point velocity pressure of each outlet. The fan's connection to the CAC resulted in 0.23 m^3/s of airflow quantity at 2485.80 Pa of static pressure closely matching the CFD model's 0.23 m^3/s airflow with 2695.61 Pa of static pressure. Moreover, the 0.23 m^3/s total airflow going through the CAC domain is the same airflow quantity provided into

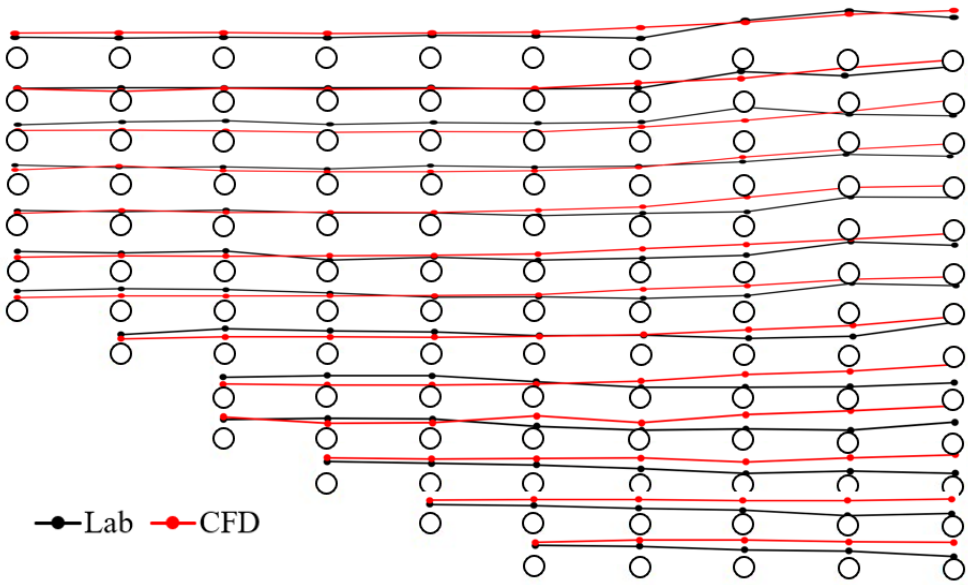

Figure 10. Comparison between laboratory experimental and CFD results based on the measured velocities for all outlets.

the fletcher CAC currently used in mines. Figure 10 showes the results of the velocities measured from each outlet in the experimental model compared with those measured from the CFD model highlighting the similarity between them. By measuring the individual output quantity from each outlet, a non-uniformity coefficient of 0.003617 was calculated for the laboratory experiment while 0.004907 was determined for the CFD model. A t-test performed to test the statistical significance between the CFD model outlet values and that of the lab unit revealed a p-value of < 0.05. This explains that there is no significant difference between airflow quantity values from the outlets measured from the CFD model and that from the laboratory experiment making the laboratory test representative of the CFD model.

4. CONCLUSION

Roof-bolters operators are exposed to elevated dust concentrations that make them prone to the onset of irreversible diseases such as CWP and silicosis. To control their exposure levels, the canopy air curtain was designed by the NIOSH to deliver filtered air on the roof bolter operators breathing zone to dilute coal dust within their working area. Additionally, this design and subsequent improvements also had a provision of perimeter flow. A high-velocity air jet emancipating from the slits downstream serves as the air curtain. This is impassable to dust particles present in the ventilation air stream lowering his exposure to respirable dust. This paper summarizes the parametric studies of the geometry of the CAC aimed at allowing near equal airflow through all the branches. The two-level manifold CAC design parameters were optimized to achieve the best possible uniformity and best efficiency.

The original perimeter profile of the third generation CAC was used in this study. A two-level manifold system was introduced into the CAC peripheral design to carry air towards the operator's breathing zone. Steady-state CFD models were developed to investigate the impact of four major parameters to the airflows. This study focused on optimizing the uniformity of the CAC by tapering the two-level manifolds to redistribute airflow across their outlets. By using the Simplex Evolutionary Operational (EVOP) optimization algorithm together with CFD the design of the two-level manifold CAC was optimized. The non-uniformity index was calculated for each CFD model performed at each optimization iteration. The design which resulted in the least non-uniformity coefficient was determined to be the optimum design of the two-level manifold-based

CAC. This design is critical for an effective dilution of dust-laden air close to the breathing zone of the miner.

Analysis of all the parameters showed that an inlet size (D_1) dimension of 10.2 cm × 4.0 cm, tapered header end size (D_2) dimension of 4.0 cm × 2.0 cm, first level manifold rectangular outlet width (R) dimension of 5.7 cm × 4.0 cm, second level manifold end size (d) of 4.0 cm × 2.7 cm, second level manifold hole size (w) of 1.27 cm in diameter and a second level manifold hole space (s) of 3.0 cm gave the optimum CAC performance. A laboratory model of this design was built and evaluated to validate the CFD results. While the CFD model resulted in a non-uniformity coefficient of 0.004907, the laboratory experiment yielded 0.003617 with the correlation between their outlet velocities having a statistical P-value of < 0.05 indicating a great correlation. This study presents an advancement in technology necessary in optimizing the uniformity of the CAC plenum to improve the efficiency of the CAC. This is important in offering protection to roof bolter operators against the inhalation of coal dust. In the long term, these advancements will protect the health of roof bolter and enhance production in coal mines. This study had limitations in testing the efficiency of this CAC model in an underground mine setting against coal dust since that was out of the scope of this study. Future studies will perform field studies to evaluate the efficiency of this CAC model.

REFERENCES

[1] D. J. Blackley, J. B. Crum, C. N. Halldin, E. Storey, and A. S. Laney, “Resurgence of progressive massive fibrosis in coal miners — Eastern Kentucky, 2016,” *Morbidity and Mortality Weekly Report*, vol. 65, no. 49, pp. 1385–1389, 2016, doi: 10.15585/mmwr.mm6549a1.

[2] A. S. Laney and M. D. Attfield, “Coal workers’ pneumoconiosis and progressive massive fibrosis are increasingly more prevalent among workers in small underground coal mines in the United States,” *Occup Environ Med*, vol. 67, no. 6, pp. 428–431, 2010, doi: 10.1136/oem.2009.050757.

[3] Mine Safety and Health Administration, “Open Government Initiative Portal - MSHA.” 2020.

[4] R. A. Cohen *et al.*, “Lung pathology in U.S. coal workers with rapidly progressive pneumoconiosis implicates silica and silicates,” *American Journal of Respiratory and Critical Care Medicine*, vol. 193, no. 6, pp. 673–680, 2016, doi: 10.1164/rccm.201505-1014OC.

[5] T. Sato, T. Shimosato, and D. M. Klinman, “Silicosis and lung cancer: Current perspectives,” *Lung Cancer: Targets and Therapy*, vol. 9, pp. 91–101, 2018, doi: 10.2147/LCTT.S156376.

[6] D. E. Pollock, J. D. Potts, and G. J. Joy, *Investigation into dust and exposures and mining practices in mines in the southern appalachian region*. Society for Mining, Mettalurgy, and Exploration, Incorporated, 2009, 2009.

[7] W. R. Reed *et al.*, “Field study results of a 3rd generation roof bolter canopy air curtain for respirable coal mine dust control,” *Int J Coal Sci Technol*, vol. 7, no. 1, pp. 79–87, 2020, doi: 10.1007/s40789-019-00280-5.

[8] J. M. Listak and T. W. Beck, “Development of a canopy air curtain to reduce roof bolters’ dust exposure,” *Min Eng*, vol. 64, no. 7, pp. 72–79, 2012.

[9] MSHA, “Lowering Miners’ Exposure to Respirable Coal Mine Dust, Including Continuous Personal Dust Monitors,” 2014. [Online]. Available: http://www.cdc.gov/niosh/docs/2008-143/pdfs/

[10] G. V. R. Goodman and J. A. Organiscak, “Laboratory Evaluation of a Canopy Air Curtain for Controlling Occupational Exposures of Roof Bolters,” *Seventh International Mine Ventilation Congress*, vol. Proceeding, pp. 299–305, 2001.

[11] W. R. Reed, G. J. Joy, B. Kendall, A. Bailey, and Y. Zheng, “Development of a roof bolter canopy air curtain for respirable dust control,” *Min Eng*, vol. 69, no. 1, pp. 33–39, 2017, doi: 10.19150/me.7010.

[12] W. R. Reed, G. J. Joy, M. Shahan, S. Klima, and G. Ross, “Laboratory results of a 3rd generation roof bolter canopy air curtain for respirable coal mine dust control,” *Int J Coal Sci Technol*, vol. 6, no. 1, pp. 15–26, 2019, doi: 10.1007/s40789-019-0237-6.

[13] S. N. Ghani, “Performance of global optimisation algorithm EVOP for non-linear non-differentiable constrained objective functions”, In Proceedings of *1995 IEEE International Conference on Evolutionary Computation*, Vol. 1, p. 320 1995

[14] Z. Zhou, Y. S. Ong, P. B. Nair, A. J. Keane and K. Y. Lum, “Combining global and local surrogate models to accelerate evolutionary optimization,” *IEEE Transactions on Systems, Man, and Cybernetics, Part C (Applications and Reviews)*, 37(1), 66-76, 2006

[15] N. Islam, S. Rana, R. Ahsan, and S. N. Ghani, “An optimized design of network arch bridge using global optimization algorithm,” *Advances in Structural Engineering*, 17(2), 197-210, 2014

[16] W. G. Hunter, and J. R. Kittrell, “Evolutionary operation: a review,” *Technometrics*, 8(3), 389-397, 1966

[17] Y. Zheng and W. R. Reed, “Effects of Roof Bolter Canopy Air Curtain on Airflow and Dust Dispersion in an Entry Using Exhaust Curtain Ventilation,” no. August, 2020, doi: 10.1007/s42461-020-00294-7.

[18] G. Xu, K. D. Luxbacher, S. Ragab, J. Xu, and X. Ding, “Computational fluid dynamics applied to mining engineering: a review,” *Int J Min Reclam Environ*, vol. 31, no. 4, pp. 251–275, 2017, doi: 10.1080/17480930.2016.1138570.

[19] P. J. Roache, “Quantification of uncertainty in computational fluid dynamics,” *Annu Rev Fluid Mech*, vol. 29, pp. 123–160, 1997, doi: 10.1146/annurev.fluid.29.1.123.

[20] J. C. K. Tong, E. M. Sparrow, and J. P. Abraham, “Geometric strategies for attainment of identical outflows through all of the exit ports of a distribution manifold in a manifold system,” *Appl Therm Eng*, vol. 29, no. 17–18, pp. 3552–3560, 2009, doi: 10.1016/j.applthermaleng.2009.06.010.

[21] J. M. Hassan, T. A. Mohamed, W. S. Mohammed, and W. H. Alawee, “Modeling the Uniformity of Manifold with Various Configurations,” *Journal of Fluids*, vol. 2014, no. April, pp. 1–8, 2014, doi: 10.1155/2014/325259.

SECTION

3. CONCLUSIONS AND RECOMMENDATIONS

3.1. CONCLUSIONS

Overexposure to respirable coal mine dust by underground coal miners has been linked to the recent increase in CWP. These studies developed novel technologies and methodologies to monitor and control coal dust exposures in underground mines. First, a new low cost, small size and light weight personal coal dust monitor was developed from a plantower PMS5003 low-cost PM sensor, achieving at least 80% decrease in costs of monitoring units. These coal dust sensors were evaluated and calibrated using simple and multiple linear regression calibration models. Since linear regression models have the drawbacks of being unable to account for multiple factors and non-linear relationships, several machine learning algorithms were applied in calibrating the sensors. Random forest regressor and artificial neural network showed significant performance increase in performance of the sensors above 95% using the PDM as a reference. The support vector machine on the other hand performed similar to the linear regression models giving no performance advantage.

While these sensors are important in detecting overexposures, it is crucial to have effective control measures, such as the canopy air curtains. This study optimized the design of the CAC using a two level manifold system and computational fluid dynamics.

3.2. RECOMMENDATIONS

While the robustness and accuracy of the low-cost PM sensors have been demonstrated in these studies to be promising, it is essential that further studies focus on exploring and improving the intrinsic safety of these sensors for coal mine application in order to prevent ignition.

Other factors that could possibly affect the performance of the sensors need to be studied. Temperature and relative humidity have been studied in these studies. It is worthwhile to study the influence of wind velocity and sensors' special directions.

BIBLIOGRAPHY

[1] I. Energy Agency, “World Energy Outlook iea.org/weo,” 2017. [Online]. Available: www.iea.org/t&c/

[2] U. Energy Information Administration, “Monthly Energy Review -- June, 2023,” 2023. [Online]. Available: www.eia.gov/mer

[3] D. Wang *et al.*, “Incidence and disease burden of coal workers’ pneumoconiosis worldwide, 1990–2019: Evidence from the global burden of disease study 2019,” *European Respiratory Journal*, vol. 58, no. 5, Nov. 2021, doi: 10.1183/13993003.01669-2021.

[4] Y. Shekarian, E. Rahimi, N. Shekarian, M. Rezaee, and P. Roghanchi, “An analysis of contributing mining factors in coal workers’ pneumoconiosis prevalence in the United States coal mines, 1986–2018,” *Int J Coal Sci Technol*, vol. 8, no. 6, pp. 1227–1237, Dec. 2021, doi: 10.1007/s40789-021-00464-y.

[5] A. Medical Association, “Letters Progressive Massive Fibrosis in Coal Miners From 3 Clinics in Virginia,” 2018. [Online]. Available: https://www.cdc.gov/niosh/topics/cwhsp/.

[6] D. N. Weissman, “Progressive massive fibrosis: An overview of the recent literature,” *Pharmacology and Therapeutics*, vol. 240. Elsevier Inc., Dec. 01, 2022. doi: 10.1016/j.pharmthera.2022.108232.

[7] D. J. Blackley, J. B. Crum, C. N. Halldin, E. Storey, and A. S. Laney, “Resurgence of progressive massive fibrosis in coal miners — Eastern Kentucky, 2016,” *Morbidity and Mortality Weekly Report*, vol. 65, no. 49, pp. 1385–1389, 2016, doi: 10.15585/mmwr.mm6549a1.

[8] J. Mo, L. Wang, W. Au, and M. Su, “Prevalence of coal workers’ pneumoconiosis in China: A systematic analysis of 2001–2011 studies,” *Int J Hyg Environ Health*, vol. 217, no. 1, pp. 46–51, Jan. 2014.

[9] S. Han, H. Chen, M. A. Harvey, E. Stemn, and D. Cliff, “Focusing on coal workers’ lung diseases: A comparative analysis of china, australia, and the united states,” *Int J Environ Res Public Health*, vol. 15, no. 11, Nov. 2018, doi: 10.3390/ijerph15112565.

[10] G. R. Zosky *et al.*, “Coal workers’ pneumoconiosis: An Australian perspective,” *Medical Journal of Australia*, vol. 204, no. 11, pp. 414-418.e2, Jun. 2016, doi: 10.5694/mja16.00357.

[11] MSHA, “Major Provisions and Effective Dates MSHA ’ s Final Rule to Lower Miners ’ Exposure to Respirable Coal Mine Dust,” vol. 2014, pp. 1–2, 2014.

[12] P. D. Monitor, “Model PDM3700,” no. 42.

[13] L. J. M. Jon C. Volkwein, Robert P. Vinson and and S. E. Mischler. Donald P. Tuchman, “Performance of a New Personal Respirable Dust Monitor for Mine Use,” *Report of Investigations 9663, National Institute for Occupational Safety and Health, Pittsburgh Research Laboratory*, pp. 1–25, 2004, [Online]. Available: papers://d0b7ba82-564e-41a5-892d-096be28ddf10/Paper/p192

[14] G. Allen *et al.*, “Evaluation of the TEOM Method for Measurement of Ambient Particulate Mass in Urban Areas PAPER Evaluation of the TEOM ® Method for Measurement of Ambient Particulate Mass in Urban Areas,” vol. 2247, 2012, doi: 10.1080/10473289.1997.10463923.

[15] J. C. Volkwein *et al.*, “Laboratory and Field Performance of a Continuously Measuring Personal Respirable Dust Monitor,” *US Department of Health and Human Services, Public Health Service, Centers for Disease Control and Prevention, National Institute for Occupational Safety and Health, Cincinnati, OH*, pp. 1–55, 2006.

[16] T. Zheng *et al.*, “Field evaluation of low-cost particulate matter sensors in high- and low-concentration environments,” *Atmos Meas Tech*, vol. 11, no. 8, pp. 4823–4846, 2018.

[17] K. E. Kelly *et al.*, “Ambient and laboratory evaluation of a low-cost particulate matter sensor,” *Environmental Pollution*, vol. 221, pp. 491–500, 2017, doi: 10.1016/j.envpol.2016.12.039.

[18] D. M. Holstius, A. Pillarisetti, K. R. Smith, and E. Seto, “Field calibrations of a low-cost aerosol sensor at a regulatory monitoring site in California,” *Atmos Meas Tech*, vol. 7, no. 4, pp. 1121–1131, 2014, doi: 10.5194/amt-7-1121-2014.

[19] D. Koestner, D. Stramski, and R. A. Reynolds, “Assessing the effects of particle size and composition on light scattering through measurements of size-fractionated seawater samples,” *Limnol Oceanogr*, vol. 65, no. 1, pp. 173–190, Jan. 2020, doi: 10.1002/lno.11259.

[20] S. Sousan, K. Koehler, L. Hallett, and T. M. Peters, “Evaluation of the Alphasense optical particle counter (OPC-N2) and the Grimm portable aerosol spectrometer (PAS-1.108),” *Aerosol Science and Technology*, vol. 50, no. 12, pp. 1352–1365, 2016, doi: 10.1080/02786826.2016.1232859.

[21] S. Sousan *et al.*, “Inter-comparison of low-cost sensors for measuring the mass concentration of occupational aerosols,” *Aerosol Science and Technology*, vol. 50, no. 5, pp. 462–473, 2016, doi: 10.1080/02786826.2016.1162901.

[22] S. Sousan, K. Koehler, L. Hallett, and T. M. Peters, “Evaluation of consumer monitors to measure particulate matter,” *J Aerosol Sci*, vol. 107, pp. 123–133, 2017, doi: 10.1016/j.jaerosci.2017.02.013.

[23] A. Manikonda, N. Zíková, P. K. Hopke, and A. R. Ferro, “Laboratory assessment of low-cost PM monitors,” *J Aerosol Sci*, vol. 102, pp. 29–40, 2016, doi: 10.1016/j.jaerosci.2016.08.010.

[24] A. D. Gillies and H. W. Wu, “A new real time personal respirable dust monitor,” *Coal 2006: Coal operator’s conference*, pp. 77–92, 2006, [Online]. Available: http://ro.uow.edu.au/coal/37

[25] J. Y. Kim, S. R. Magari, R. F. Herrick, T. J. Smith, and D. C. Christiani, “Comparison of fine particle measurements from a direct-reading instrument and a gravimetric sampling method,” *J Occup Environ Hyg*, vol. 1, no. 11, pp. 707–715, 2004, doi: 10.1080/15459620490515833.

[26] Y. Wang, J. Li, H. Jing, Q. Zhang, J. Jiang, and P. Biswas, “Laboratory Evaluation and Calibration of Three Low-Cost Particle Sensors for Particulate Matter Measurement,” *Aerosol Science and Technology*, vol. 49, no. 11, pp. 1063–1077, 2015, doi: 10.1080/02786826.2015.1100710.

[27] A. L. Northcross, R. J. Edwards, M. A. Johnson, Z. Wang, K. Zhu, and K. R. Smith, “A low-cost particle counter as a realtime fine-particle mass monitor,” *Environmental Sience: processes & Impacts*, vol. 15, no. 2, pp. 433–439, 2013, doi: 10.1039/c2em30568b.

[28] C. Barrett, E. Sarver, E. Cauda, J. Noll, S. Vanderslice, and J. Volkwein, “Comparison of Several DPM Field Monitors for Use in Underground Mining Applications,” pp. 2367–2380, 2019, doi: 10.4209/aaqr.2019.06.0319.

[29] J. Noll and S. Janisko, “Using laser absorption techniques to monitor diesel particulate matter exposure in underground stone mines,” *Smart Biomedical and Physiological Sensor Technology V*, vol. 6759, p. 67590P, 2007, doi: 10.1117/12.737790.

[30] Marinov, “Performance Evaluation of Low-cost Particulate Matter Sensors,” pp. 13–16, 2017.

[31] G. Olivares, I. Longley, and G. Coulson, “Development of a low-cost device for observing indoor particle levels associated with source activities in the home,” *10th International Conference on Healthy Buildings 2012*, vol. 3, no. July, pp. 2456–2462, 2012.

[32] K. E. Kelly *et al.*, “Ambient and laboratory evaluation of a low-cost particulate matter sensor,” *Environmental Pollution*, vol. 221, pp. 491–500, 2017, doi: 10.1016/j.envpol.2016.12.039.

[33] A. Leavey *et al.*, “Air quality metrics and wireless technology to maximize the energy efficiency of HVAC in a working auditorium,” *Build Environ*, vol. 85, pp. 287–297, 2015, doi: 10.1016/j.buildenv.2014.11.039.

[34] B. Feenstra *et al.*, “Performance evaluation of twelve low-cost PM2.5 sensors at an ambient air monitoring site,” *Atmos Environ*, vol. 216, no. February, p. 116946, 2019, doi: 10.1016/j.atmosenv.2019.116946.

[35] C. Lin, J. Gillespie, M. D. Schuder, W. Duberstein, I. J. Beverland, and M. R. Heal, “Evaluation and calibration of Aeroqual series 500 portable gas sensors for accurate measurement of ambient ozone and nitrogen dioxide,” *Atmos Environ*, vol. 100, no. 2, pp. 111–116, 2015, doi: 10.1016/j.atmosenv.2014.11.002.

[36] W. R. Reed *et al.*, “Field study results of a 3rd generation roof bolter canopy air curtain for respirable coal mine dust control,” *Int J Coal Sci Technol*, vol. 7, no. 1, pp. 79–87, 2020, doi: 10.1007/s40789-019-00280-5.

[37] MSHA, “Coal dust samples data set .” https://arlweb.msha.gov/OpenGovernmentData/OGIMSHA.asp#msha-datasets (accessed Jul. 28, 2023).

[38] J. M. Listak and T. W. Beck, “Development of a canopy air curtain to reduce roof bolters’ dust exposure,” *Min Eng*, vol. 64, no. 7, pp. 72–79, 2012.

[39] G. V. R. Goodman and J. A. Organiscak, “Laboratory Evaluation of a Canopy Air Curtain for Controlling Occupational Exposures of Roof Bolters,” *Seventh International Mine Ventilation Congress*, vol. Proceeding, pp. 299–305, 2001.

[40] W. R. Reed, G. J. Joy, B. Kendall, A. Bailey, and Y. Zheng, “Development of a roof bolter canopy air curtain for respirable dust control,” *Min Eng*, vol. 69, no. 1, pp. 33–39, 2017, doi: 10.19150/me.7010.

[41] W. R. Reed, G. J. Joy, M. Shahan, S. Klima, and G. Ross, “Laboratory results of a 3rd generation roof bolter canopy air curtain for respirable coal mine dust control,” *Int J Coal Sci Technol*, vol. 6, no. 1, pp. 15–26, 2019, doi: 10.1007/s40789-019-0237-6.

[42] W. R. Reed, G. J. Joy, M. Shahan, S. Klima, and G. Ross, “Laboratory results of a 3rd generation roof bolter canopy air curtain for respirable coal mine dust control,” *Int J Coal Sci Technol*, vol. 6, no. 1, pp. 15–26, 2019, doi: 10.1007/s40789-019-0237-6.

[43] J. C. K. Tong, E. M. Sparrow, and J. P. Abraham, “Geometric strategies for attainment of identical outflows through all of the exit ports of a distribution manifold in a manifold system,” *Appl Therm Eng*, vol. 29, no. 17–18, pp. 3552–3560, 2009, doi: 10.1016/j.applthermaleng.2009.06.010.

[44] J. M. Hassan, T. A. Mohamed, W. S. Mohammed, and W. H. Alawee, “Modeling the Uniformity of Manifold with Various Configurations,” *Journal of Fluids*, vol. 2014, no. April, pp. 1–8, 2014, doi: 10.1155/2014/325259.

[45] A. Tomor and G. Kristóf, “Validation of a discrete model for flow distribution in dividing-flow manifolds: Numerical and experimental studies,” *Periodica Polytechnica Mechanical Engineering*, vol. 60, no. 1, pp. 41–49, 2016, doi: 10.3311/PPme.8518.

[46] M. S. Gandhi, A. A. Ganguli, J. B. Joshi, and P. K. Vijayan, “CFD simulation for steam distribution in header and tube assemblies,” *Chemical Engineering Research and Design*, vol. 90, no. 4, pp. 487–506, Apr. 2012, doi: 10.1016/j.cherd.2011.08.019.

VITA

Nana Kobina Amoako Amoah was born and raised in Tarkwa, Ghana. He obtained his undergraduate degree in environmental and safety engineering from the University of Mines and Technology in Ghana graduating with a first class. He entered the Missouri University of Science and Technology in January 2020. He received a Doctor of Philosophy Degree in Mining Engineering in December 2023.